**CRADA FINAL REPORT
FOR
CRADA NO. NFE-04-00699**

STRUCTURAL ANALYSIS OF SANDWICH FOAM PANELS

April 2010

Prepared by

X. Sharon Huo, Ph.D., P. E.
Associate Professor of Civil Engineering
Tennessee Technological University
P.O. Box 5032
Cookeville, Tennessee 38505

and

Jan Kosny Ph.D.
Oak Ridge National Laboratory
Building 3147
P.O. Box 2008
Oak Ridge, TN 37831-6070

UT–BATTELLE
ORNL-27 (4-00)

Energy and Transportation Science Division

CRADA FINAL REPORT
FOR
CRADA NO. NFE-04-00699

STRUCTURAL ANALYSIS OF SANDWICH FOAM PANELS

Submitted to

SGI Ventures, Inc.
1800 Bering Drive
Suite 501
Houston, TX 77057

OAK RIDGE NATIONAL LABORATORY
Oak Ridge, Tennessee 37831-6283
managed by
UT-BATTELLE, LLC
for the
U.S. DEPARTMENT OF ENERGY
under contract DE-AC05-00OR22725

April 2010

TABEL OF CONTENTS

LIST OF TABLES

LIST OF FIGURES

NOTATIONS AND DEFINITION

The following notations and definitions are utilized throughout the report:

(a) Notations:

E :   Modulus of elasticity

v :   Poisson's ratio

ρ :   Density

t :   Thickness

F_y : Yield strength

(b) Definitions:

Slenderness Ratio: The ratio of the effective length of a column to the radius of gyration of the column, both with respect to the same axis of bending. In algebra form, the slenderness ratio is: KL/r. The slenderness ratio was an important term for columns behavior. A column with larger slenderness ratio is unstable. According to the AISC LRFD Specifications, Article B7, the slenderness ratio of a compression member, KL/r, should not exceed 200.

($r = \sqrt{\dfrac{I}{A}}$, A is the area of cross section of the column; I = the least moment of inertia of the column section; K = the effective coefficient; L = the actual length of the column. KL = effective length (length of an equivalent hinged-hinged column)).

Maximum Deflection: The maximum value of member deformation along its length. Limitation for the maximum deflection is normally specified in the Design code. The deflection limitation of basic panel deformation was L/240 = 0.45 inch, and the limitation of column deformation was L/360 = 0.3 inch.

Maximum Rotation: The maximum value of rotated angle about member axis along its length.

Maximum tensile (compressive) stress: The maximum positive (negative) value of the node

stress. The limitation of the maximum stress of the steel facing is:

$\phi F_{steel} = 0.85 \times 33ksi = 28.05ksi$ (Yield strength $F_y = 33ksi$).

PROJECT SUMMARY

The Sandwich Panel Technologies including Structural Insulated Panels (SIPs) can be used to replace the conventional wooden-frame construction method. The main purpose of this Cooperative Research and Development Agreement (CRADA) between UT-Battelle, LLC and SGI Venture, Inc. was to design a novel high R-value type of metal sandwich panelized technology. This CRADA project report presents design concept discussion and numerical analysis results from thermal performance study of this new building envelope system. The main objective of this work was to develop a basic concept of a new generation of wall panel technologies which will have R-value over R-20 will use thermal mass to improve energy performance in cooling dominated climates and will be 100% termite resistant.

The main advantages of using sandwich panels are as follows: (1) better energy saving structural panels with high and uniform overall wall R-value across the elevation that could not be achieved in traditional walls; and (2) reducing the use of raw materials or need for virgin lumber. For better utilization of these Sandwich panels, engineers need to have a thorough understanding of the actual performance of the panels and system. Detailed analysis and study on the capacities and deformation of individual panels and its assembly have to be performed to achieve that goal. The major project activity was to conduct structural analysis of the stresses, strains, load capacities, and deformations of individual sandwich components under various load cases. The analysis simulated the actual loading conditions of the regular residential building and used actual material properties of the steel facings and foam.

PROJECT OBJECTIVES

The main purpose of this Cooperative Research and Development Agreement (CRADA) between UT-Battelle, LLC and SGI Venture Inc. was to design a novel high R-value type of metal sandwich panelized technology This CRADA project report presents design concept discussion and numerical analysis results from thermal performance study of this new building envelope system. The main objective of this work was to develop a basic concept of a new generation of wall panel technologies which will have R-value over R-20 will use thermal mass to improve energy performance in cooling dominated climates and will be 100% termite resistant.

In recent years, increased levels of insulation, high-performance windows, improved construction practices that reduce air leakage and sensible and latent heat-recovery ventilators have significantly reduced heating and cooling loads. Continued improvements in these building envelope technologies suggests that in the near future residences could be routinely constructed with very low heating and cooling loads. Thus, it is clear that developing very low-energy houses will require improved integration between the traditional building envelope and new features like active thermal mass, radiant barriers, cool surfaces, etc.

The proposed building envelope technology maximizes this integration by utilizing a highly-efficient building envelope with high-R thermal insulation, active thermal mass and superior air-tightness. The project team approach was to combine four common building technologies in a novel way. Structural Insulated Panel (SIP) technology was utilized as a structural vehicle and for high-R thermal insulation. Novel approach to panel-to-panel connections provided excellent air and moisture tightness, but it also works in a similar way as conventional wall framing.

Thermal mass effect will be provided by proprietary thermally-active inserts. It is anticipated that, these new wall panels will utilize internal radiant barriers. Application of steel panel facing will provide impermeable surfaces minimizing degradation of the system R-value (foam aging process caused by the emission to the atmosphere of the foam blowing agent). An application of only steel components (no wood) will provide 100% termite resistance of the proposed wall technology. In addition, the panels are lightweight and will be 100% recyclable. Structures made of the panels can be dismantled, moved and reconfigured into a different structure. We believe that the research proposed here points the way to a new generation of affordable, comfortable, very-low energy buildings that are easily integrated with renewable and fuel cell energy-conversion technologies.

The major objective of the project was to conduct structural analysis of the stresses, strains, load capacities, and deformations of individual sandwich components under various load cases. The analysis simulated the actual loading conditions of the regular residential building and used actual material properties of the steel facings and foam. The research team used ANSYS 8.0 software to perform the proposed analysis. The obtained results include the stress and strain levels, deformation, and load capacities of the structural components of sandwich system, such as panels, columns, and header, under various loading conditions. The analytical results would enhance the understanding of the structural performance of sandwich panels.

The research revealed the following results: (a) For the panel with metal facing Gage 24, 25 and 26, the maximum deformation occurred at about middle height of the panels, the maximum tensile stress in longitudinal direction occurred at the bottom of the front steel facing and the maximum compressive stress occurs at about 45" from the top surface of the front steel facing. The magnitude of the column deformation depended on the modulus of elasticity of foam.

(b) The slenderness ratios of C-channel columns and Delta columns were less than the limitation of 200 and the columns were acceptable. The slenderness ratios of original columns, however, were larger than the specified limitation, and the columns were not acceptable for lateral stability. Torsional deformation (twist) could be clearly observed in the C-shape columns under loading due to the asymmetry about the weak axis in the cross-section. The delta-shape and original columns exhibited flexural buckling deformation only. The analysis of stresses and deformations showed Delta columns made of 16 gage and 18 gage steel were the only columns that met structural requirements for load scenario when columns were subjected to wind load based on 36 in wide tributary area;

In the window header, the maximum tensile and compressive stresses in steel occurred at the bottom of the front facing, close to the support while the maximum compressive stress in the PU foam were almost equal to zero, indicating the steel facings carried almost all of the loads on the window header.

CRADA BENEFITS TO DOE

The main purpose of this Cooperative Research and Development Agreement (CRADA) between UT-Battelle, LLC and SGI Venture Inc. was to design a basic concept of a new generation of metal sandwich panelized technologies. The primary goal of this CRADA was conceptual development of a new type of building envelope technology which will have an R-value over R-20 and will use thermal mass to improve energy performance in cooling dominated climates and will be 100% termite resistant. The second project goal was experimental and numerical analysis of the structural performance of metal sandwich panels with relatively complex, multilayer configuration of two or more different materials or subsystems, including intermediate panel connectors, novel structural members, core foam materials, and the occasional use of phase change materials.

Performed numerical analysis demonstrated excellent structural performance of new sandwich panels. It was found that twist or torsional deformation could be clearly observed in the C-shape columns under loading due to the asymmetry about the weak axis in the cross-section. The newly developed delta-shape and original columns exhibited flexural buckling deformation only. The maximum deformations of delta-shape and original columns occurred at about 45"- 46" from the top surfaces of the columns. The stresses, deformations and slenderness ratios in C-channel columns and Delta columns were acceptable when columns were subjected to wind load based on the column area only. The slenderness ratio of original columns was unacceptable. Only Delta columns made of 16 and 18 gage steel met all of the design criteria when the columns subjected to wind load based on 36 in wide tributary area (24 in. for C-shape column). For columns with the same Gage and under the same loads, the Delta column had the smallest stress and the original column had the largest stress. Considering the deformation, slenderness ratio

and stresses of the columns, Delta-columns made of 16 and 18 gage steel were the best choice among the columns studied in this project.

We believe that the research results described here points the way to a new generation of affordable, comfortable, very-low energy buildings.

ACKNOWLEDGEMENTS

CHAPTER 1

INTRODUCTION

Most residential buildings in the USA are made of wood-frames, constructed with lumbers and nailed together to form the skeleton of the buildings. Although these buildings are economical to build, they have faced concerns on effective utilization of natural resources (wood) and their durability performance. As construction grows, experts are expecting a shortage in construction material supply, especially the raw materials. The shortage of the construction materials would lead to the price increase for the materials and as a result, the increasing price gouges the homeowners and construction industry. It is very common that, the wood-framed buildings are susceptible to moisture and air leakage to and from outside the building, which generates higher energy consumption, and very often moisture-related durability problem. In case of using steel-studs, the overall R-value of the building is reduced considerably by thermal bridging. Furthermore, the thermal shorts along the wall can often lead to local de-colorization of the wall surfaces or sometimes water condensation that can attract mildew. Therefore, a development of structural insulated building panels that could overcome the shortcomings of the wood-frames structures is in high demand now. The sandwich panels developed by Dr. Jan Kosny at the Oak Ridge National Laboratory (ORNL) are the ones to meet these needs for residential buildings. This technology consists of insulation foam core and structural metal facings. The foam core can be made of expanded polystyrene (EPS), polyurethane or polyisocyanurate foam and is sandwiched between two metal skins.

When these panels are engineered and assembled properly, they will act as load bearing structural members and need no frame of skeleton. For better utilization of these panels, engineers need to have a thorough understanding of the actual performance of the panels and

1

other system components. Detailed analysis of the load capacities and potential deformation of individual panels and their assembly had to be performed to achieve this goal.

The main objective of this project is to conduct structural analysis of the stresses, strains, load capacities, and deformations of individual technology components under various load cases. The analysis simulated the actual loading conditions of the regular residential building and used actual material properties of the steel facing of steel structural columns and foam. The research team used ANSYS 8.0 software to perform the proposed analysis. The analytical results would enhance the understanding of the structural performance of the sandwich wall system.

The following research approaches were undertaken to achieve the objectives of this study.

The material properties of the panel components including skins and foam were carefully selected first because the accuracy of the material properties is crucial to correctness of the analysis. The basic dimensions of the panels and columns were obtained from the information provided by Dr. Kosny from the ORNL.

The modeling and analysis began with the main sandwich panel component. The panel was precisely modeled following the finalized dimensions and collected material properties. Three gages of the steel facing, gages 24, 25, and 26, were considered in the analysis. The loads on the panel simulated the actual load conditions in low-rise residential buildings that included the gravity load and wind load. The analytical results included the stresses and strains, the axial and flexural load capacities, and deformations of the panels.

The system columns were modeled in a similar manner as the panel.   The system column was the most important structural elements in the structural insulated panel (SIP) system. A total of three types of system columns were analyzed, they are originally proposed columns, C-channel columns, and Delta columns. For each column type, two or more metal gages of the

steel facings were considered. A comparison of the structural performance of the analyzed columns was also conducted. In addition, the slenderness ratio of each column type was examined.

The window/door header was the flexural member in the sandwich system. The top and bottom C-shape tracks in the header were the major element in carrying the bending moment. These elements were modeled precisely in accordance to the header details. Distributed loads were applied along the length of the header. The load capacity on the header was determined based on the maximum allowable stresses in the header components.

This report summarizes the findings of the research activities conducted on the request of SustainBuild, LLC. The results include the stress and strain levels as well as the deformation of the panels, columns, and header under various loading conditions. The load capacities of these structural components are also presented in the report.

CHAPTER 2

GENERAL INFORMATION OF STRUCTURAL INSULTED PANELS (SIPs)

2.1 Foam Properties

The foam properties used in this study were mostly based on the information found Dyplast Products Polyisocyanurate insulation (ISO-C1) Specifications. DP-ISO-C1 is rigid closed-cell polyisocyanurate thermal insulation foam that can be fabricated into any required shape. The ISO-C1 has been tested according to 18 ASTM Specifications for various material properties. Based on ASTM E84 standards, ISO-C1 has a Class 1 flame spread/smoke development rating, and the highest R-value per inch of any commercially available insulation. The Dyplast Product ISO-C1 was available in 2, 2.5, 3, and 4 lb/ft^3 densities. Tables 2.1 through 2.4 show the physical properties of the ISO-C1 Polyisocyanurate rigid foam insulation used in analysis.

Table 2.1 Polyisocyanurate rigid foam insulation (nominal 2 lb. density)

Physical Properties	ASTM Method	English Units	
Density	D 1622	2.1	lb/ft^3
Compressive Strength	D 1621		
Parallel to Rise (Thickness)		26	lb/in^2
Perpendicular to Rise (Width)		29	lb/in^2
Shear Strength: Parallel and Perpendicular	C 273	27	lb/in^2
Shear Modulus	C 273	346	lb/in^2
Tensile Strength: Parallel and Perpendicular	D 1623	33	lb/in^2
Flexural Strength: Parallel and Perpendicular	C 203	54	lb/in^2
Flexural Modulus	C 203	864	lb/in^2
Closed Cell Content	D 2856	>95	%
Buoyancy		TBD	lb/ft^3
Water Absorption	C 272	0.24	% by volume
Water Vapor Permeance	E 96	2.33	perm-inch
Service Temperature[3]		-297 to +300	°F

Table 2.2 Polyisocyanurate rigid foam insulation (nominal 2.5 lb. density)

Physical Properties	ASTM Method	English Units	
Density	D 1622	2.5	lb/ft^3
Compressive Strength	D 1621		
Parallel to Rise (Thickness)		37	lb/in^2
Perpendicular to Rise (Width)		31	lb/in^2
Shear Strength: Parallel and Perpendicular	C 273	26	lb/in^2
Shear Modulus	C 273	253	lb/in^2
Tensile Strength: Parallel and Perpendicular	D 1623	43	lb/in^2
Flexural Strength: Parallel and Perpendicular	C 203	56	lb/in^2
Flexural Modulus	C 203	961	lb/in^2
Closed Cell Content	D 2856	>98	%
Buoyancy		TBD	lb/ft^3
Water Absorption	C 272	<0.1	% by volume
Water Vapor Permeance	E 96	2.23	perm-inch
Service Temperature[3]		-297 to +300	°F

Table 2.3 Polyisocyanurate rigid foam insulation (nominal 3 lb. density)

Physical Properties	ASTM Method	English Units	
Density	D 1622	3	lb/ft^3
Compressive Strength[3]	D 1621		
Parallel to Rise (Thickness)		45	lb/in^2
Perpendicular to Rise (Width)		38	lb/in^2
Shear Strength: Parallel and Perpendicular	C 273	30	lb/in^2
Shear Modulus	C 273	289	lb/in^2
Tensile Strength: Parallel and Perpendicular	D 1623	47	lb/in^2
Flexural Strength: Parallel and Perpendicular	C 203	70	lb/in^2
Flexural Modulus	C 203	1290	lb/in^2
Closed Cell Content	D 2856	>98	%
Buoyancy		TBD	lb/ft^3
Water Absorption	C 272	<0.1	% by volume
Water Vapor Permeance	E 96	1.98	perm-inch
Service Temperature[3]		-297 to +300	°F

Table 2.4 Polyisocyanurate rigid foam insulation (nominal 4 lb. density)

Physical Properties	ASTM Method	English Units	
Density[3]	D 1622	4	lb/ft^3
Compressive Strength[3]	D 1621		
Parallel to Rise (Thickness)		82	lb/in^2
Perpendicular to Rise (Width)		73	lb/in^2
Shear Strength: Parallel and Perpendicular	C 273	34.4	lb/in^2
Shear Modulus	C 273	315	lb/in^2
Tensile Strength: Parallel and Perpendicular	D 1623	61	lb/in^2
Flexural Strength: Parallel and Perpendicular	C 203	123	lb/in^2
Flexural Modulus	C 203	2331	lb/in^2
Closed Cell Content	D 2856	>98	%
Buoyancy		TBD	lb/ft^3
Water Absorption	C 272	<0.1	% by volume
Water Vapor Permeance	E 96	0.7	perm-inch
Service Temperature[3]		-297 to +300	°F

The research team also collected the information on properties from the BASF Corporation. Their product Elastospray 82302 was a two component, polyurethane spray foam system with a unit weight ranging from 2.0 to 3.0 lb/ft^3. Although, according to the data sheet, the available structural property was the compressive strength only, the information was helpful in determining the material properties used for analysis of the ORNL sandwich panels. Table 2.5 shows the approximate properties of PU foam with a density of 3 lb/ft^3 used in this research.

Table 2.5 Properties of PU foam of SIPs system

Physical Properties	English Units	
Density[3]	3	lb/ft^3
Shear Modulus	1000	lb/in^2
Poisson's ratio	0.4	/
Compressive strength	50	psi
Tensile strength	70	psi
Shear strength	50	psi
Flexural strength	70	psi

2.2 Variation of steel thickness Gages and associated sandwich components

In this research, the panels, columns, and system header made of different steel thicknesses were investigated. The use of varied metal gages allowed the research team to conduct a parametric study for the performance of wall sandwiches and other system components. Table 2.6 shows the properties of steel facings. Table 2.7 lists the basic panel, system columns and window header studied in this research.

Table 2.6 Material property of the steel facings of the SIPs panel

Steel thickness	t (in.)	$F_y(ksi)$	$E(ksi)$	v	$\rho(pci)$
16 Gage	0.0598	33	29000	0.3	0.284
18 Gage	0.0478	33	29000	0.3	0.284
20 Gage	0.0359	33	29000	0.3	0.284
24 Gage	0.0239	33	29000	0.3	0.284
25 Gage	0.0209	33	29000	0.3	0.284
26 Gage	0.0179	33	29000	0.3	0.284

Table 2.7 SIP system components studied

Steel thickness	Basic panel	C-shape column		Delta-shape column		Original column	Window header
		2×4	2×6	Welded	Non-welded		
16 Gage	N	Y	Y	Y	Y	Y	Y
18 Gage	N	N	N	Y	Y	Y	N
20 Gage	N	Y	Y	Y	Y	Y	N
24 Gage	Y	N	N	N	N	N	N
25 Gage	Y	N	N	N	N	N	N
26 Gage	Y	N	N	N	N	N	N

Note: Y denotes the gage will be studied; N denotes the gage won't be studied.

2.3 Loads

Loads applied on the analyzed sandwich wall system include the dead loads, live loads and wind load. Dead loads of the panel include the self-weight of the studied component. Live loads and wind load were introduced based on the analysis of residential building. The plane dimensions of low-rise residential buildings were assumed as shown in Figure 2.1. The height of the basic wall panel and system column was 9 ft (108 inches).
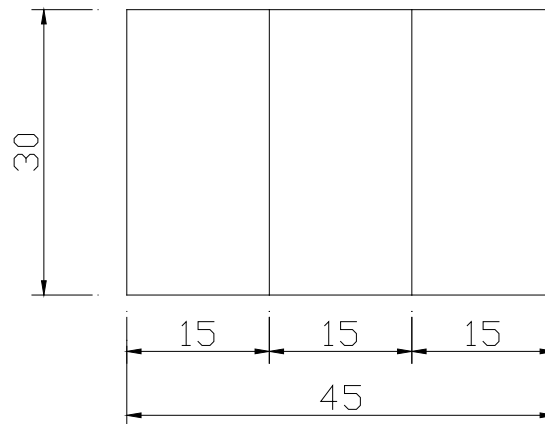
Figure 2.1 The plan view of the low-rise residential building (unit: feet)

2.3.1 Loads of the basic panel

2.3.1.1 Live load of the panels

The live load of the basic panel was calculated according the ASCE – 7 Standard Specifications – Minimum Design Loads for Buildings and Other Structures (ASCE 7-98).

Live load (floor): L_fl = 50psf; Live load (Roof): L_rf = 20psf;

From Figure 2.1, the circumference of the building C = 150 ft and the area A = 1,350 ft^2. The average width of the basic panel Width = 3.04 in. Therefore, live load due to occupancy: L= L_fl ×A/C/Width = 12.34 psi; and roof live load: Lr = L_rf ×A/C/Width = 24.93 psi. The summation of the live load on the basic panel L_L = L + Lr =17.27 psi.

2.3.1.2 Rain load of the panels

The design rainfall for the building is 3 inches per hour, and the runoff quantity for each scupper is $Q = 0.0104$ Ai $= 42.12$, assuming the scuppers are 4 inches above the roof surface. Referring to the specification, the hydraulic head at this flow rate for the scupper used dh=1.754. The design roof rain load, then, was Rain $= 5.2$ (ds + dh) $= 30$psf. The rain load on the basic panel was:

R= Rain ×A/C/Width = 7.40 psi

2.3.1.3 Snow load of the panels

According to the specification, Snow load was assumed: Snow $= 20$ psf. Snow load on the basic panel S $=$ Snow $\times$ A/C/Width $= 4.93$psi

2.3.1.4 Wind load of the panels

In wind load calculation, the basic wind load was taken as V $= 100$ mph; Important factor: I $= 1.0$; Directionality factor $K_d = 0.85$; Velocity pressure exposure coefficient $K_z = 0.912$; $GC_{pf} = 0.8$ (The external pressure coefficient, which was found using Figures 6-5 to 6-7 in ASCE 7-98); $GC_{pi}=0.18$ (The internal pressure coefficient and was found on Table 6-7 in ASCE 7-98); The velocity pressure, pounds per square foot, was computed from the equation

$q_h = 0.00256K_dK_zV^2I = 19.85$ psf

The design pressure, in units of pounds per square foot, for wind loads acting on the components and cladding of a low-rise building was specified in Section 6.5.12.4.1 of ASCE 7-98. That pressure can then be calculated from

$P = q_h[(GC_{pf}) \pm (GC_{pi})] = 19.6$ psf $= 0.136$ psi

2.3.2 Loads of the system column

The two following cases of column loading conditions were considered in the study;

Case 1- column carried wind load based on column area only;

Case 2- column carried wind load based on 36 in wide tributary area (column spacing) for Delta-shape and original system columns and 24 in wide tributary area for C-shape column. The deformations and stresses of the system columns were determined under the Case1 load and Case 2 load, respectively.

2.3.2.1 Live load of the system column

The values of the vertical loads which were applied on the column were determined according to the dimensions of column and directly connected panel. For example, the circumference of the Delta-shape column was $C_{delta} = 24.002$ inches; the area of the basic panel $A_p = 110.4934$ inch^2; the live load applied on the panel was $L_L = L + Lr = 17.27$ psi. Then the live load applied the Delta-shape was: $P_L = L_L * A_p / C_{delta} = 79.503$ (lb/in). The live loads of the other system columns were calculated according to the similar procedure.

2.3.2.2 Wind load of the system column

The width of the front side of Delta-shape column was 3.5 in. When the Delta-shape column was to carry wind load based on 36 in wide tributary area (column spacing), the wind load of the Delta-shape column in load Case 2 became: W=0.136 psi *36in./3.5in. =1.3989 psi. The wind load of the other system column was calculated according to the similar procedure.

2.3.3 Loads of the window header

The header carries the vertical load that was transferred from the weight of the panel. The height of the basic panel above the window header was assumed as 3 feet, which was one-third of the height of the basic panel. The self-weight of the basic panel was 35.476 lbs for foam and 96.61 lbs for steel facings. The cross-sectional area of the window header $A_h = 37.833$ in^2. Then, the gravity load of the window header $P_h = (35.476+96.61)/A_h/3 = 1.164$psi.

2.4 Finite Element Analysis Procedure

ANSYS finite element analysis software is used in the modeling of the ORNL sandwich wall system. Shell elements (Shell181) are used to model the metal facings and solid elements (Solid45) are used to model the foam between the facings.

SOLID45 is used for the 3-D modeling of solid structures. The element is defined by eight nodes having three degrees of freedom at each node: translations in the nodal x, y, and z directions. The element has plasticity, creep, swelling, stress stiffening, large deflection, and large strain capabilities. A reduced integration option with hourglass control is available. Figure 2.2 shows the geometry of Solid45.

SHELL181 is suitable for analyzing thin to moderately-thick shell structures. It is a 4-node element with six degrees of freedom at each node: translations in the x, y, and z directions, and rotations about the x, y, and z-axes. SHELL181 is well-suited for linear, large rotation, and/or large strain nonlinear applications. Change in shell thickness is accounted for in nonlinear analyses. In the element domain, both full and reduced integration schemes are supported. SHELL181 accounts for follower (load stiffness) effects of distributed pressures. Figure 2.3 shows the geometry of Shell181.
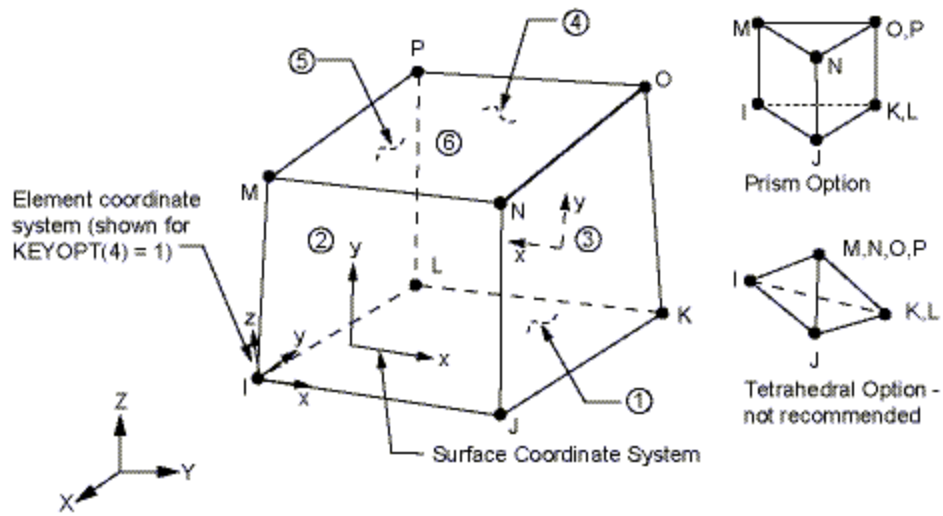
Figure 2.2 Solid45 Geometry
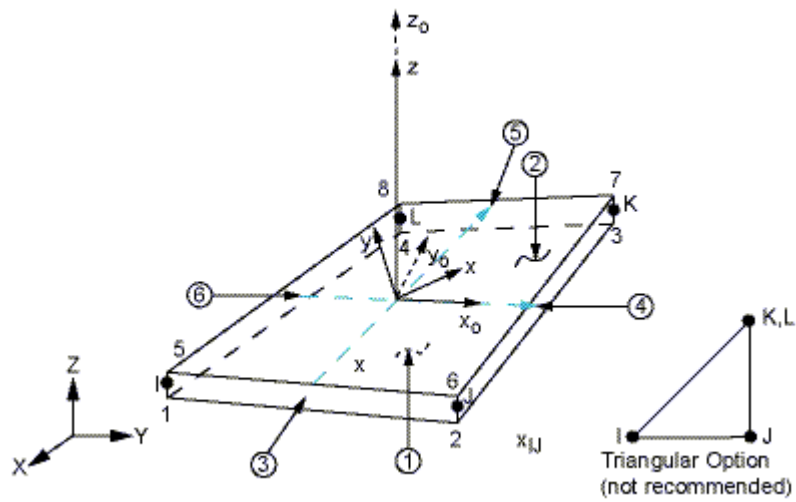
Figure 2.3 Shell181 Geometry

CHAPTER 3

MODELING AND ANALYSIS OF WALL PANELS

The basic panel was the first structural system component to be modeled and analyzed.

Three following thicknesses of the wall panel facings were studied, 24, 25, 26 -gage.

3.1 Description of input and modeling of the basic panel

3.1.1 Dimensions and modeling of the basic panel

Figure 3.1 shows the basic dimension of the cross-section of the panel and Figure 3.2 shows

the longitudinal dimension of the panel.
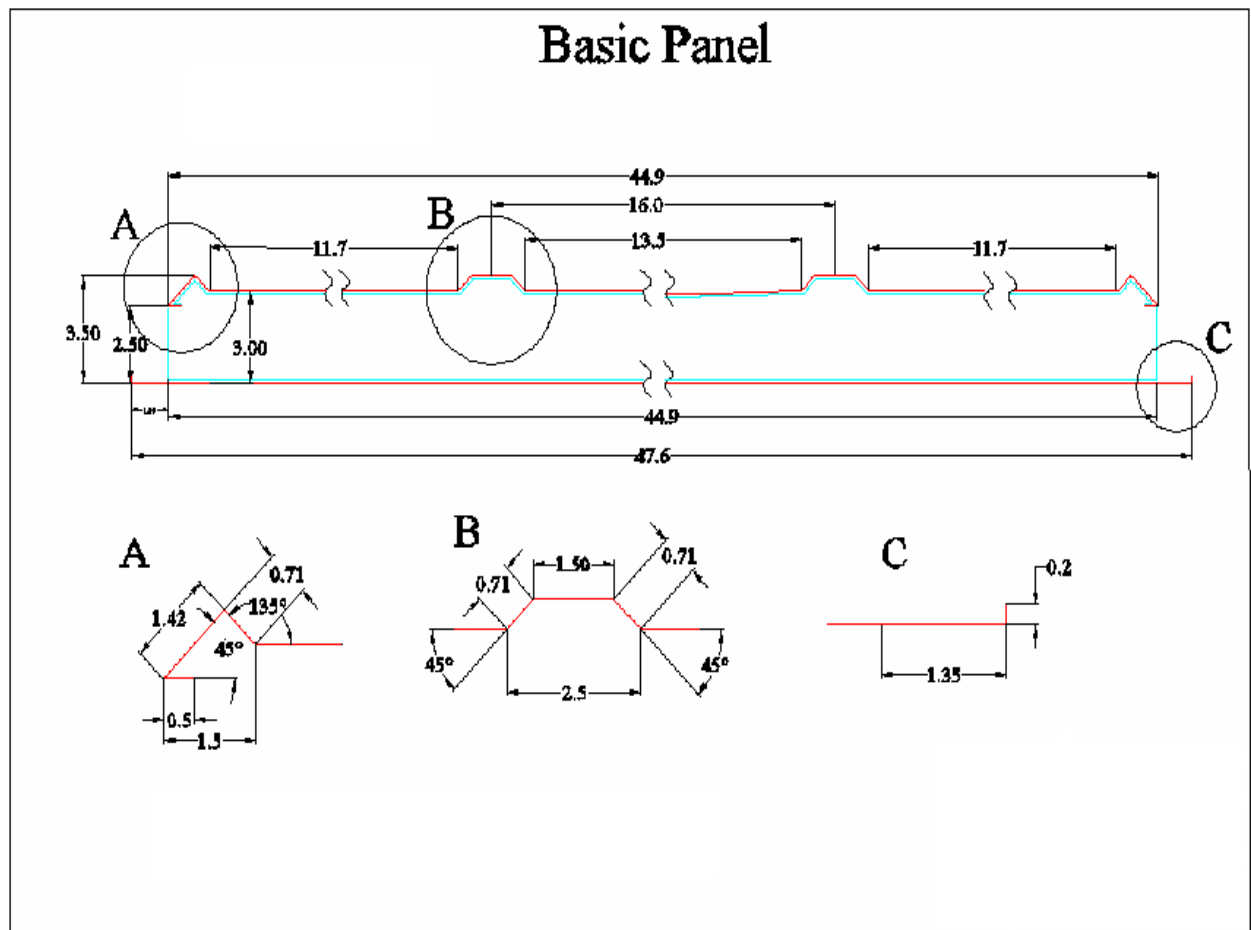
Figure 3.1 Cross-section of the basic panel model (unit: inches)
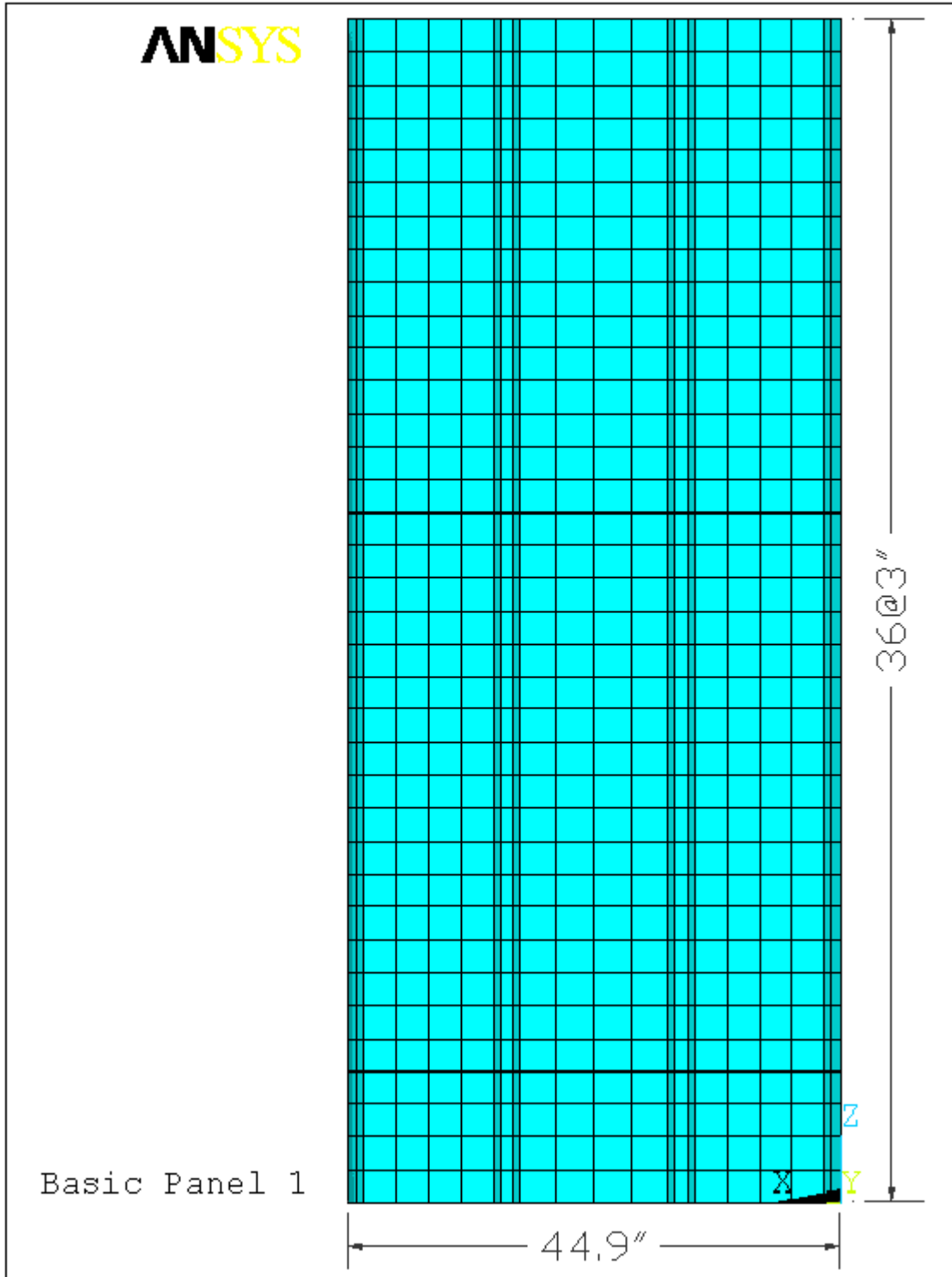
Figure 3.2 Elevation of the panel model

3.1.2 Finite element model of basic sandwich panel

Shell elements (Shell181) were used to model the metal facings and solid elements (Solid45) were used to model the foam core between the facings. As shown in Figure. 3.4, the model was restrained with pin supports at the top of the panel and fix supports at the bottom except the rotation about x direction.
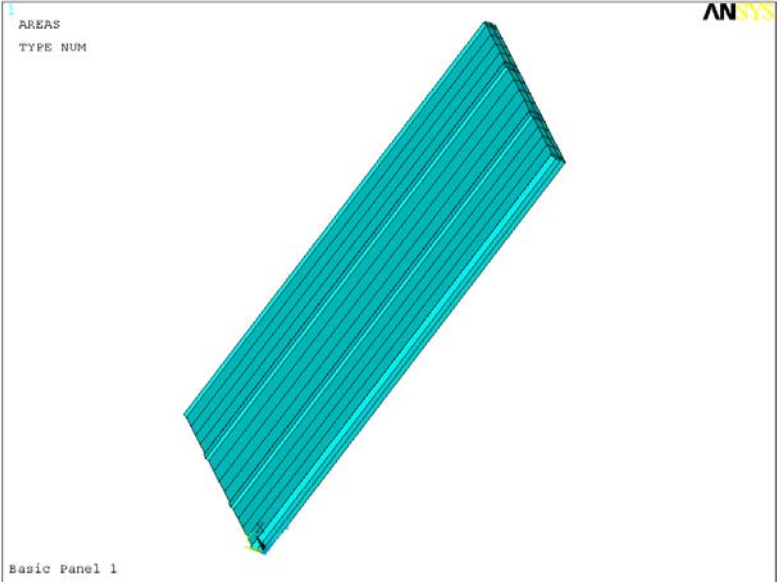
Figure 3.3 Basic panel model
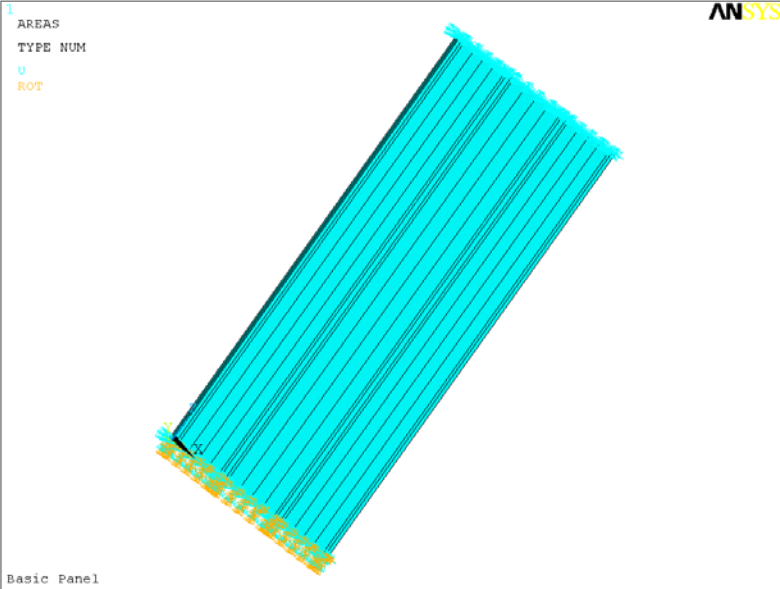
Figure 3.4 Panel model with end restrains

3.1.3 Loads

Live load: 2487 $psf = 17.27\ psi$, applied on the top of the panel.

Wind load: 19.60 $psf = 0.136\ psi$, applied on the steel facing of the panel.

Dead load: Self-weight of the panel are listed in Table 3.1.

Table 3.1 Dead load of the panel (unit: lbs)

	24 Gage	25 Gage	26 Gage
Foam	35.476	35.476	35.476
Steel Sheets	96.61	84.48	72.36
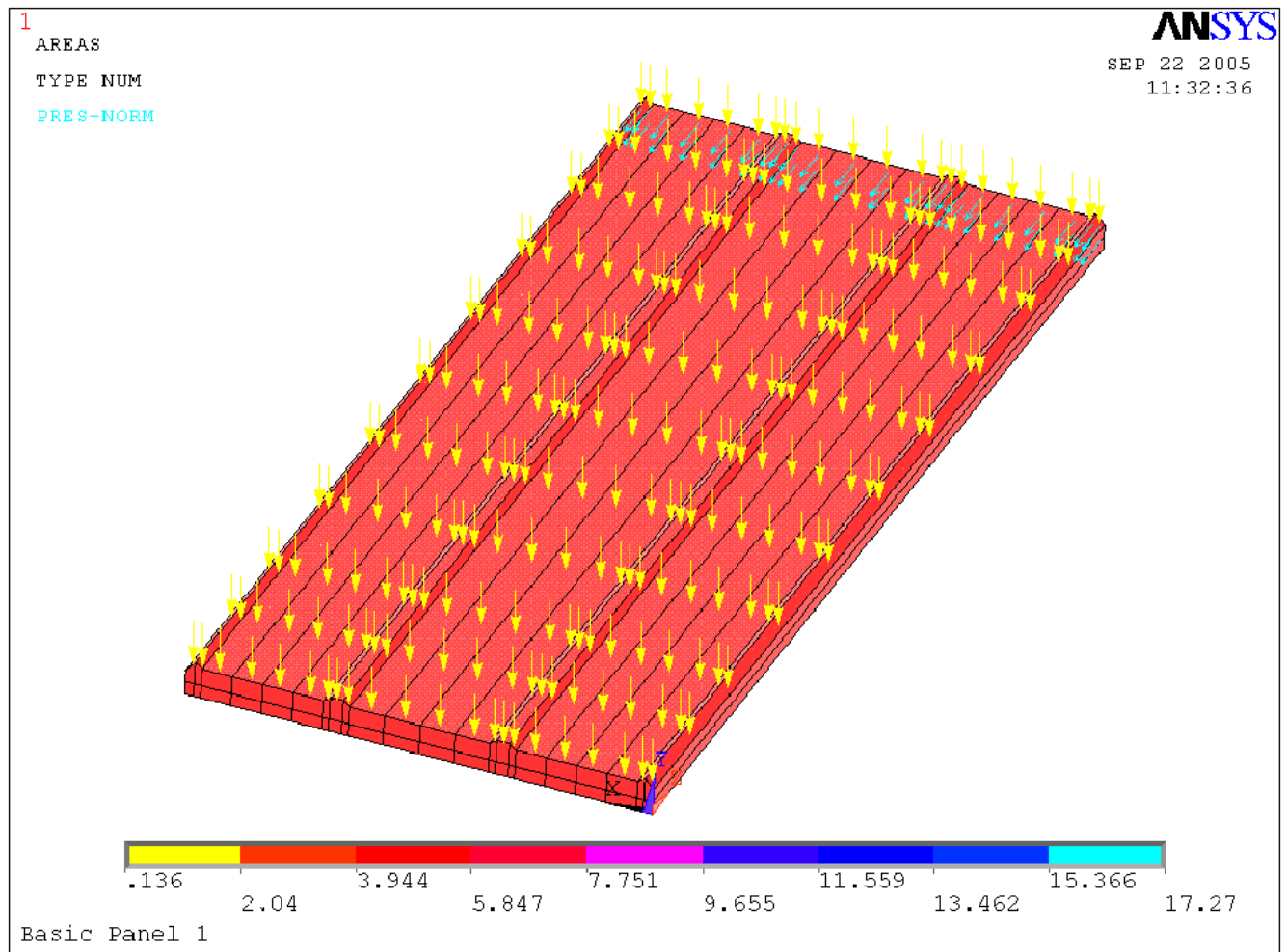
Figure 3.5 Loads on the panel model

3.2 Analytical Results of the Sandwich Panel

3.2.1 Deformation

Figures 3.6, 3.7 and 3.8 show the lateral deformation of panels with 24, 25 and 26 gage,

respectively. As the thickness of the steel facing increased, the deformation of the panel decreased.
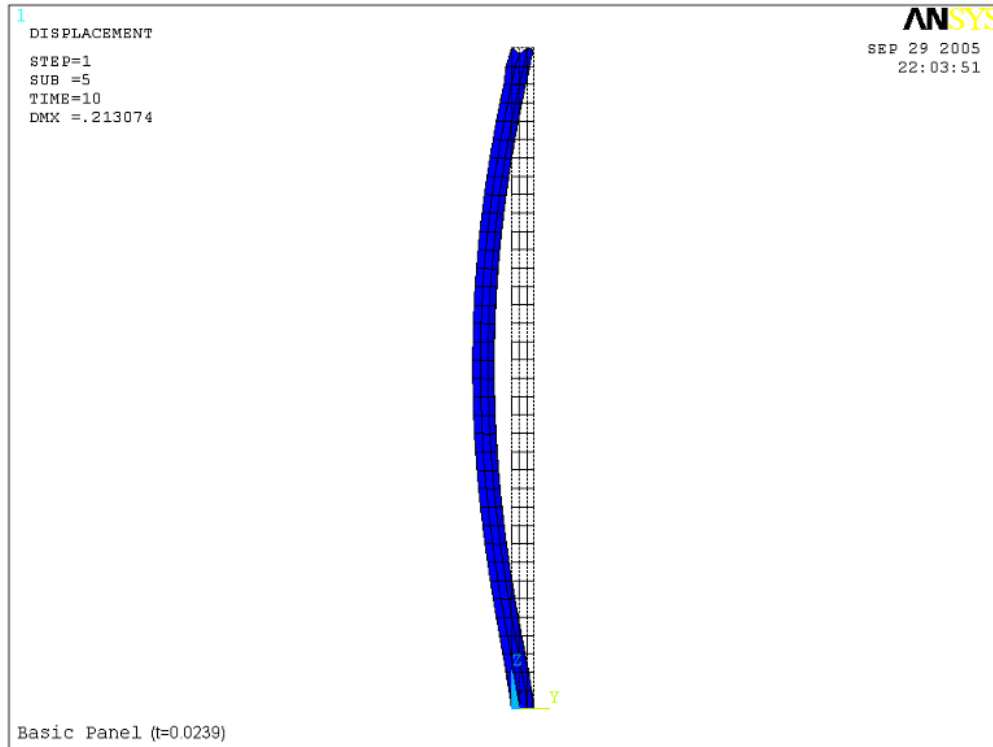
Figure 3.6 Deformation of the panel with 24 Gage (unit: inches)
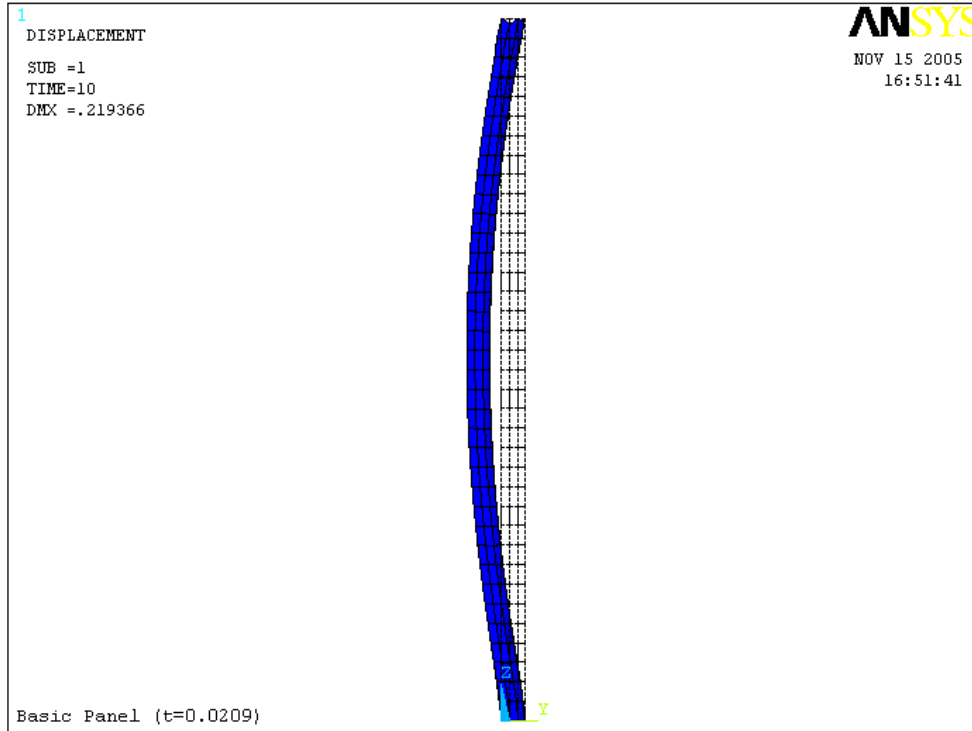
Figure 3.7 Deformation of the panel with 25 Gage (unit: inches)
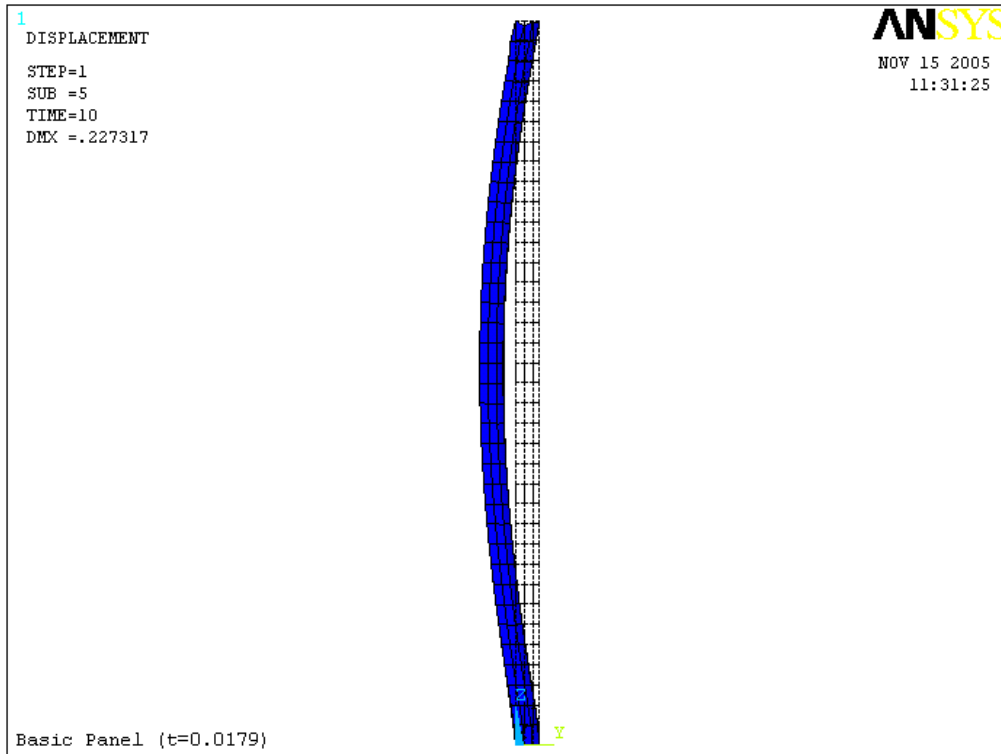
Figure 3.8 Deformation of the panel with 26 Gage (unit: inches)

20

3.2.2 Stress and strain

Figures 3.9 through 3.14 show the stresses in steel facings of the panels and Figures 3.15 through 3.20, show the stresses in the longitudinal direction (z direction) in foam of the panels. The panels were composed of 24, 25 or 26 gage steel facings. The panel stresses were presented in the format of stress contours. The stress values in steel facings and foams were shown in the stress value bar that matched with the color in the contour.
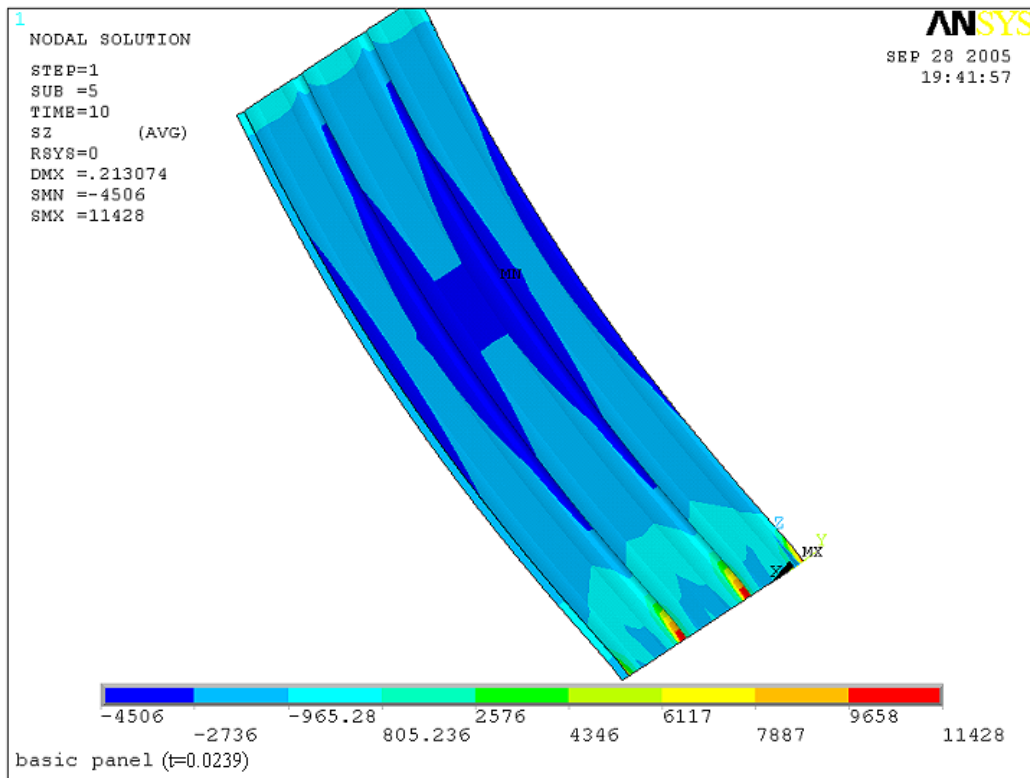
Figure 3.9 Stresses in z direction in the front steel facing with 24 Gage (unit: psi)
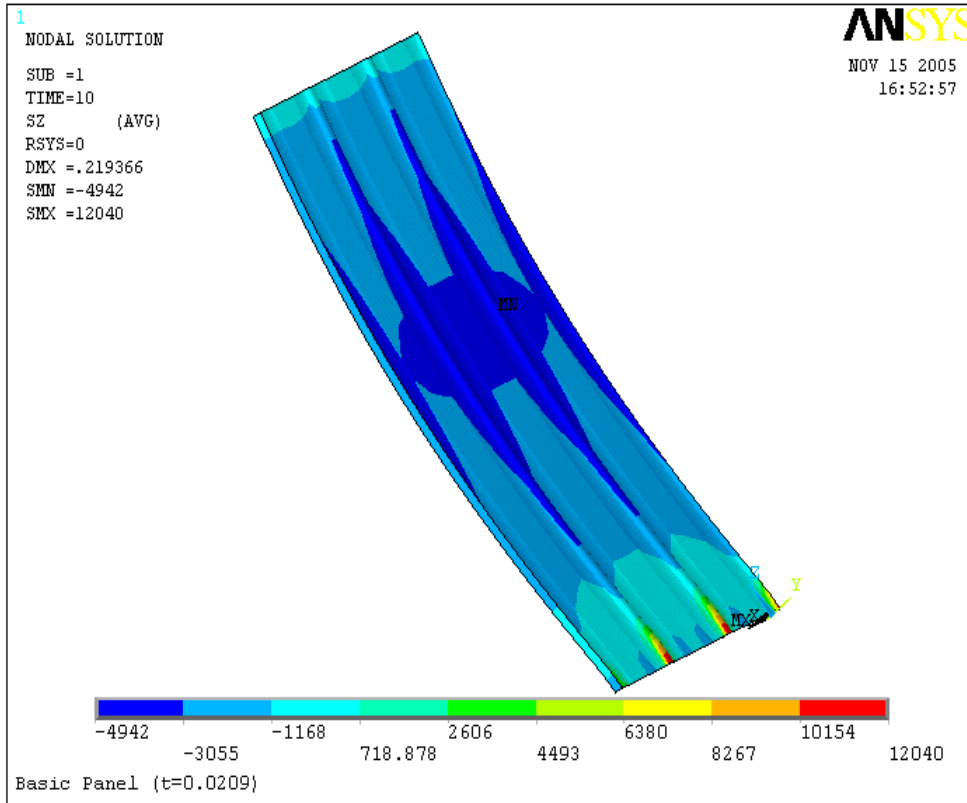
Figure 3.10 Stresses in z direction in the front steel facing with 25 Gage (unit: psi)
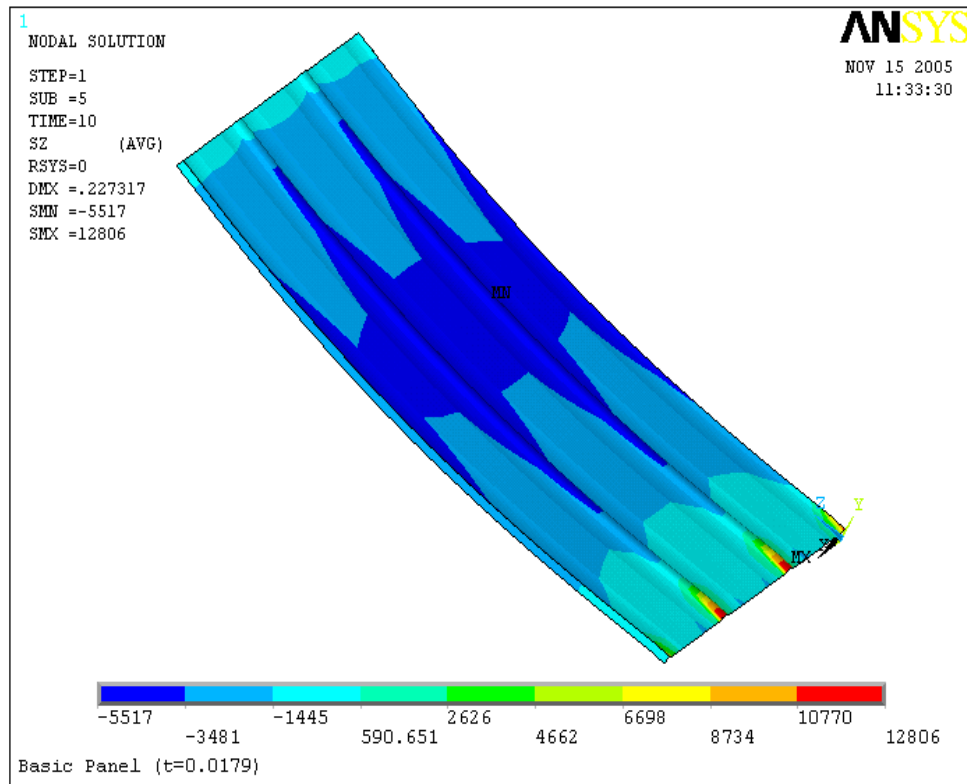
Figure 3.11 Stresses in z direction in the front steel facing with 26 Gage (unit: psi)
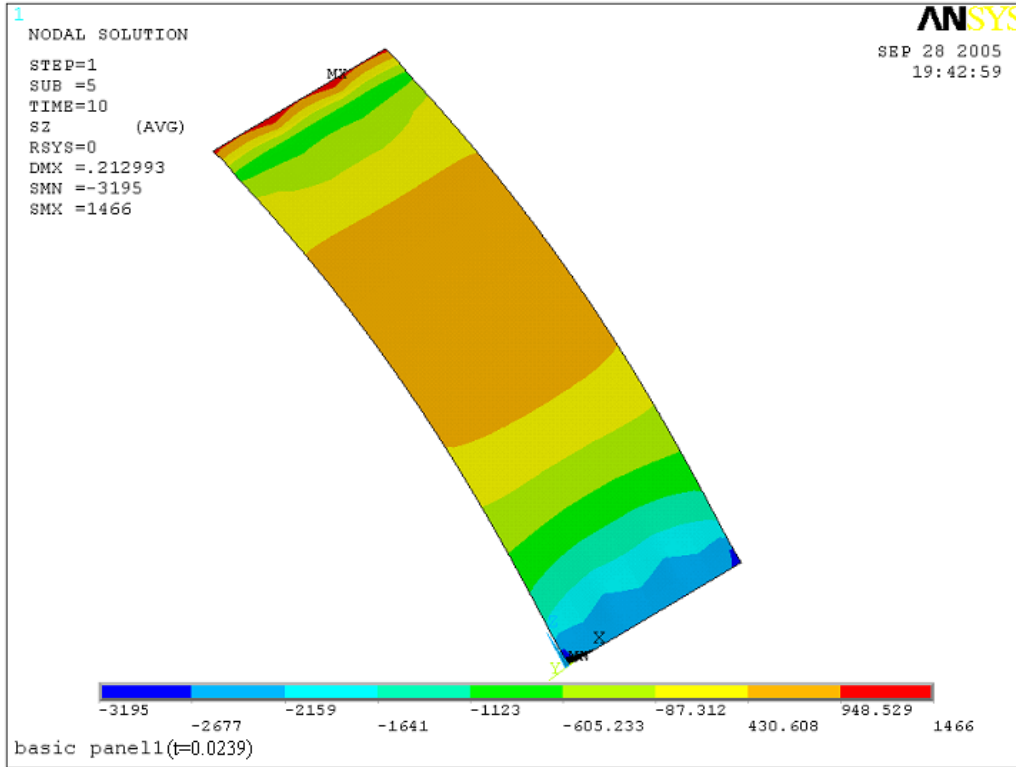
Figure 3.12 Stresses in z direction in the back steel facing with 24 Gage (unit: psi)
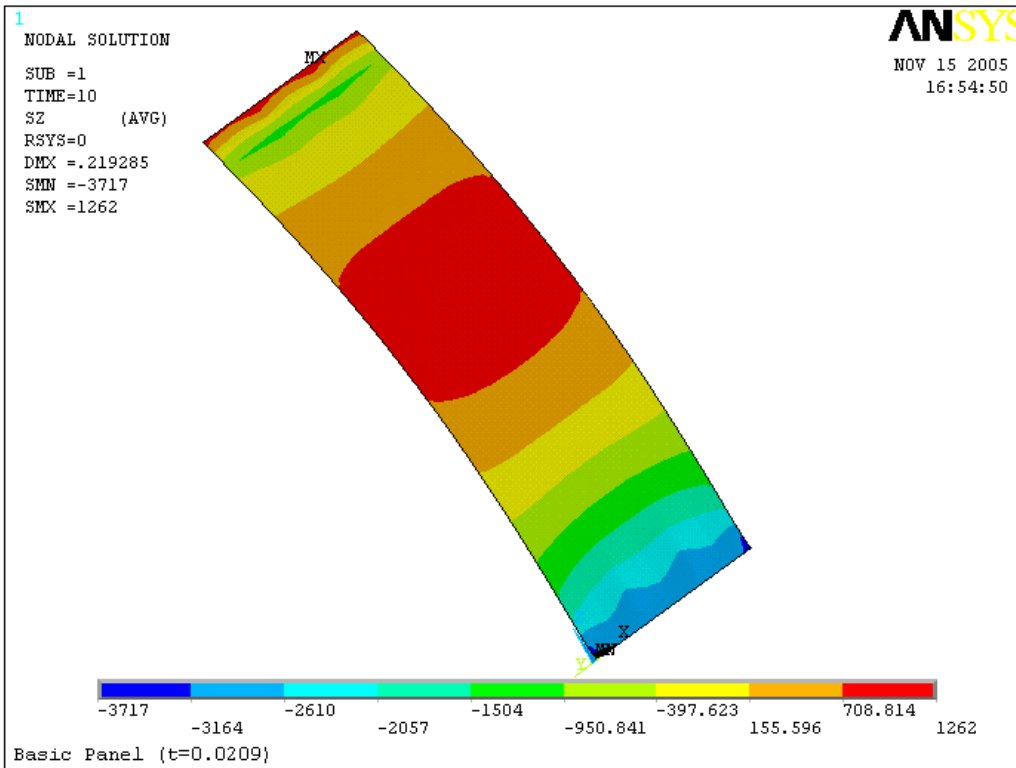
Figure 3.13 Stresses in z direction in the back steel facing with 25 Gage (unit: psi)
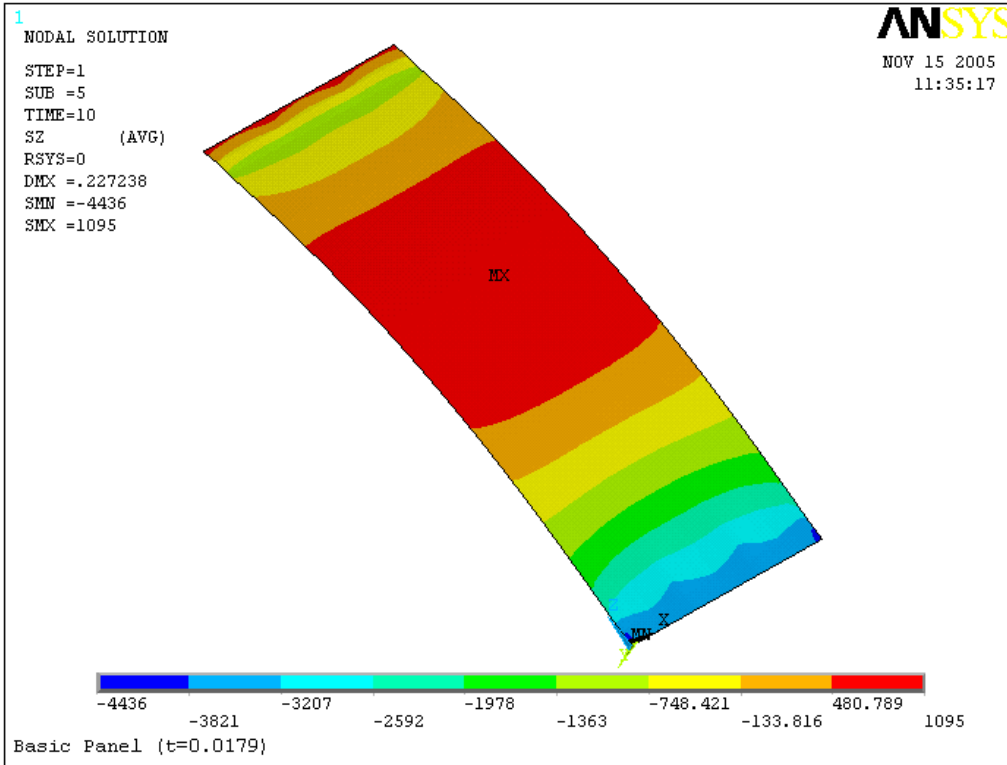
Figure 3.14 Stresses in z direction in the back steel facing with 26 Gage (unit: psi)
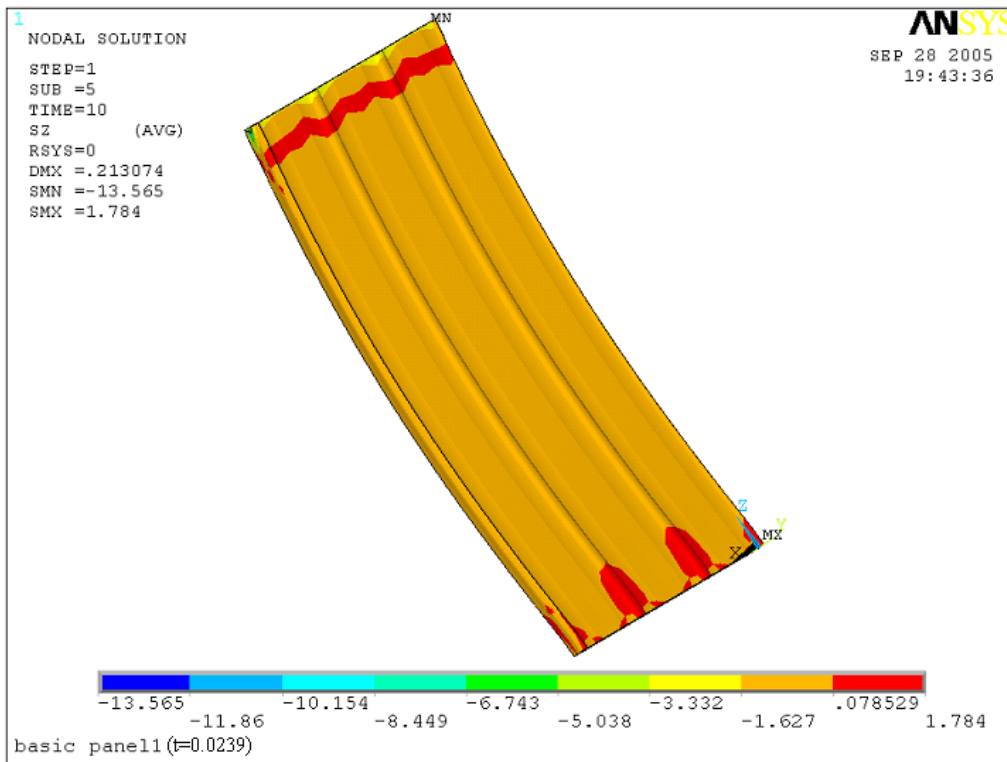
Figure 3.15 Stresses in z direction in the front side of foam with 24 Gage (unit: psi)

24
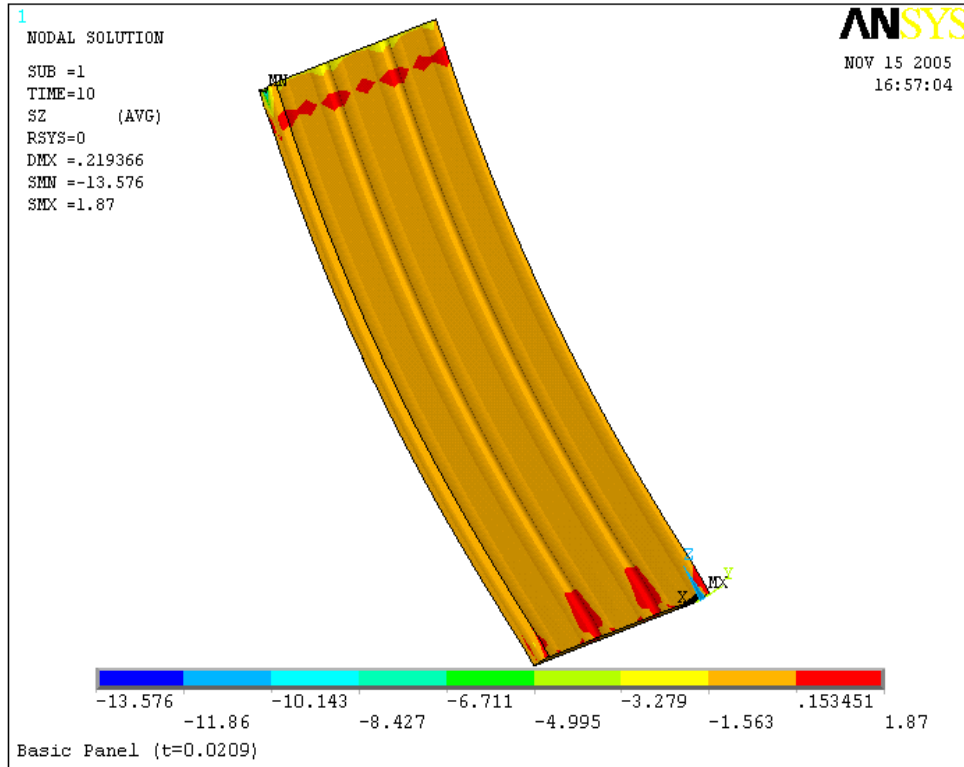
Figure 3.16 Stresses in z direction in the front side of foam with 25 Gage (unit: psi)
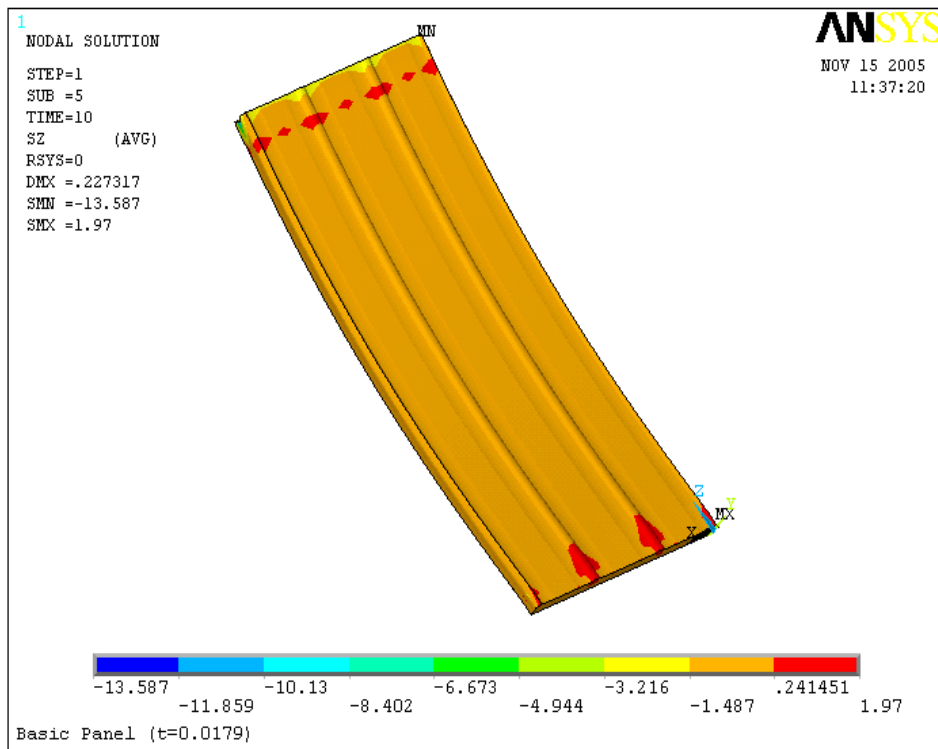
Figure 3.17 Stresses in z direction in the front side of foam with 26 Gage (unit: psi)
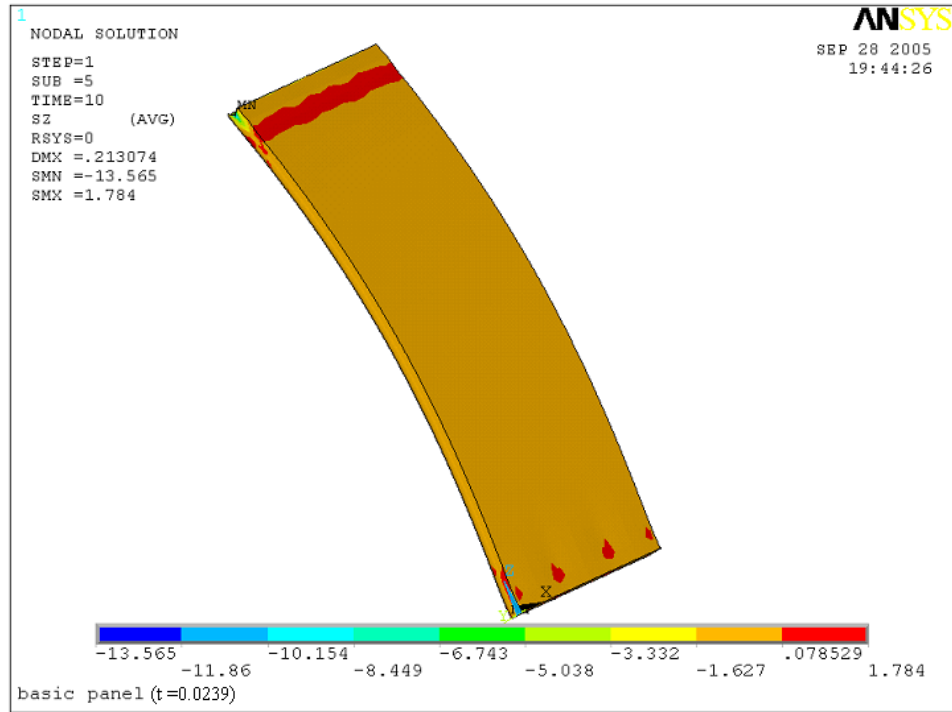
Figure 3.18 Stresses in z direction in the back side of foam with 24 Gage (unit: psi)
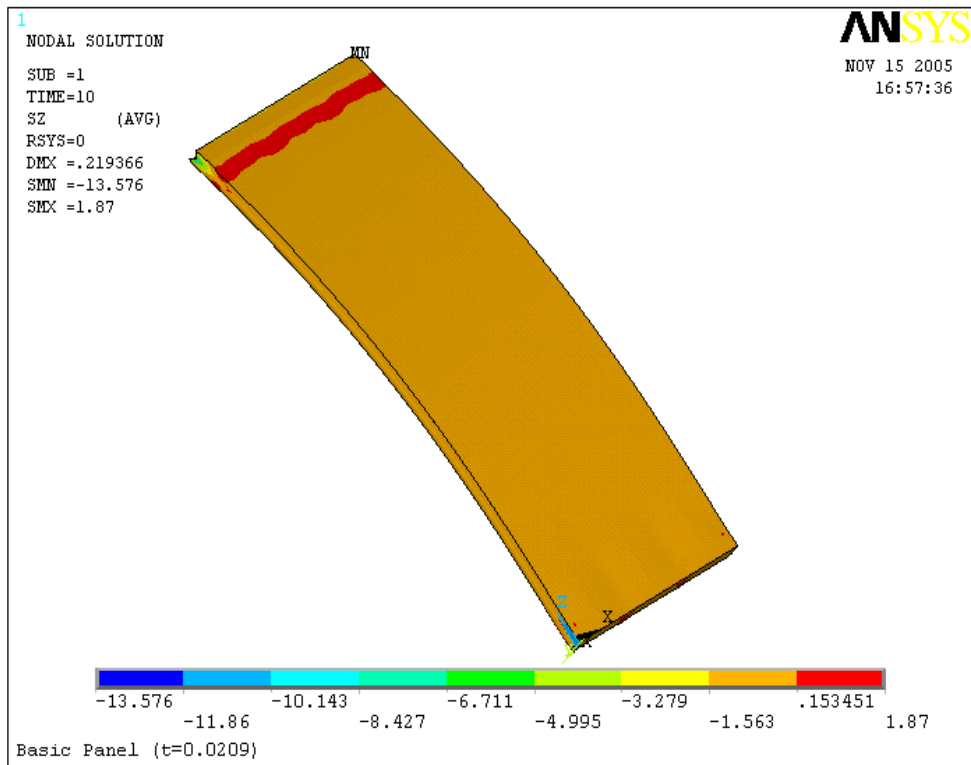
Figure 3.19 Stresses in z direction in the back side of foam with 25 Gage (unit: psi)
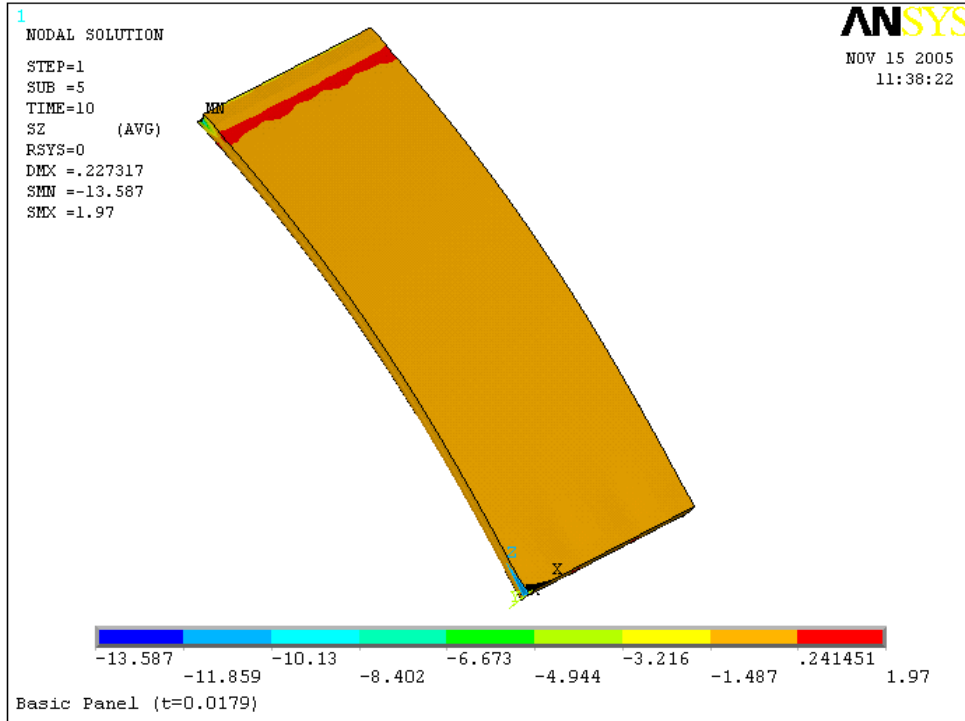
Figure 3.20 Stresses in z direction in the back side of foam with 26 Gage (unit: psi)

3.3 Results Comments of the Sandwich Panels

(a) The maximum deformations and stresses of the panels studied are listed in Table 3.2

Table 3.2 Summary of the maximum deformation and stresses of the panels

Gage#	Maximum Deformation(in.)	Maximum positive stress (Tension) (psi)			Maximum negative stress (Compression) (psi)		
		Steel sheet (front)	Steel sheet (back)	PU foam	Steel sheet (front)	Steel sheet (back)	PU foam
Gage 24	0.213	11428	1466	1.784	4506	3195	13.565
Gage 25	0.219	12040	1262	1.87	4942	3717	13.576
Gage 26	0.227	12806	1095	1.97	5517	4436	13.587

(b) For the panel of 24, 25 and 26 gage, the maximum deformation occurred at about 51"

from the top surface. The maximum tensile stress in longitudinal direction occurred at the bottom

of the front steel facing, while the maximum compressive stress occurred at about 45" from the

top surface of the front steel facing.

(c) The magnitude of deformation was dependent on the modulus of elasticity of foam, E_{foam}, as shown in Figure 3.21 through 3.23.
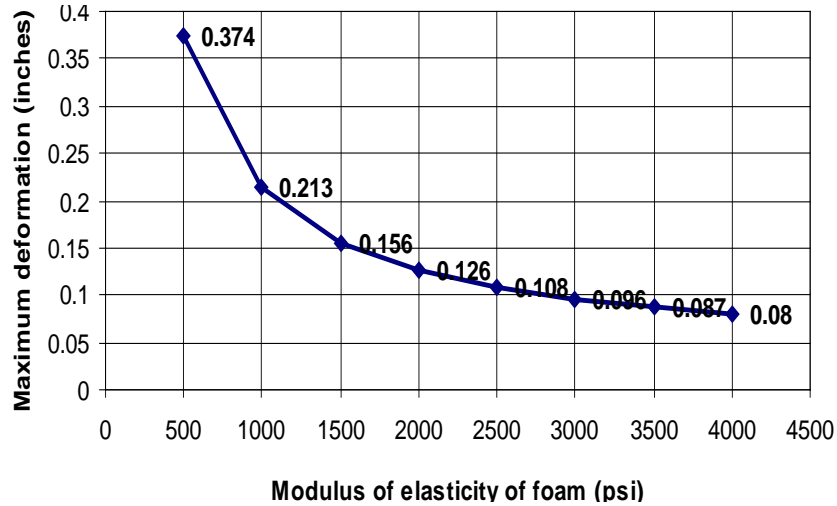
Figure 3.21 Maximum deformation of panel vs. modulus of elasticity of foam (24 Gage)
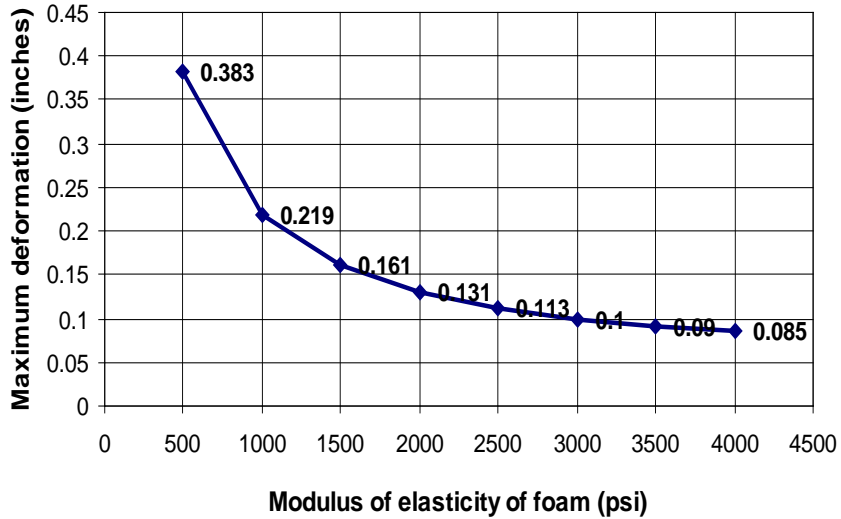
Figure 3.22 Maximum deformation of panel vs. modulus of elasticity of foam (25 Gage)
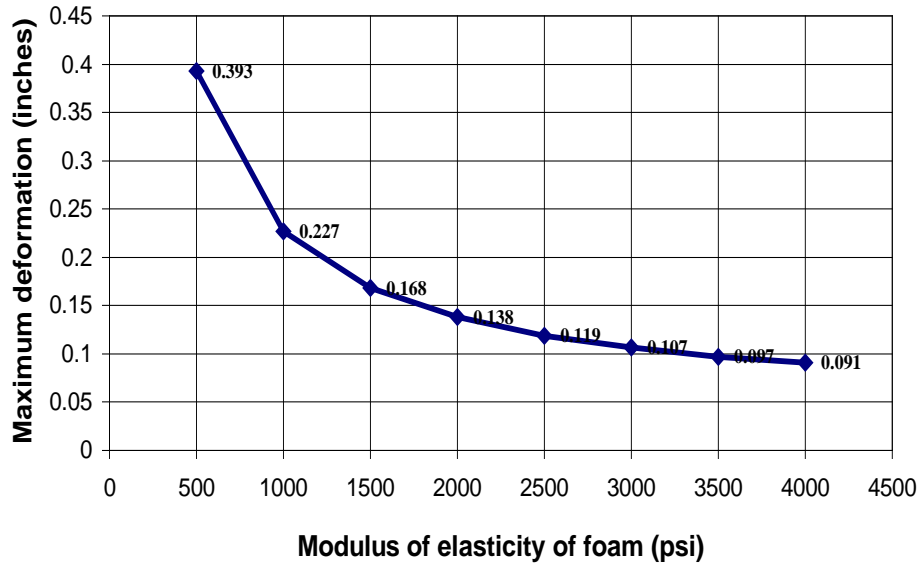
Figure 3.23 Maximum deformation of panel vs. modulus of elasticity of foam (26 Gage)

3.4 Load Capability of the Basic Sandwich Panel

The load capabilities of the panel were determined from the following factored combinations:

$$1.2D+1.6L+0.5(L_r \text{ or } S \text{ or } R) \qquad (1)$$

$$1.2D+1.6(L_r \text{ or } S \text{ or } R)+(0.5L \text{ or } 0.8W) \qquad (2)$$

$$1.2D+1.6W+0.5L+0.5(L_r \text{ or } S \text{ or } R) \qquad (3)$$

Where D= dead load; L = live load due to occupancy; Lr = roof live load; S = snow load; R = nominal load due to initial rainwater or ice exclusive of the ponding contribution; and W = wind load

The initial values of the above loads are: L =12.340 psi; Lr = 4.930 psi; S = 4.930 psi; R = 7.400 psi; and W = 0.136 psi

3.4.1 Vertical load capability of the basic panels

Vertical load capability of the panels was determined based on load combination (2) - 1.2D+1.6R+0.8W. The dead load and wind load remained unchanged in the analysis; the only

variable was the vertical rain load. The maximum vertical load was controlled by the allowable compressive stresses in the foam.

Table 3.3 Vertical load capability (Rain load) of the basic panel

Steel thickness	R(psi)	Stress in foam(psi)		Stress in steel (ksi)	
		Maximum positive stress (Tension)	Maximum negative stress (Compression)	Maximum positive stress (Tension)	Maximum negative stress (Compression)
24 Gage	**40.58**	5.136	**50.990**	5.98	9.43
25 Gage	**40.54**	5.037	**50.988**	6.027	9.22
26 Gage	**40.51**	4.943	**50.997**	6.037	9.349

Note: 1. $\phi F_{foam} = 0.85 \times 60 = 51 psi$; $\phi F_{steel} = 0.85 \times 33 = 28.05 ksi$
 2. Dead load and wind load are constants.

3.4.2 Wind load capability of the basic panels

Wind load capability of the panels was determined based on load combination (3) - 1.2D+1.6W+0.5L+0.5S. In this analysis, the dead load, live load and roof live load were constant. The only variable was wind load. The wind load capacity was controlled by the allowable steel tensile stress.

Table 3.4 Horizontal load capability (Wind load) of the basic panel

Steel thickness	W(psi)	Stress in foam(psi)		Stress in steel(ksi)	
		Maximum positive stress (Tension)	Maximum negative stress (Compression)	Maximum positive stress (Tension)	Maximum negative stress (Compression)
24 Gage	**0.1919**	4.142	6.784	**28.046**	8.262
25 Gage	**0.182**	4.126	6.788	**28.050**	8.544
26 Gage	**0.1711**	4.098	6.792	**28.048**	8.916

Note: 1. $\phi F_{foam} = 0.85 \times 60 = 51 psi$; $\phi F_{steel} = 0.85 \times 33 = 28.05 ksi$
 2. Dead load, live load and snow load are constants.

3.4.3 Deflection capability of the basic panels

Deflection capability of the panels was determined based on service load combination

D+W+L+S (or Lr). Except for the wind load, all of the other loads were kept as constants. The

maximum deformation was limited to a common accepted requirement for buildings (AISC

LRFD Specifications). Under the maximum deformation, the tensile stress in steel facing was

very close to the allowable stress.

Table 3.5 Deformation vs. wind load (W) of the basic panel

Steel thickness	W (psi)	Maximum deformation (inches)	Stress in foam (psi)		Stress in steel (ksi)	
			Maximum positive stress (Tension)	Maximum negative stress (Compression)	Maximum positive stress (Tension)	Maximum negative stress (Compression)
24 Gage	0.286	**0.450**	3.825	13.566	25.462	8.269
25 Gage	0.278	**0.449**	3.901	13.576	26.035	8.797
26 Gage	0.268	**0.449**	3.968	13.587	26.655	9.458

Note: 1. $\phi F_{foam} = 0.85 \times 60 = 51 psi$; $\phi F_{steel} = 0.85 \times 33 = 28.05 ksi$
  2. Dead load, live load and snow load are constants.
  3. The limitation of panel deformation was L/240=0.45 inch.

CHAPTER 4

MODELING AND ANALYSIS OF C-SHAPE COLUMNS

Three System columns of various cross-sections were studied for column performance. The three sections were C-shape profile, Delta-shape and original columns. In the Delta-shape column, both welded and non-welded cross sections were considered in the analysis. There were two sizes of the C-shape profiles – 2×4 channel (3.5 inch web) and 2×6 channel (5.5 inch web). In addition, various steel facing gages for all profiles were considered as described in chapter 2. This chapter presents the study on C-shape profiles.

4.1 Description of Input and Modeling of the C-shape Profiles

4.1.1 Dimensions and modeling of the C-shape profiles

(a) 2×4   (b) 2×6
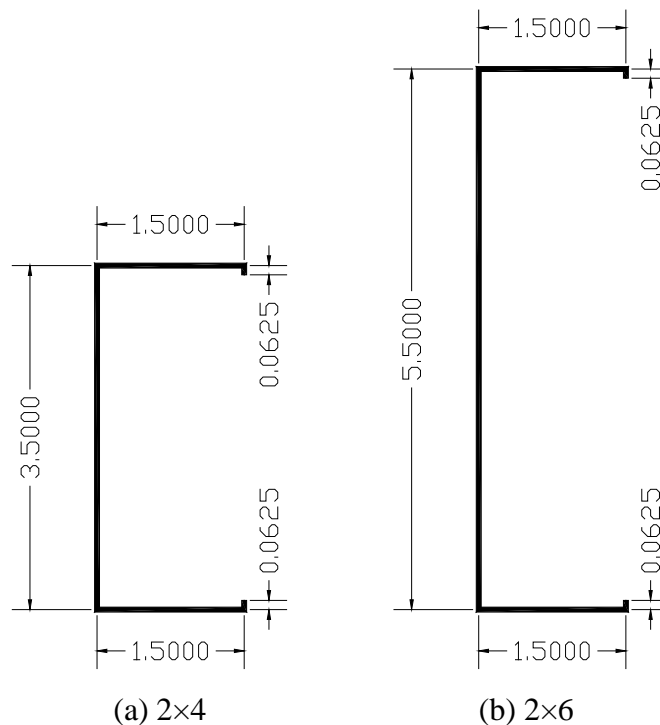
Figure 4.1 Cross-section of C-shape profile (unit: inches)

(a) Column with 2X4 C-shape

(b) Column with 2X6 C-shape
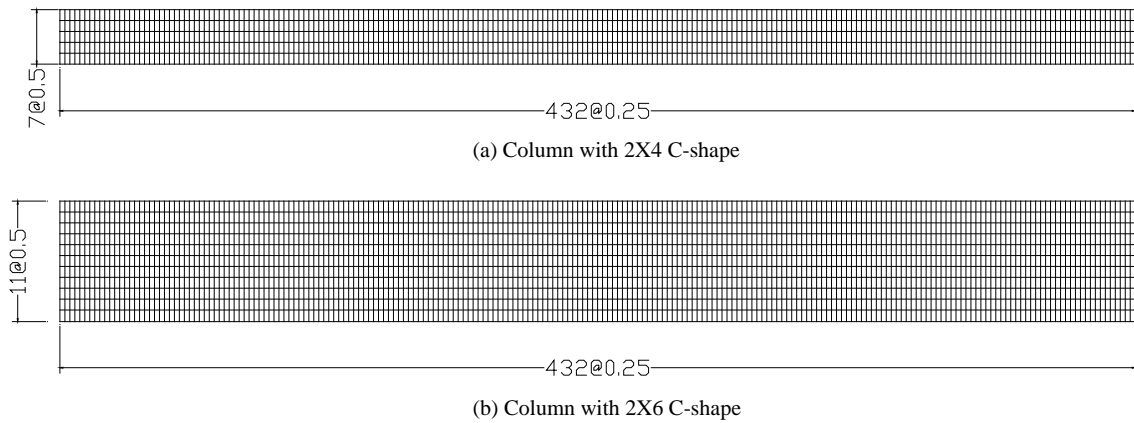
Figure 4.2 Modeling of C-shape profile

4.1.2 Finite element model of column with C-shape Profile

Shell elements (Shell181) were used to model the C-shape profile. Figure 4.3 shows the three-dimensional view of the C-shape column model. The model was restrained with pin supports at the top of the column and fix supports at the bottom except the rotation about Y direction, as shown in Figure. 4.4
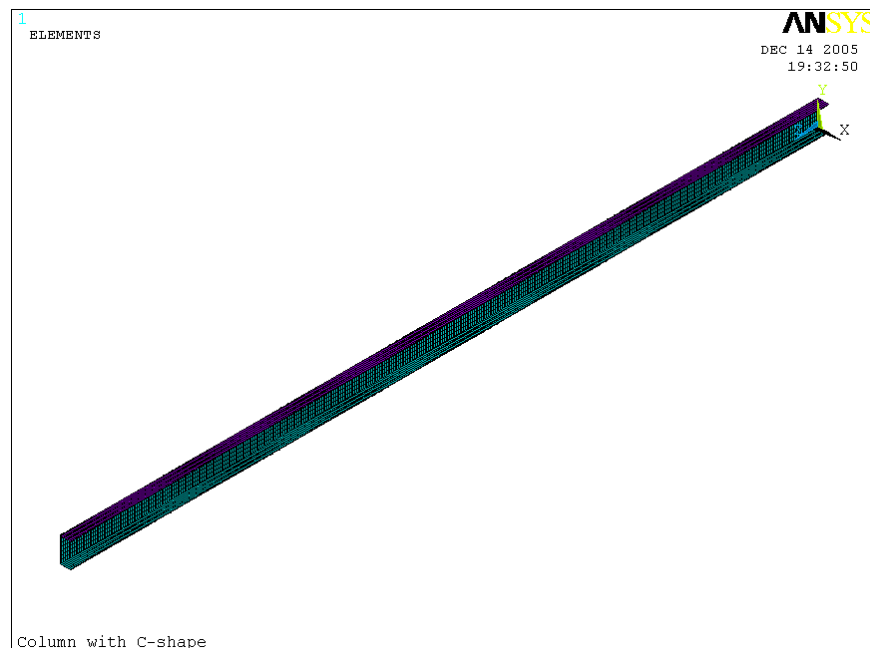
Figure 4.3 The 3-D C-shape profile model
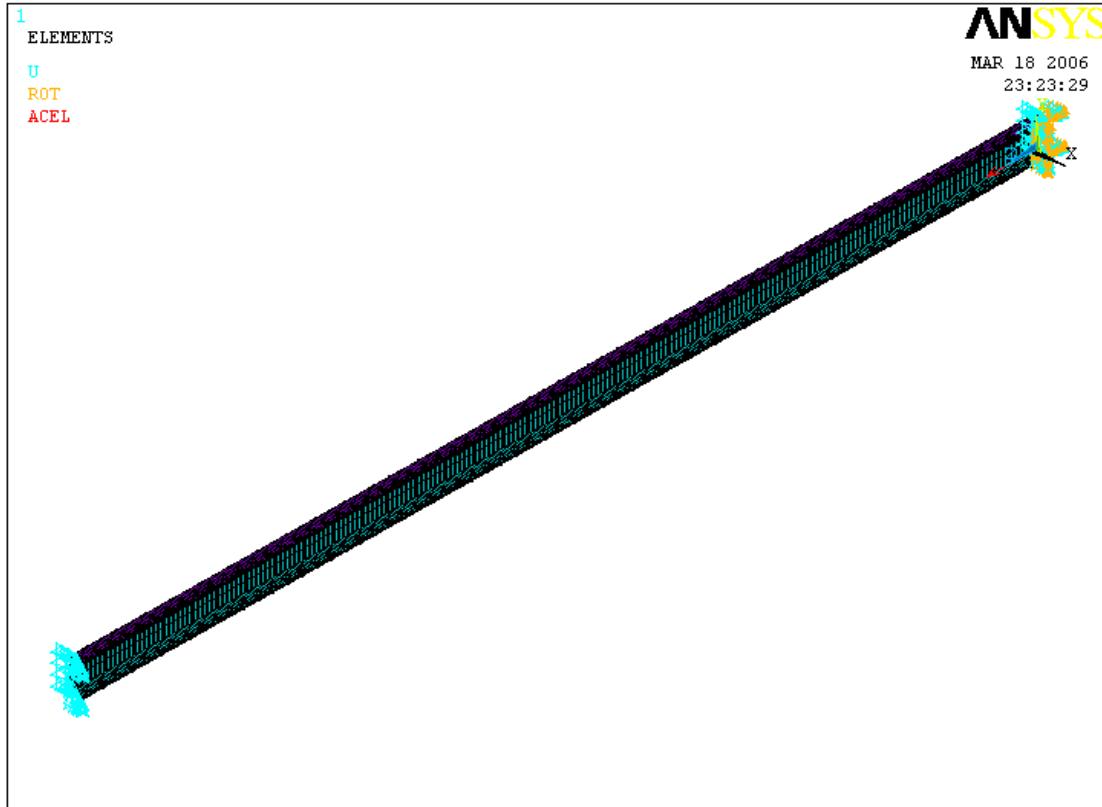
Figure 4.4 Model of the C-shape profile with end restrains

4.1.3 Loads

Table 4.1 Loading on the C-shape profiles

Gage #		Dead load (lbs)	Live load (lb/in)	Wind load(psi)	
				Case 1	Case 2
Gage 16	2×4	12.13	192.022	0.136	2.176
	2×6	15.80	147.495	0.136	2.176
Gage 20	2×4	7.28	192.022	----	---
	2×6	9.48	147.495	---	---

Note:
   1. Case 1 denotes columns carry the wind load based on the profile area only;
   2. Case 2 denotes columns carry the wind load based on 24 in wide tributary area.

Figure 4.5 was an example of the C-shape profile with loads. It was assumed that the profile resists wind load on its flange.
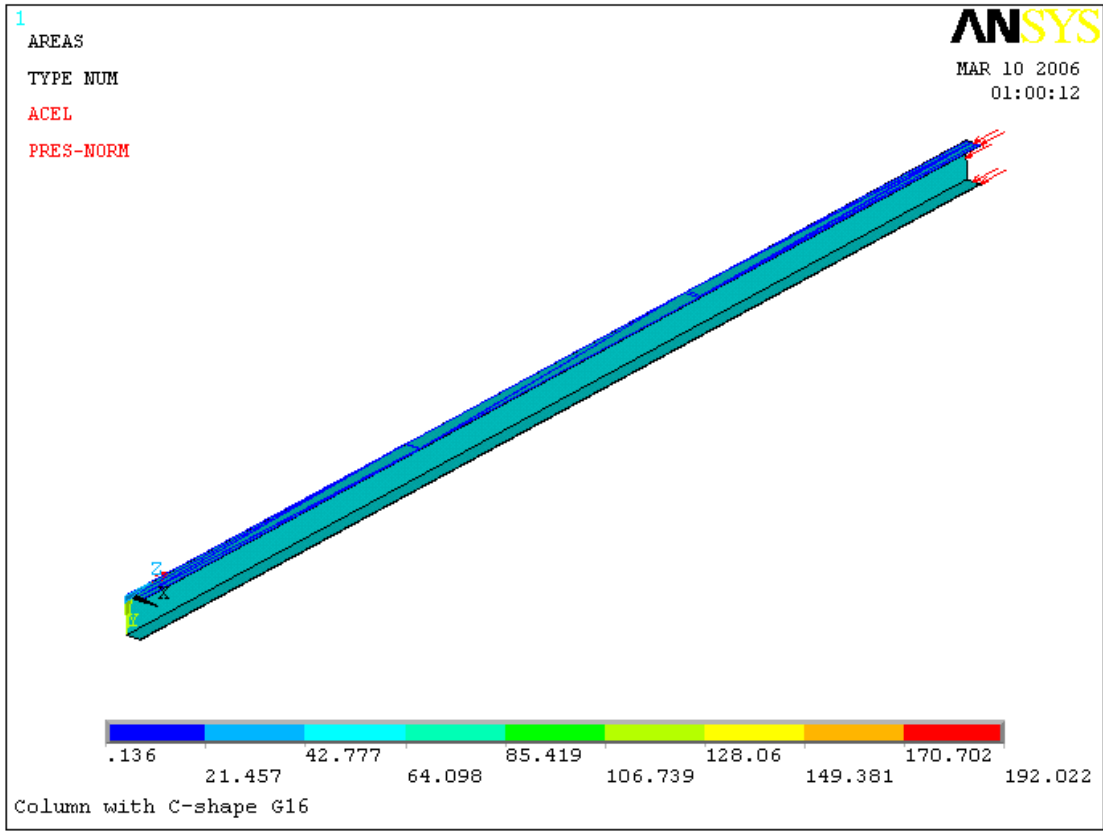
Figure 4.5 Loads on the C-shape profile

(Positive values denote the pressure act into the areas)

4.2 Analytical Results of the C-shape Profile

4.2.1 Deformation

Figures 4.6 through 4.9 show the deformation summations of C-shape profiles with 16 gage and 20 gage under the load Case 1. A large rotation was observed in the C-shape profiles when they were under loading. To show the rotation deformation, the column was cut at different longitudinal positions along the column. Figures 4.10 through 4.13 show the cross-sectional rotation of C-shape profiles with 16 gage and 20 gage under load Case 1. Similarly, Figures 4.14 and 4.15 show the deformation summations of the C-shape profiles with 16 gage under load Case 2 and Figures 4.16 through 4.17 shows the cross-sectional rotation of the columns under the same load case.

4.2.1.1 Deformation of C-shape profile under the load Case 1
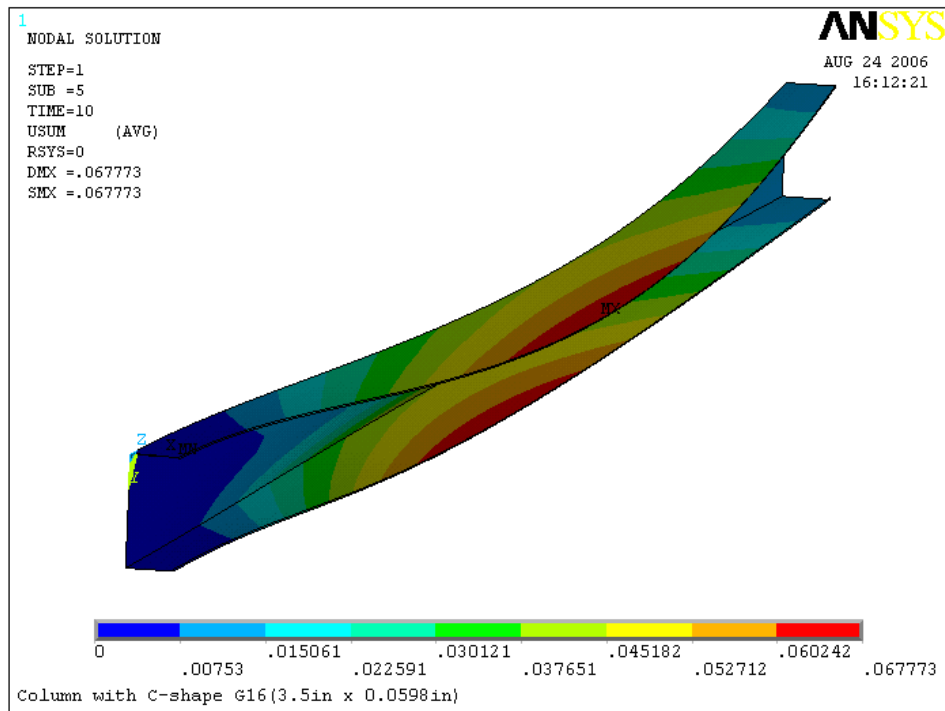
Figure 4.6 Deformation of C2×4 C-shape profile with 16 Gage (unit: inches)
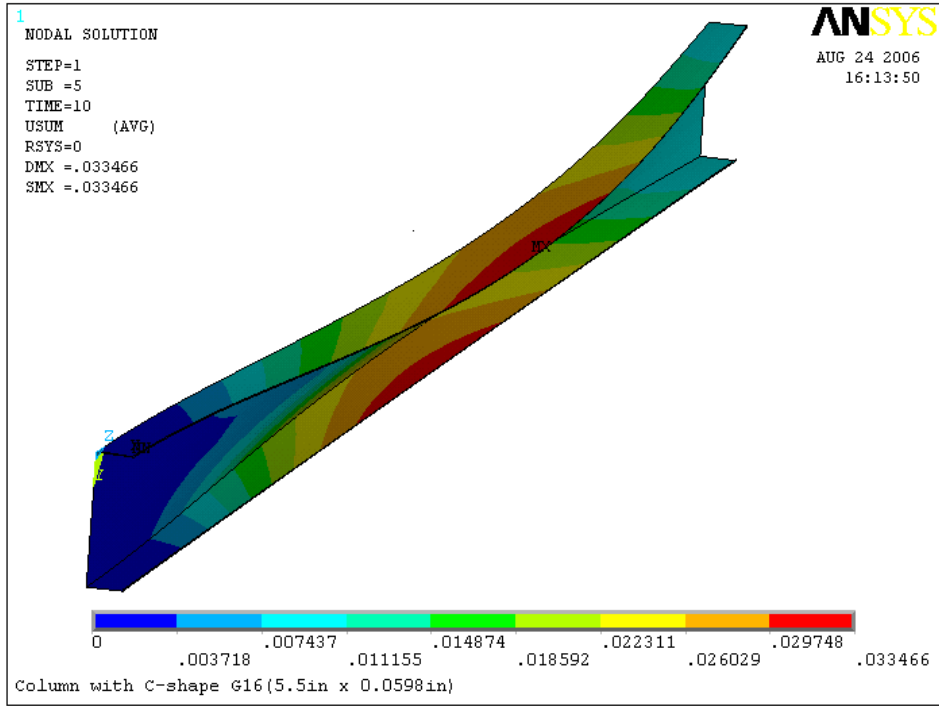
Figure 4.7 Deformation of C2×6 C-shape profile with 16 Gage (unit: inches)
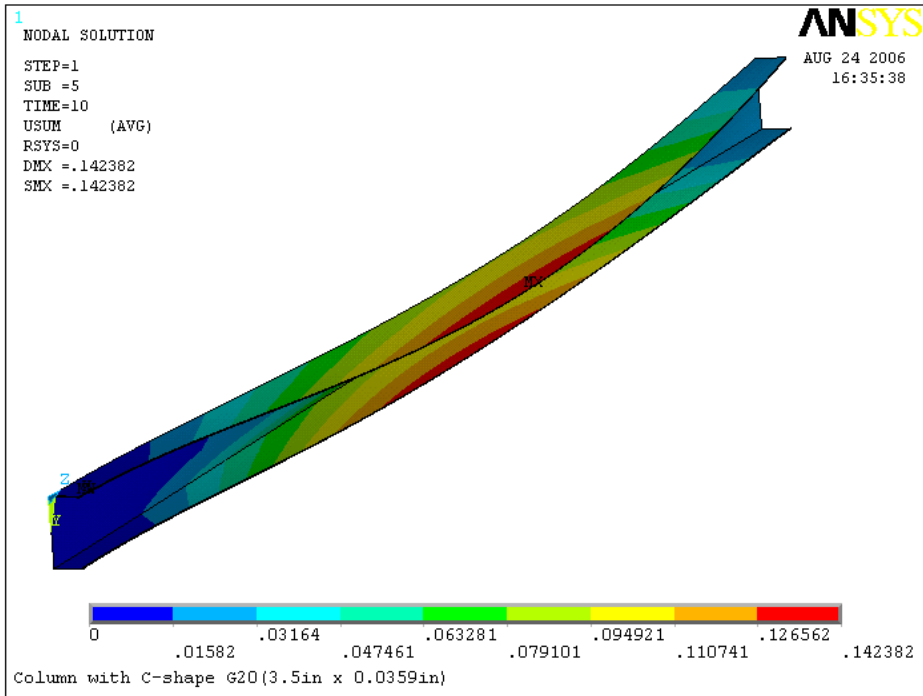
Figure 4.8 Deformation of C2×4 C-shape profile with 20 Gage (unit: inches)
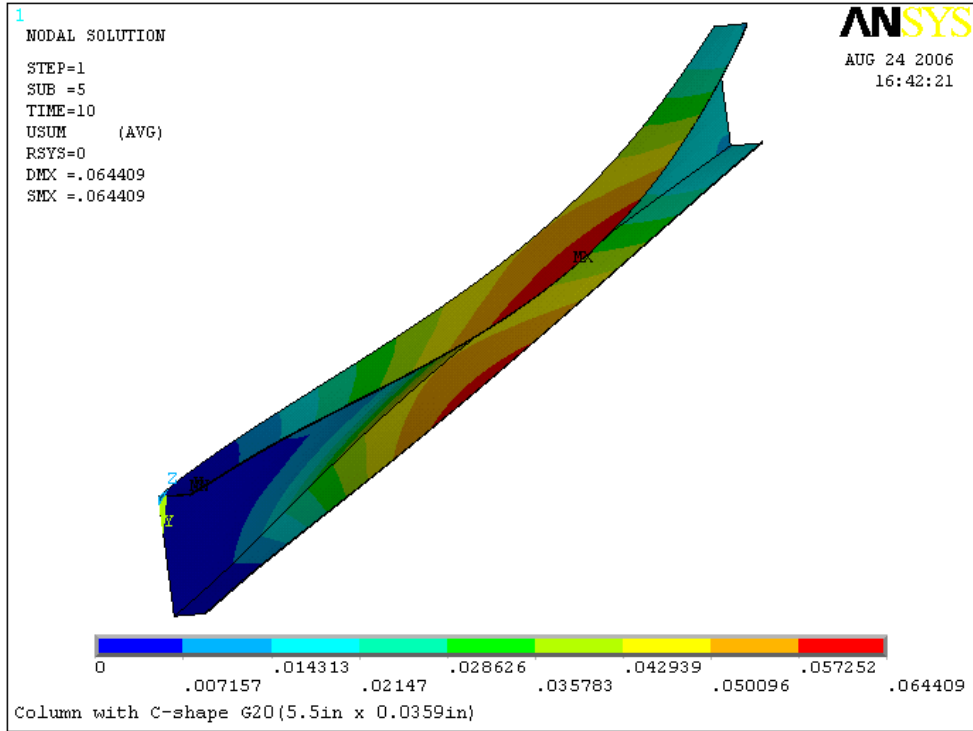
Figure 4.9 Deformation of C2×6 C-shape profile with 20 Gage (unit: inches)

4.2.1.2 Rotation of C-shape column under the load Case 1

(a) Cross-section view (Z=0.0 in.)

(b) Cross-section view (Z=20.0 in.)

(c) Cross-section view (Z=30.0 in.)

(d) Cross-section view (Z=54.0 in.)

(e) Cross-section view (Z=90.0 in.)

(f) Cross-section view (Z=108.0 in.)

Figure 4.10 Cross-section view of C-shape 16 Gage (C2×4)
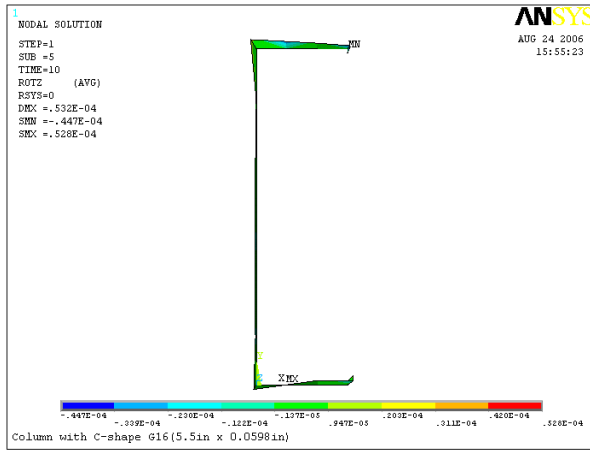
(a) Cross-section view (Z=0.0 in.) (b) Cross-section view (Z=20.0 in.) (c) Cross-section view (Z=30.0 in.)
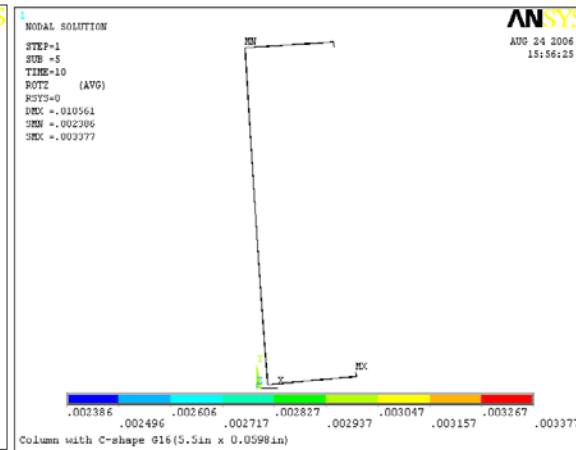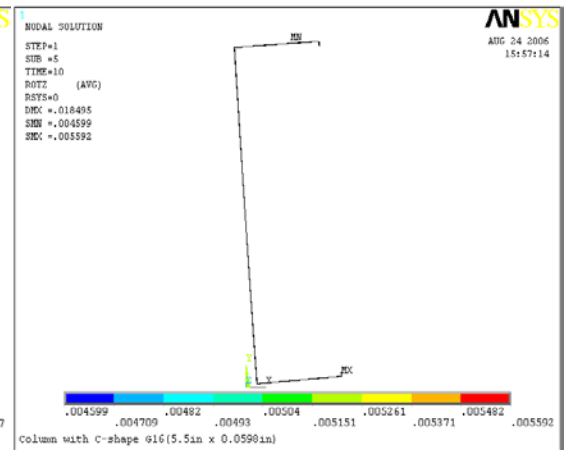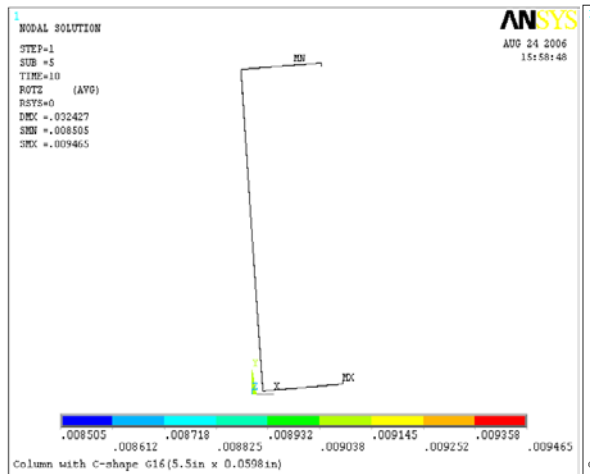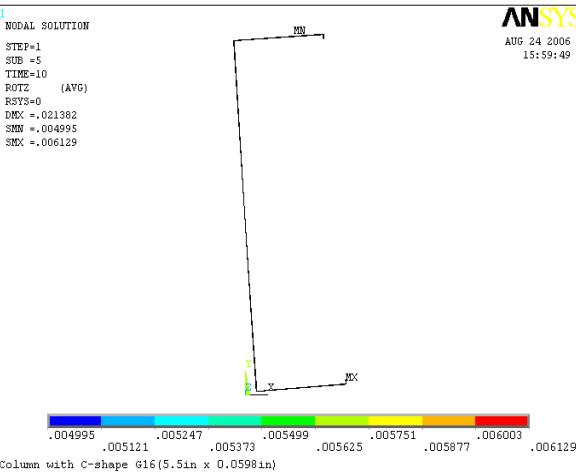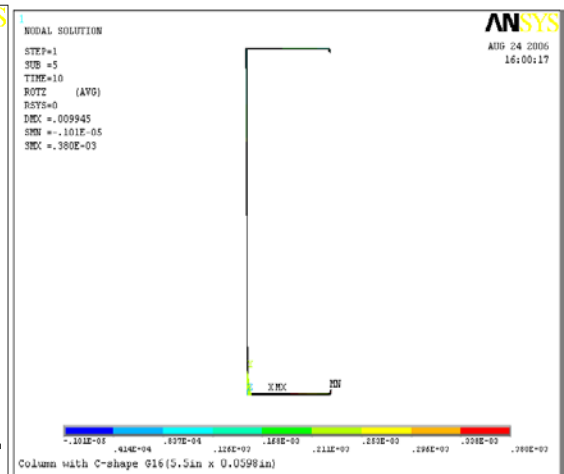
(d) Cross-section view (Z=54.0 in.) (e) Cross-section view (Z=90.0 in.) (f) Cross-section view (Z=108.0 in)

Figure 4.11 Cross-section view of C- shape 16 Gage (C2×6)
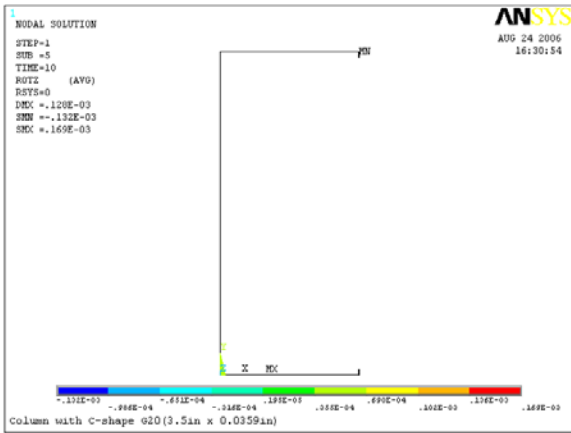
(a) Cross-section view (Z=0.0 in.) (b) Cross-section view (Z=20.0 in.) (c) Cross-section view (Z=30.0 in.)
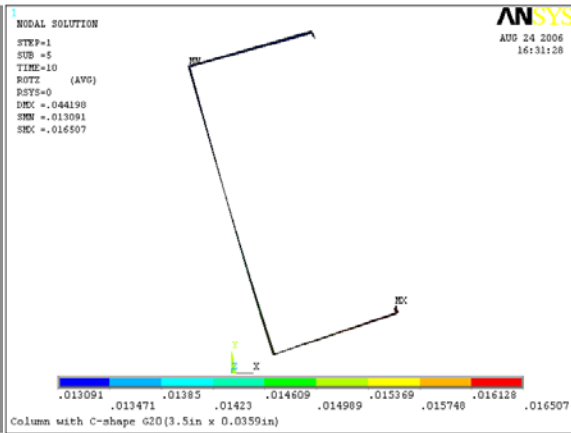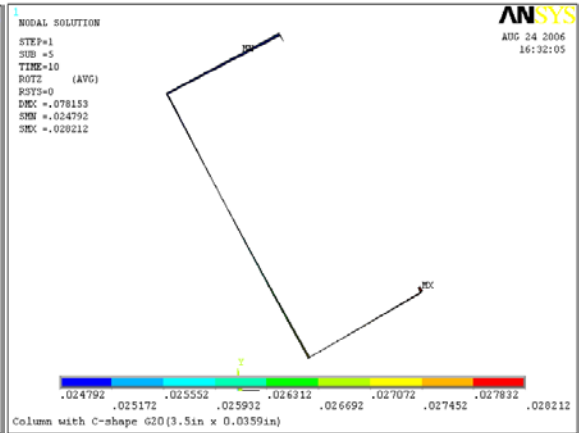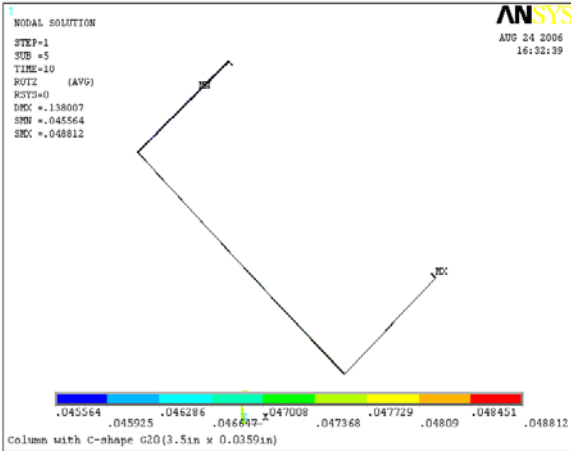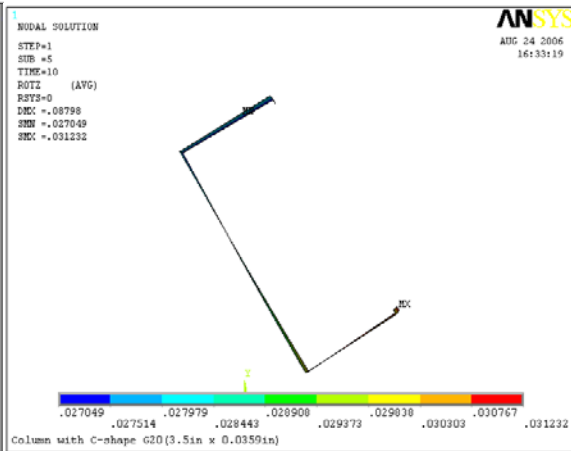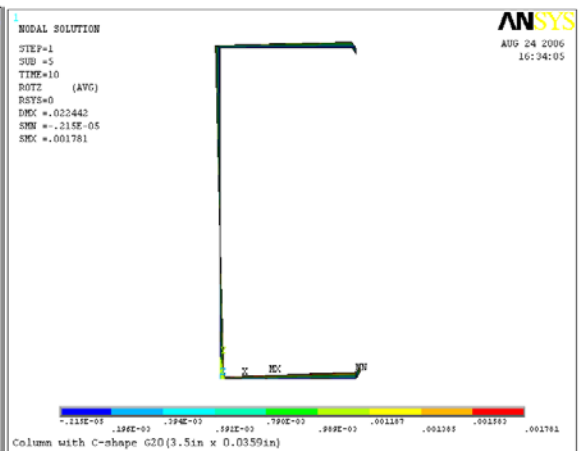
(d) Cross-section view (Z=54.0 in.) (e) Cross-section view (Z=90.0 in.) (f) Cross-section view (Z=108.0 in)

Figure 4.12 Cross-section view of C- shape 20 Gage (C2×4)
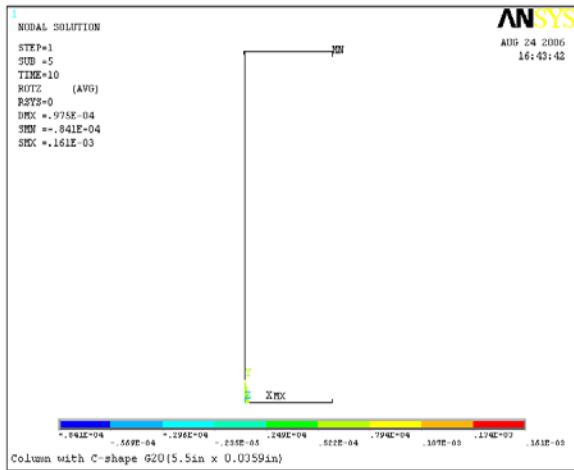
(a) Cross-section view (Z=0.0 in.)   (b) Cross-section view (Z=20.0 in.)   (c) Cross-section view (Z=30.0 in.)
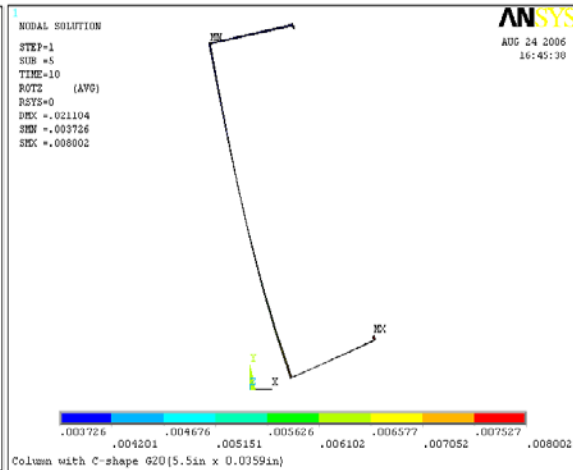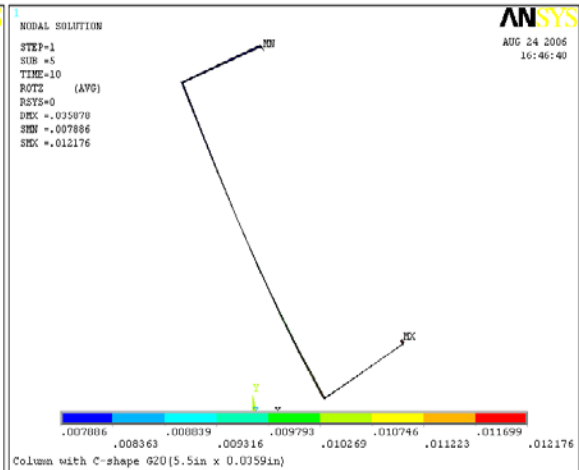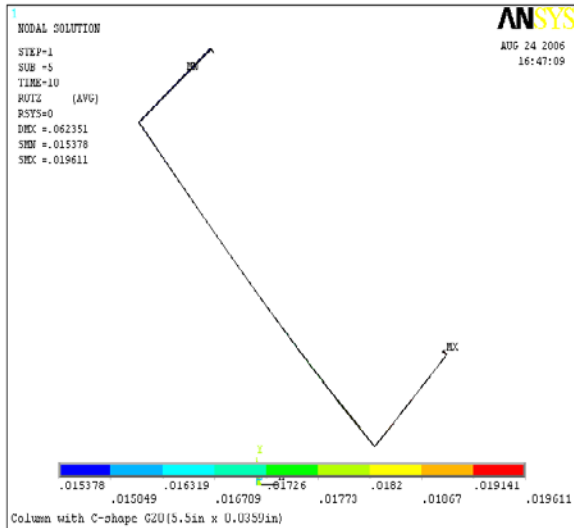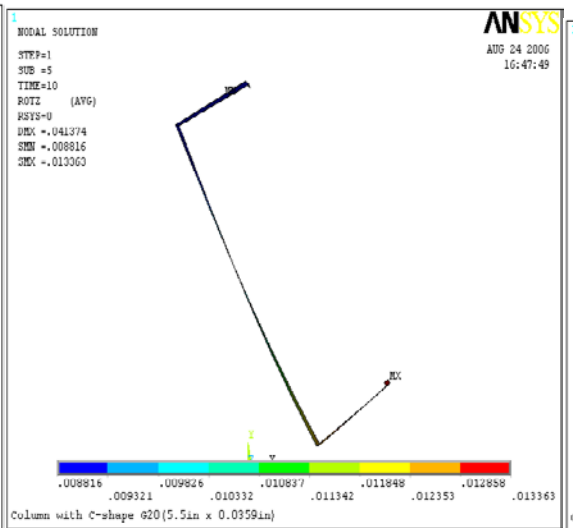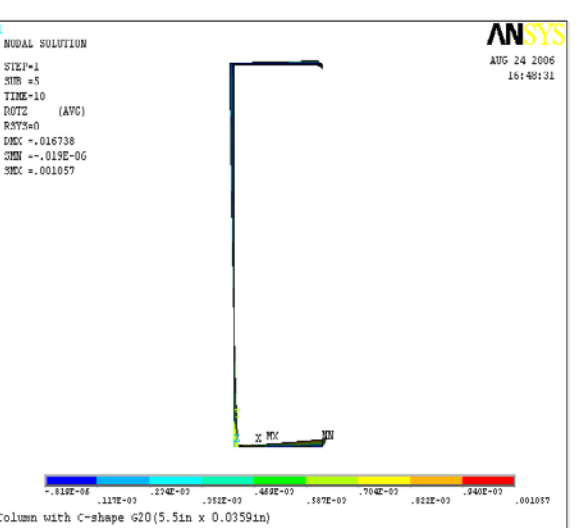
(d) Cross-section view (Z=54.0 in.)   (e) Cross-section view (Z=90.0 in.)   (f) Cross-section view (Z=108.0 in)

Figure 4.13 Cross-section view of C- shape 20 Gage (C2×6)

43

4.2.1.3 Deformation of C-shape column under the load Case 2
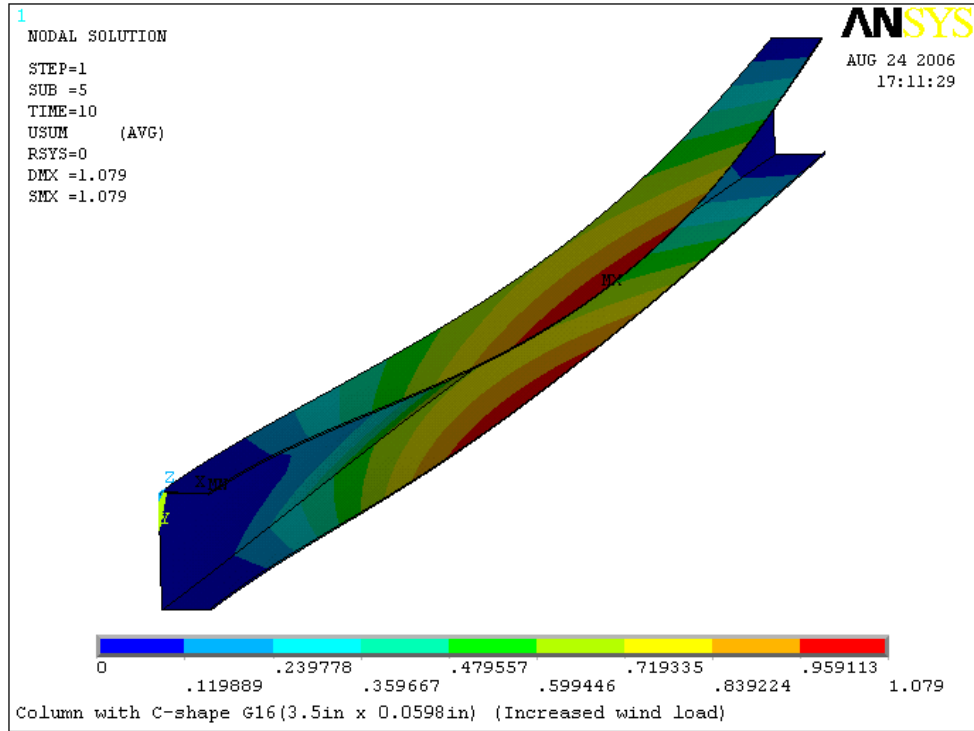
Figure 4.14 Deformation of C2×4 C-shape profile with 16 Gage (unit: inches)
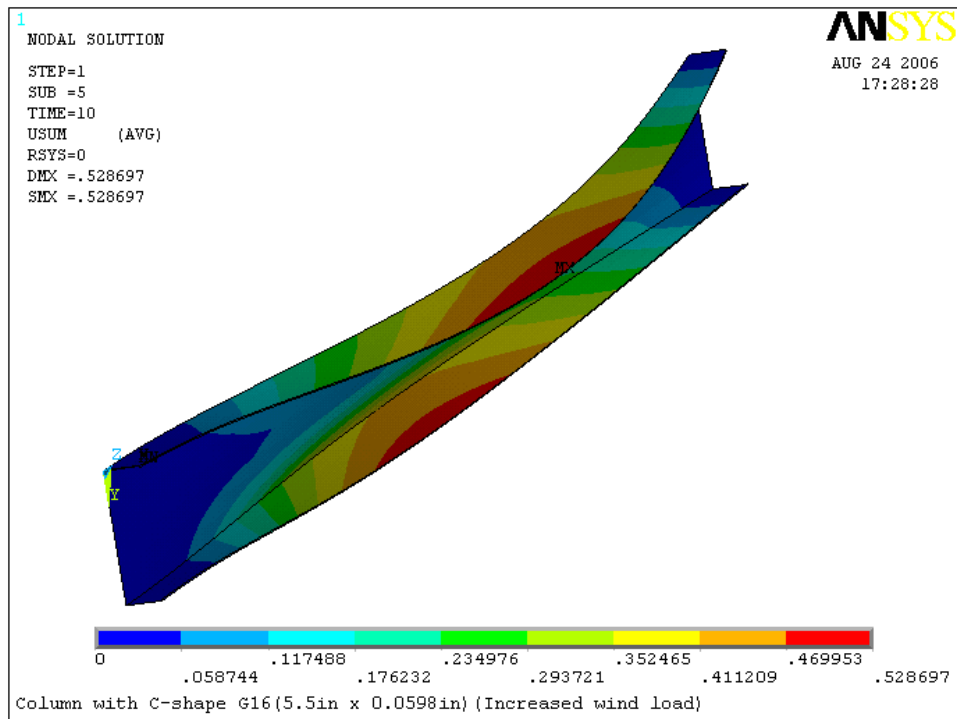
Figure 4.15 Deformation of C 2×6 C-shape profile with 16 Gage (unit: inches)

4.2.1.4 Rotation of C-shape column under the load Case 2

(a) Cross-section view (Z=0.0 in.)   (b) Cross-section view (Z=20.0 in.)   (c) Cross-section view (Z=30.0 in.)

(d) Cross-section view (Z=54.0 in.)   (e) Cross-section view (Z=90.0 in.)   (f) Cross-section view (Z=108.0 in)
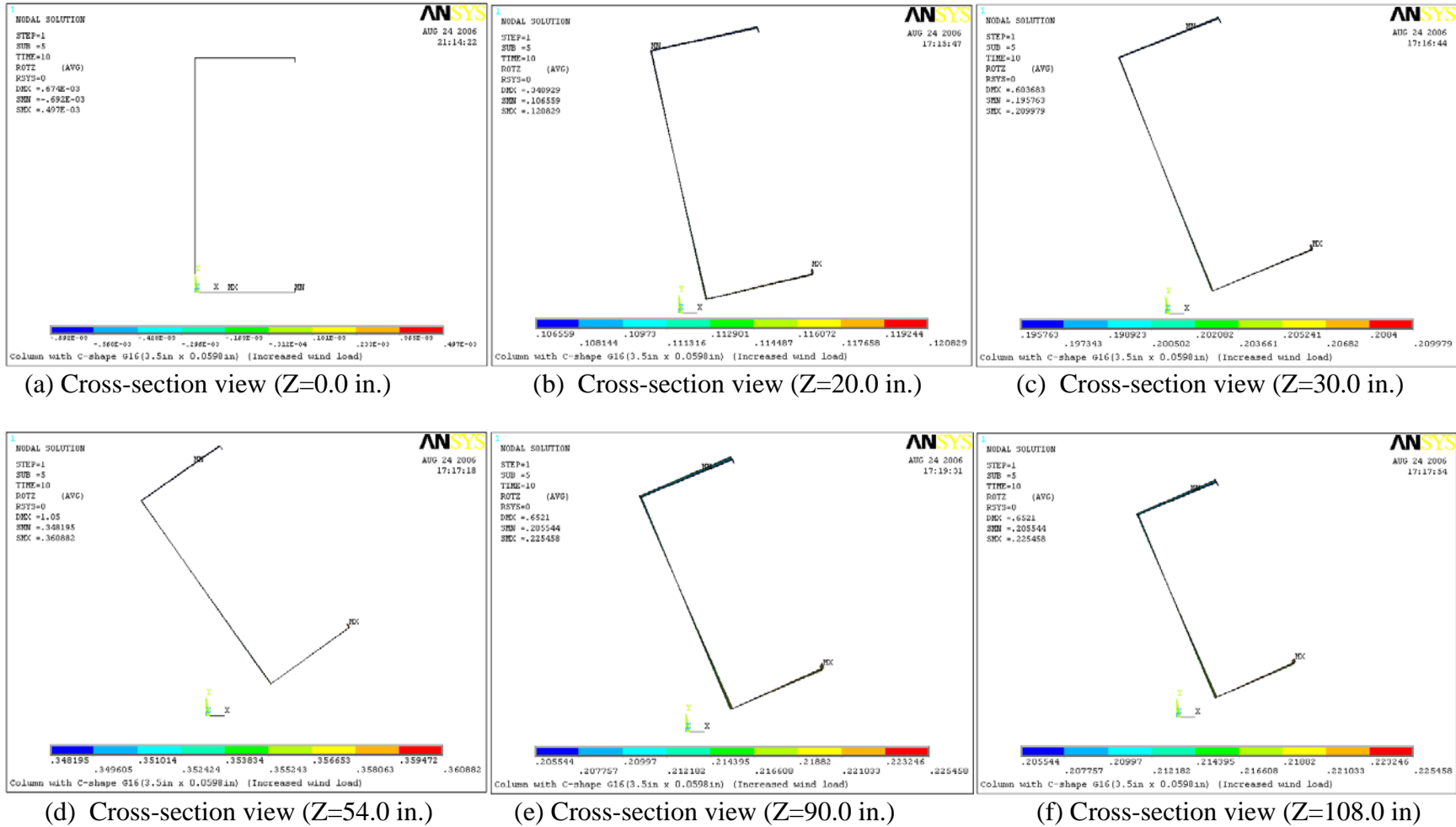
Figure 4.16 Cross-section view of C-shape 16 Gage (C2×4)
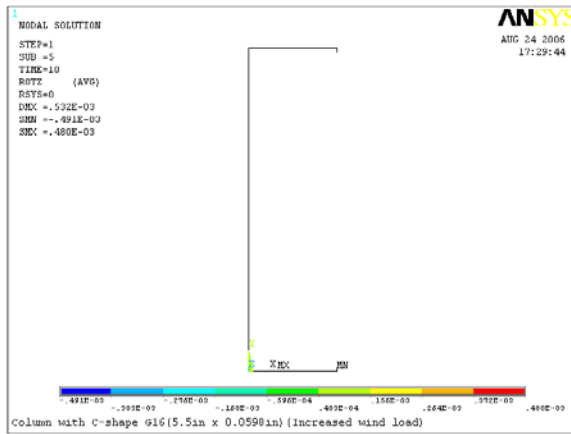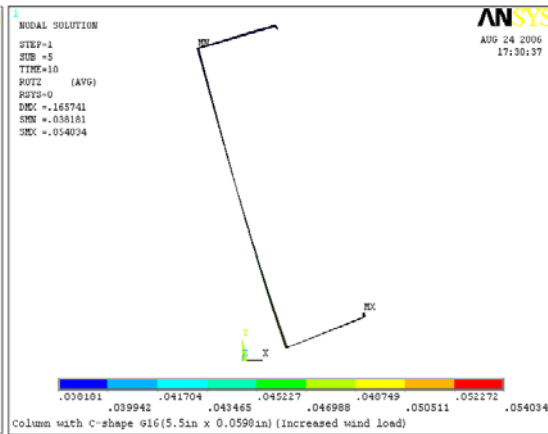
45

(a) Cross-section view (Z=0.0 in.)   (b) Cross-section view (Z=20.0 in.)   (c) Cross-section view (Z=30.0 in.)
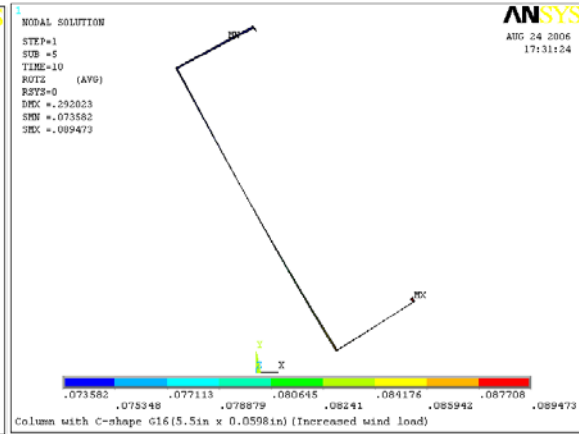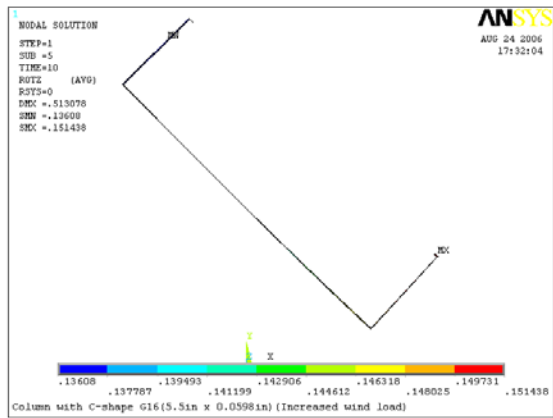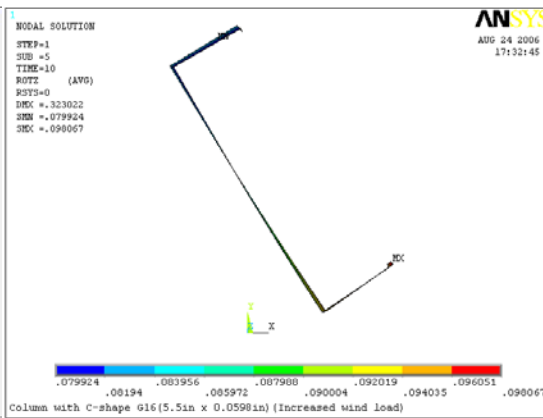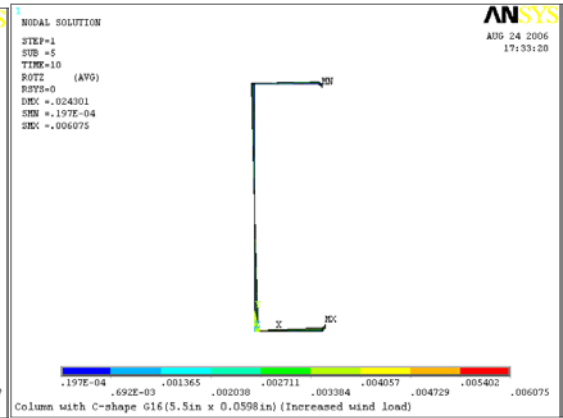
(d) Cross-section view (Z=54.0 in.)   (e) Cross-section view (Z=90.0 in.)   (f) Cross-section view (Z=108.0 in)

Figure 4.17 Cross-section view of C- shape 16 Gage (C2×6)

It was observed that the maximum deformation of the C-shape profiles increased as the thickness of the steel decreased. For example, the maximum deformation of the 2×4 C-shape profile increased from 0.0678 in to 0.142 in when steel thickness changed from 16 gage to 2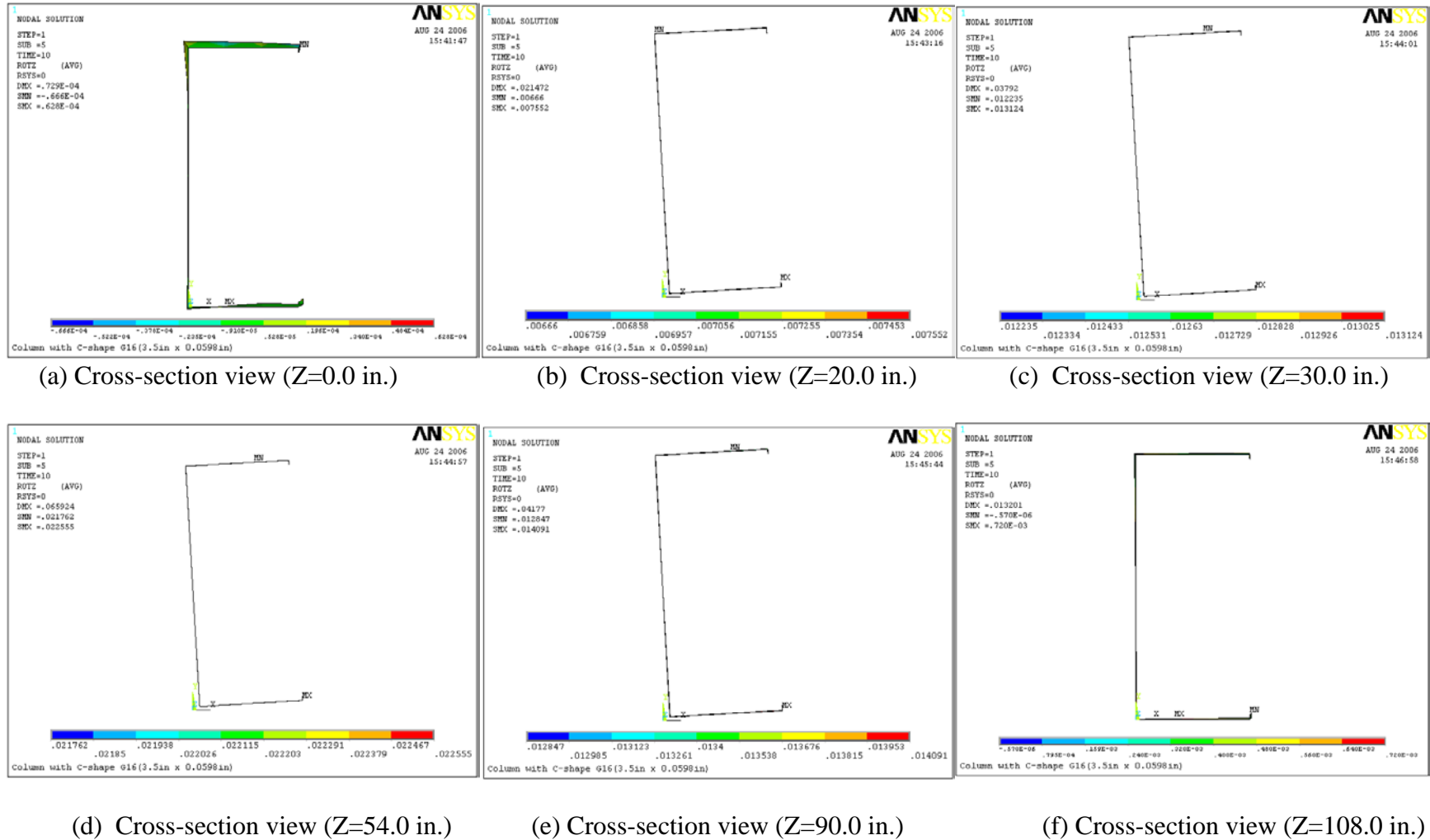0 gage. For the same steel thickness, the maximum deformation of the C-shape profiles decreased as the height of the channel-web increased. For example, the maximum deformation of the C-shape profile with 16 gage thickness varied from 0.0678 in. to 0.033 in. when the height of the web increased from 3.5 in. to 5.5 in.

The maximum rotations of the C-shape profiles follow the same trend as the maximum deformation: increased as the thickness of the steel decreased and decreased as height of the web increased. For example, the maximum rotation of the 2×6 C-shape profile varied from 0.0097 rad to 0.0202 rad when the steel thickness changed from 16 gage to 20 gage; For the same thickness of the steel, the maximum rotation of the C-shape profile made of 20 gage steel decreased from 0.0503 rad to 0.0202 rad when the height of the web increased from 3.5 in. to 5.5 in.

4.2.2 Stresses of the C-shape profiles

Figures 4.18 through 4.25 show the stresses in longitudinal direction of the C-shape profiles made of 16 Gage and 20 Gage steel under the load Case 1. Figures 4.26 through 4.29 show the stresses in longitudinal direction of C-shape profile made of 16 Gage steel under the load Case 2. The figures present the stresses in the front side and back side of each profile with deformed shape.

4.2.2.1 Stresses in longitudinal direction of C-shape profile under the load Case 1
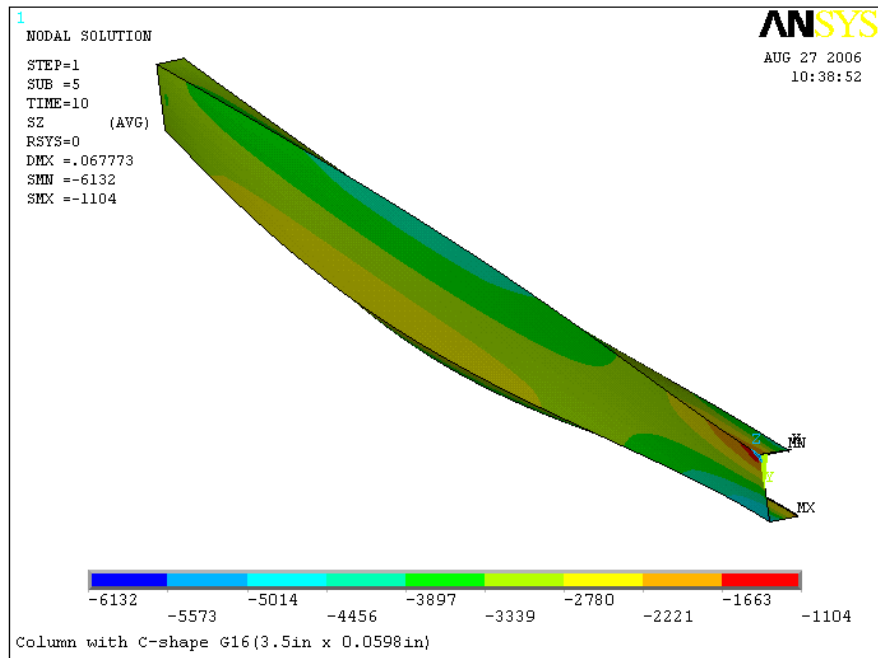
Figure 4.18 Stresses in the back side of C2×4 profile with 16 Gage (units: psi)
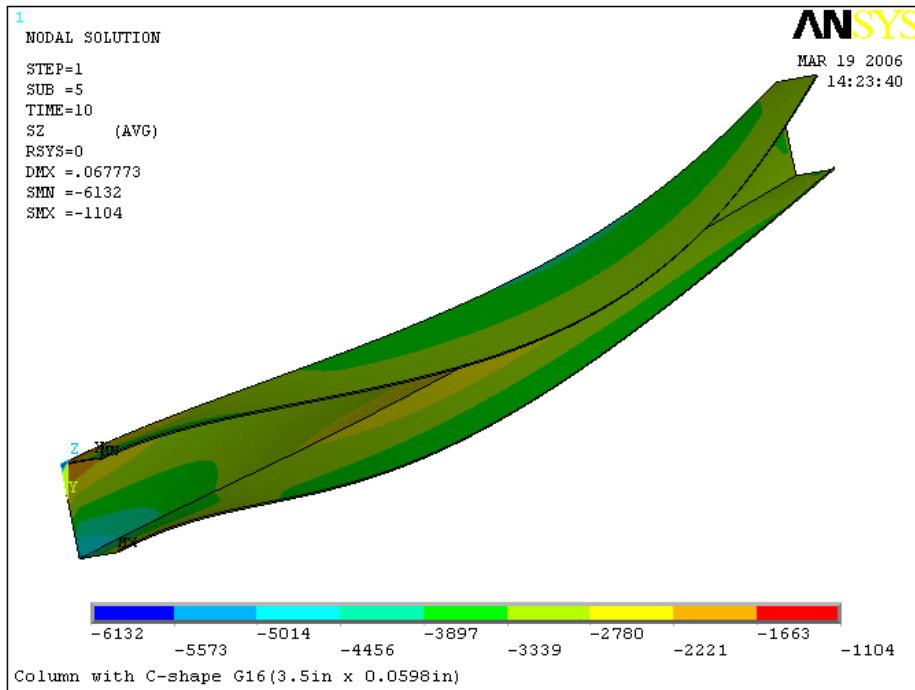
Figure 4.19 Stresses in the front side of C2×4 profile with 16 Gage (units: psi)
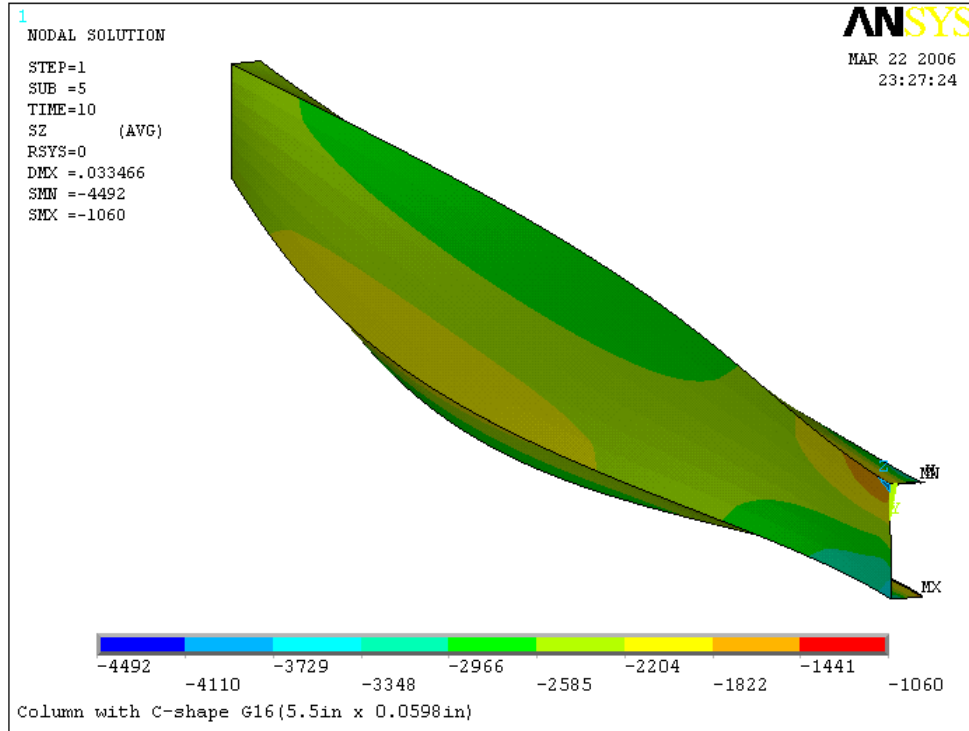
Figure 4.20 Stresses in the back side of C2×6 profile with 16 Gage (units: psi)
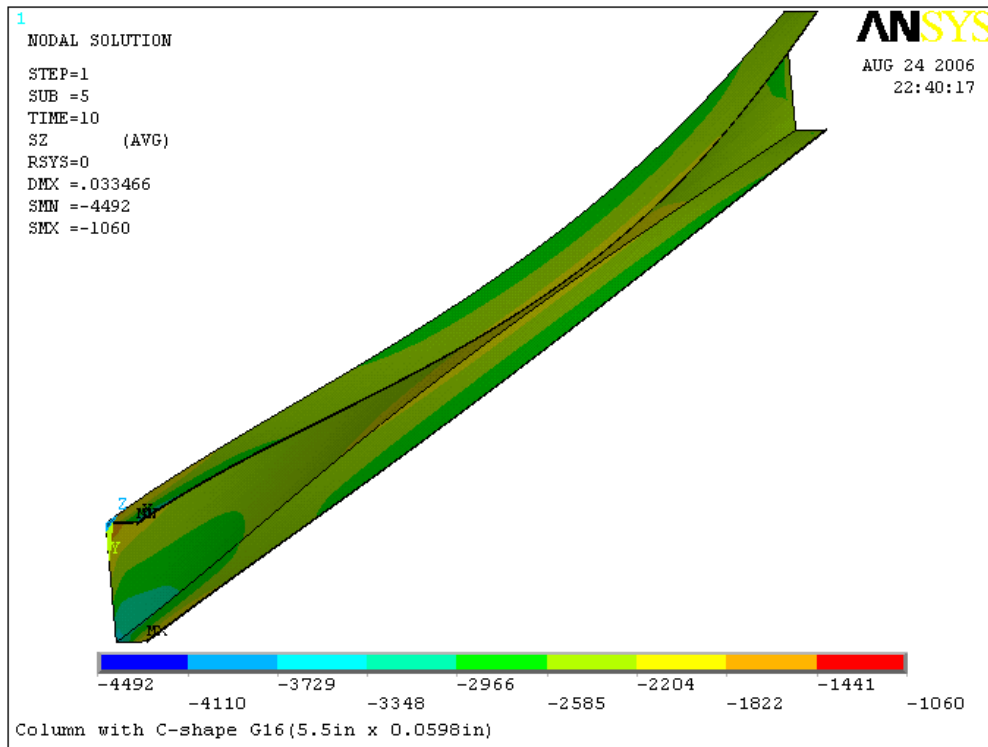
Figure 4.21 Stresses in the front side of C2×6 profile with 16 Gage (units: psi)
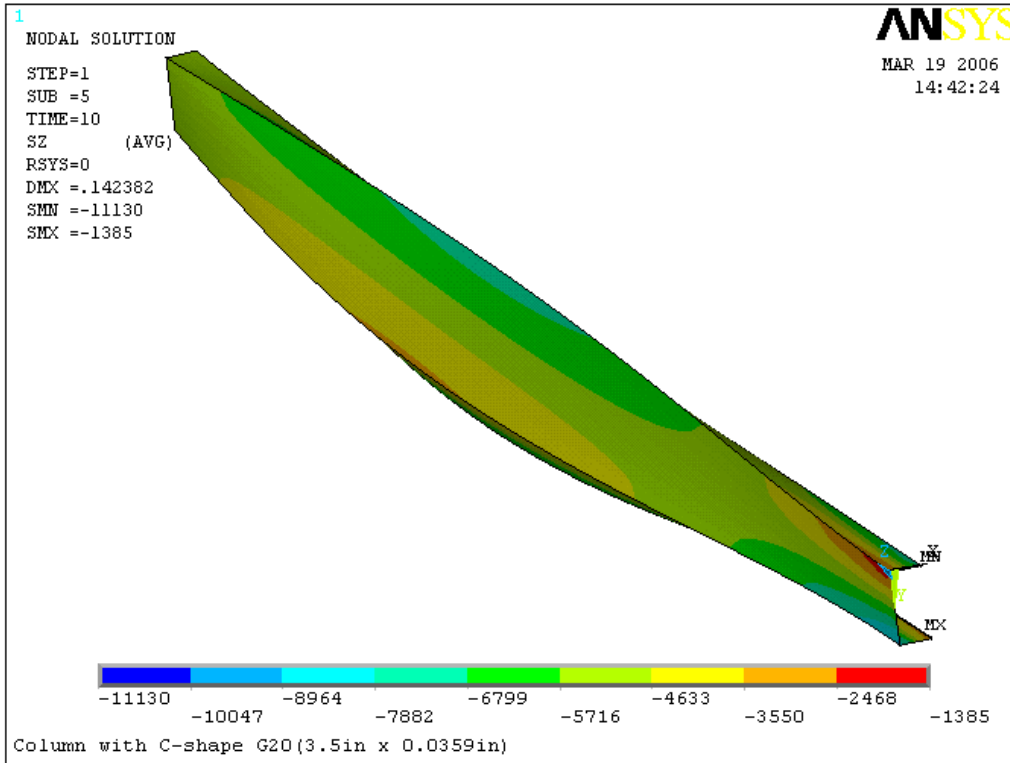
Figure 4.22 Stresses in the back side of C2×4 profile with 20 Gage (units: psi)
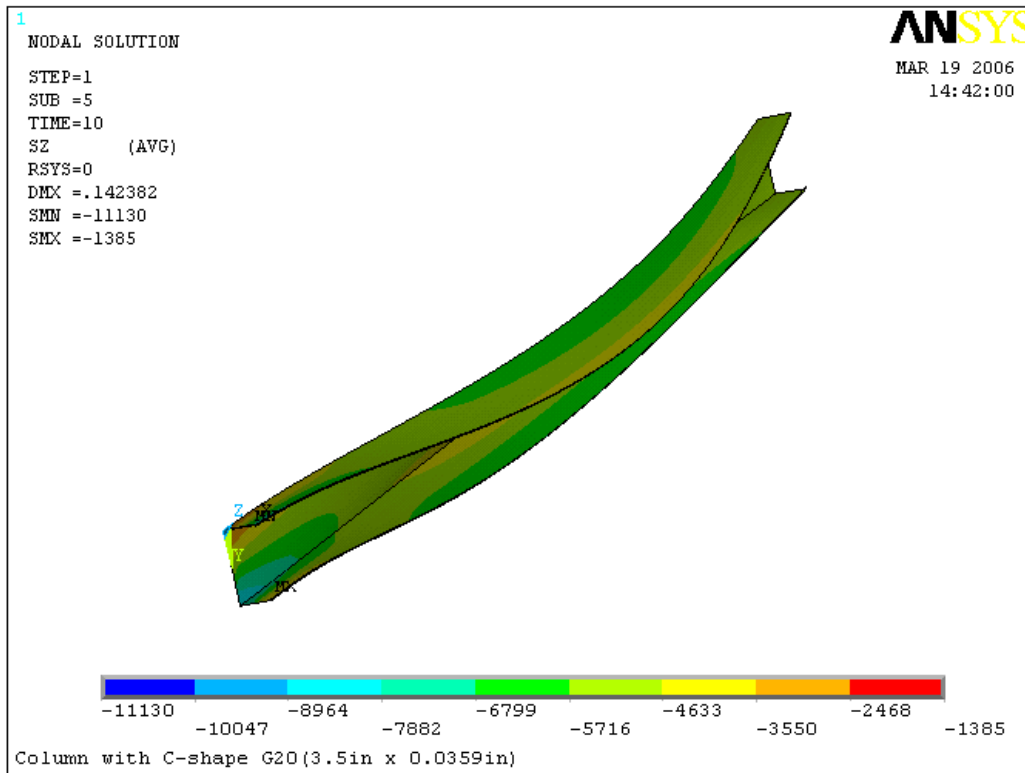
Figure 4.23 Stresses in the front side of C2×4 profile with 20 Gage (units: psi)

50
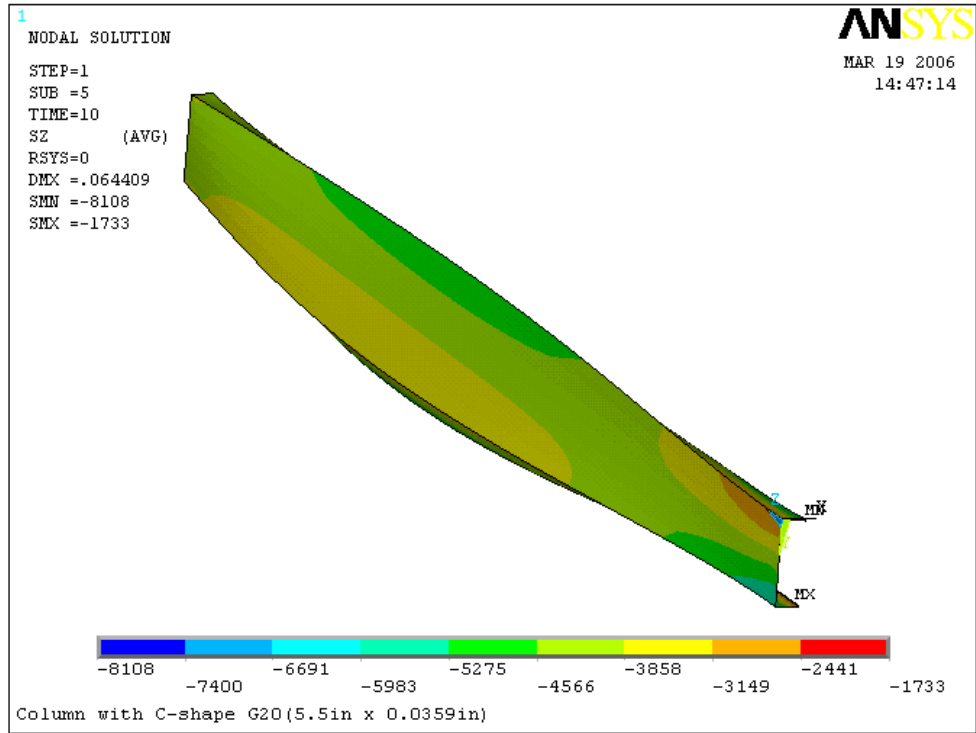
Figure 4.24 Stresses in the back side of C2×6 profile with 20 Gage (units: psi)
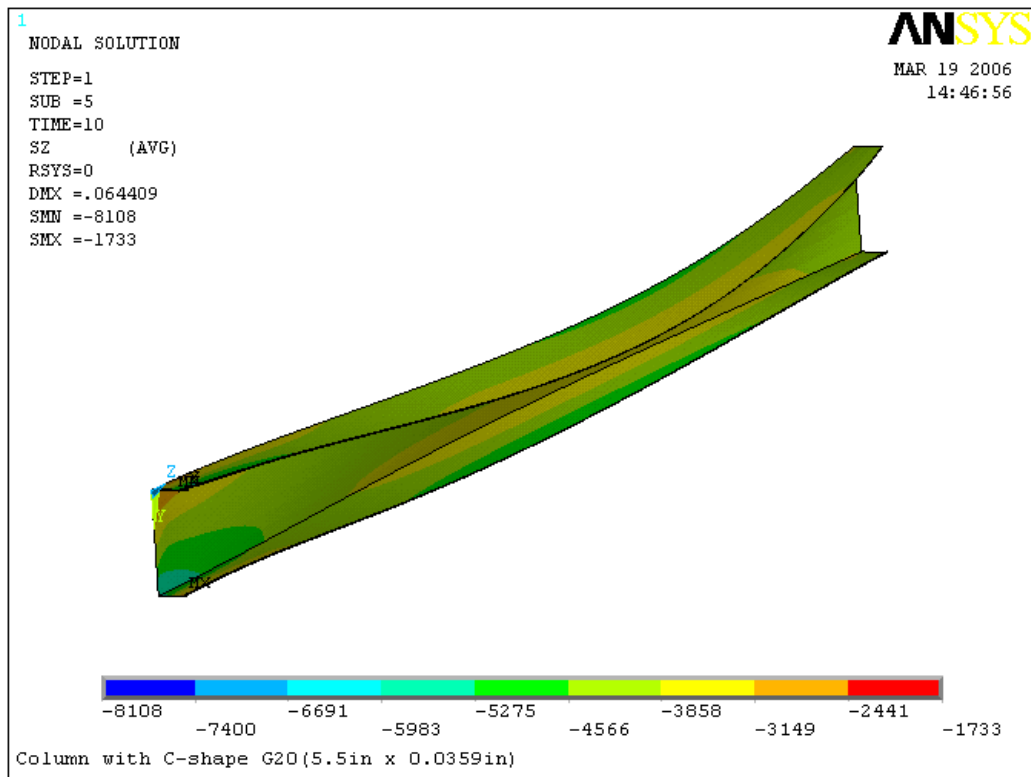
Figure 4.25 Stresses in the front side of C2×6 profile with 20 Gage (units: psi)

4.2.2.2 Stresses in longitudinal direction of C-shape profile under the load Case 2
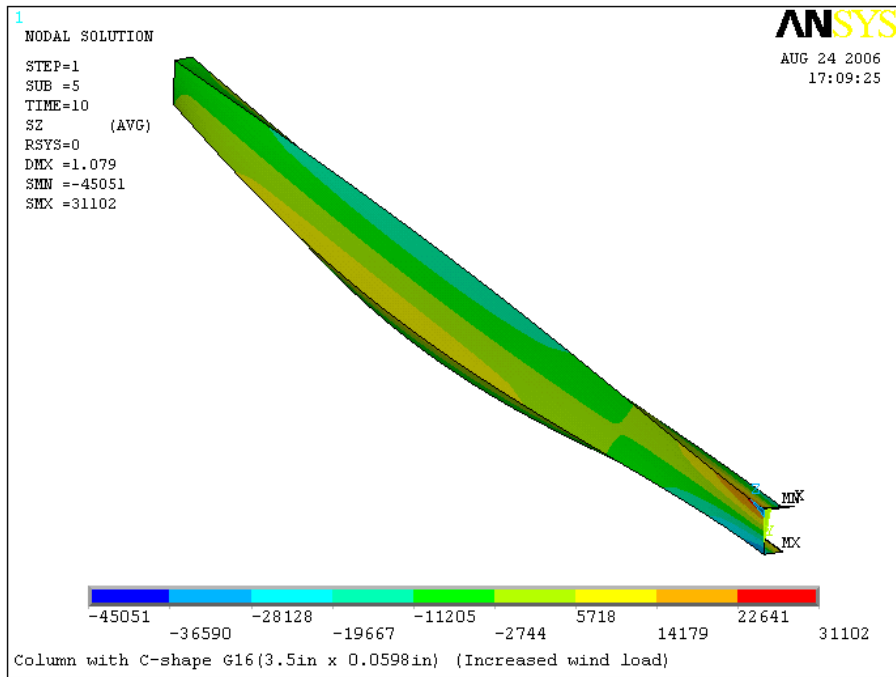
Figure 4.26 Stresses in the back side of C2×4 profile with 16 Gage (units: psi)
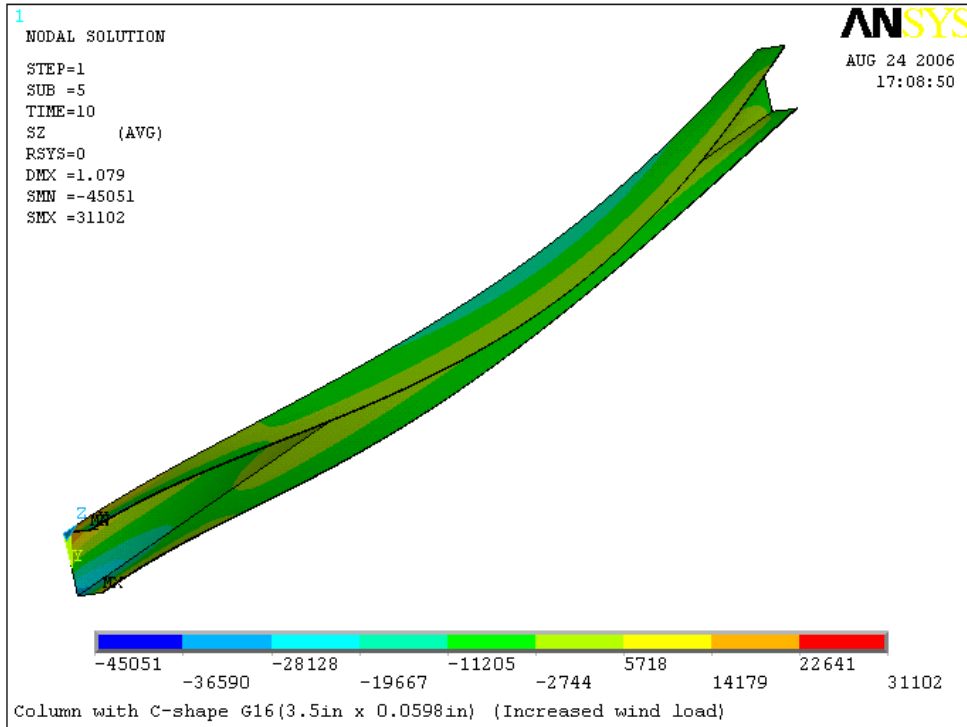
Figure 4.27 Stresses in the front side of C2×4 profile with 16 Gage (units: psi)
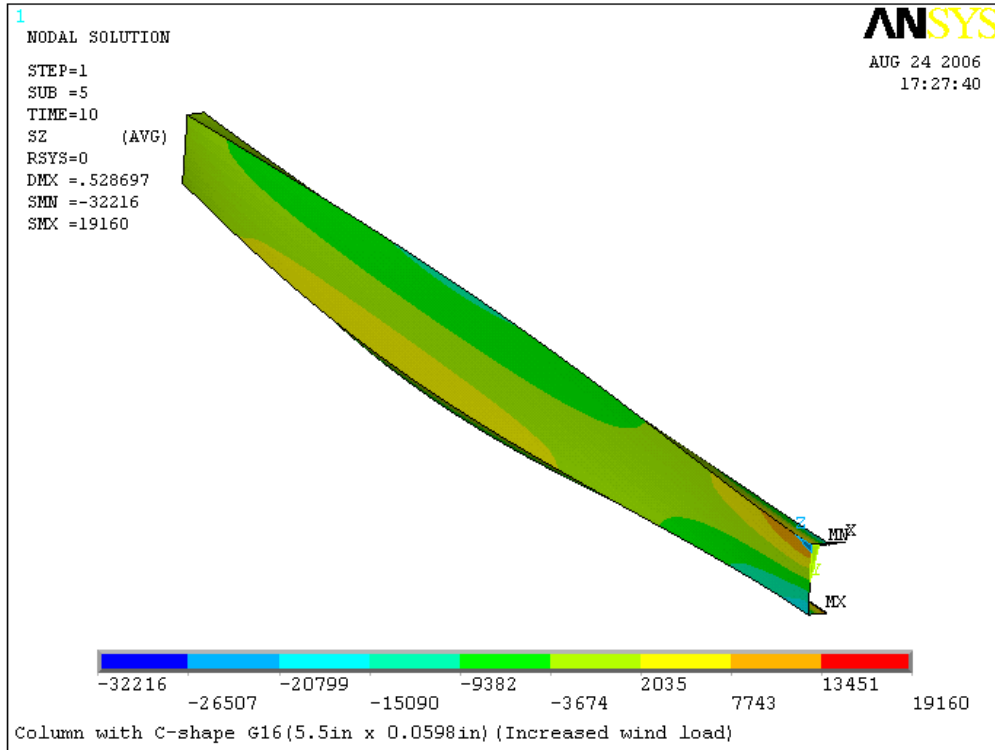
Figure 4.28 Stresses in the back side of C2×6 profile with 16 Gage (units: psi)
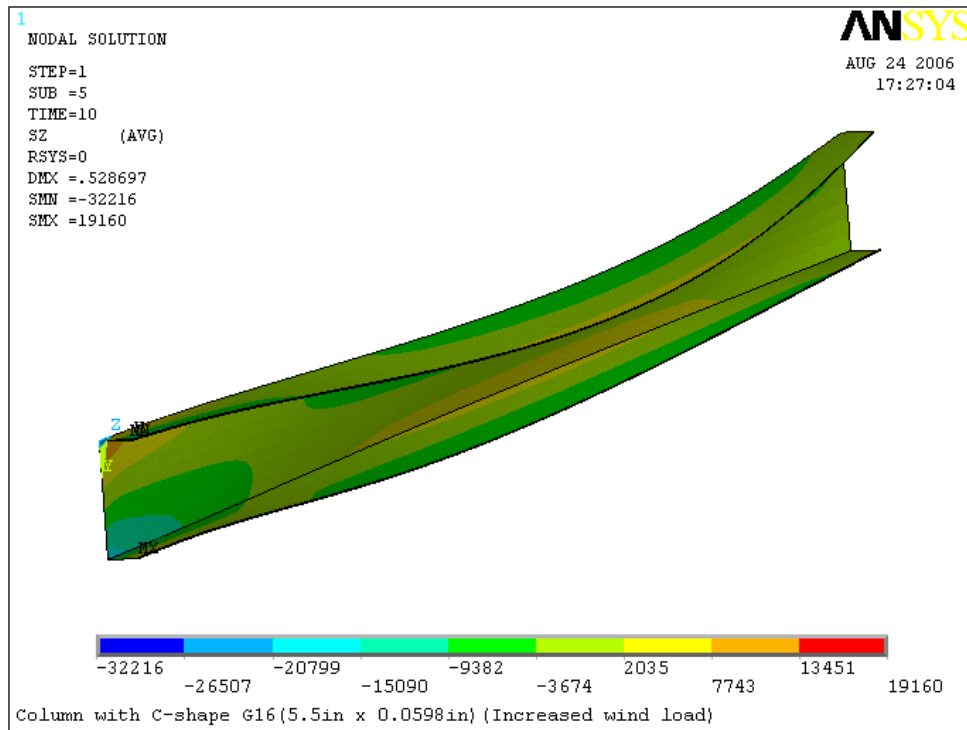
Figure 4.29 Stresses in the front side of C2×6 profile with 16 Gage (units: psi)

The maximum stresses of the C-shape profiles increased as thickness of the steel decreased, while the maximum stresses of the profiles decreased as the height of channel-web increased. For example, the maximum stresses of the 2×4 C-shape profile decreased from 6132 psi to 4492 psi when the steel thickness changed from 16 gage to 20 gage. For the same steel thickness, the maximum stresses of the C-shape profile made of 16 gage steel varied from 6132 psi to 4492 psi when the height of the web increased from 3.5 in. to 5.5 in.

4.3 Load Capability of the C-shape Profile under the load Case 1

The load capabilities of the C-shape profiles were determined from the following factored combinations:

$$1.2D+1.6L+0.5(L_r \text{ or } S \text{ or } R) \qquad\qquad (1)$$

$$1.2D+1.6(L_r \text{ or } S \text{ or } R)+(0.5L \text{ or } 0.8W) \qquad\qquad (2)$$

$$1.2D+1.6W+0.5L+0.5(L_r \text{ or } S \text{ or } R) \qquad\qquad (3)$$

Where D = dead load; L = live load due to occupancy; Lr = roof live load; S = snow load; R = nominal load due to initial rainwater or ice exclusive of the ponding contribution; and W = wind load

The initial values of the above loads are: L =12.340 psi; Lr = 4.930 psi; S = 4.930 psi; R = 7.400 psi; and W = 0.136 psi

4.3.1 Vertical load capability of the C-shape profile

Vertical load capability of the C-shape profile can be determined from combination (2):

1.2D+1.6R+0.8W

Table 4.2 Vertical load capability (Rain load) of the C-shape profile

| Gage # | Profile | R(psi) | Stress in steel (ksi) | |
			Maximum positive stress (Tension)	Maximum negative stress (Compression)
Gage 16	2×4	75.85	-----	**28.044**
	2×6	100.3	-----	**28.015**
Gage 20	2×4	44.09	-----	**28.022**
	2×6	57.8	-----	**28.027**

Note: 1. $\phi F_{steel} = 0.85 \times 33 = 28.05 ksi$

2. Dead load and wind load are constants.

4.3.2 Wind load capability of the C-shape profile

Wind load capability of the C-shape profile can be determined from combination (3):

1.2D+1.6W+0.5L+0.5S

Table 4.3 Horizontal load capability (Wind load) of the C-shape profile

| Gage # | Profile | W(psi) | Maximum deformation (inches) | Stress in steel (ksi) | |
				Maximum positive stress (Tension)	Maximum negative stress (Compression)
Gage 16	2×4	0.860	0.6823	20.112	**28.043**
	2×6	1.228	0.4757	17.753	**28.035**
Gage 20	2×4	0.392	0.6538	15.845	**28.031**
	2×6	0.571	0.4261	13.078	**28.049**

Note: 1. $\phi F_{steel} = 0.85 \times 33 = 28.05 ksi$

2. Dead load, live load and snow load are constants.

4.3.3 Wind capability of the C-shape profile based on deflection limitation

Deflection capability of the C-shape profile can be determined from combination:

D+W+L+S (or Lr)

Table 4.4 Deformation vs. wind load (W) of the C-shape profile

Gage #	Profile	W(psi)	Maximum deformation (inches)	Stress in steel (ksi)	
				Maximum positive stress (Tension)	Maximum negative stress (Compression)
Gage 16	2×4	0.604	**0.30**	6.078	15.060
	2×6	1.22	**0.30**	9.177	19.216
Gage 20	2×4	0.283	**0.30**	2.784	17.038
	2×6	0.638	**0.30**	6.393	22.338

Note: 1. $\phi F_{steel} = 0.85 \times 33 = 28.05 ksi$

2. Dead load, live load and snow load are constants.

3. The limitation of C-shape deformation was L/360=0.3 inch.

The capacities of the C-shape profiles under the load Case 2 were not studied herein because C-shape profiles under the normal loads were unacceptable (AISC LRFD Specifications).

CHAPTER 5

MODELING AND ANALYSIS OF DELTA-SHAPE COLUMNS

5.1 Description of Input and Modeling of Delta-shape Columns

Delta-shaped column was developed recently by Dr. Jan Kosny at ORNL. The column has a larger stiffness in the cross section. The Delta-shaped column could be made with welds at joint or without welds at joint. This chapter presents the results for both welded and unwelded conditions.

5.1.1 Dimensions and modeling of the Delta-shape column

Figure 5.1 shows the typical cross-section of the Delta-shaped column.
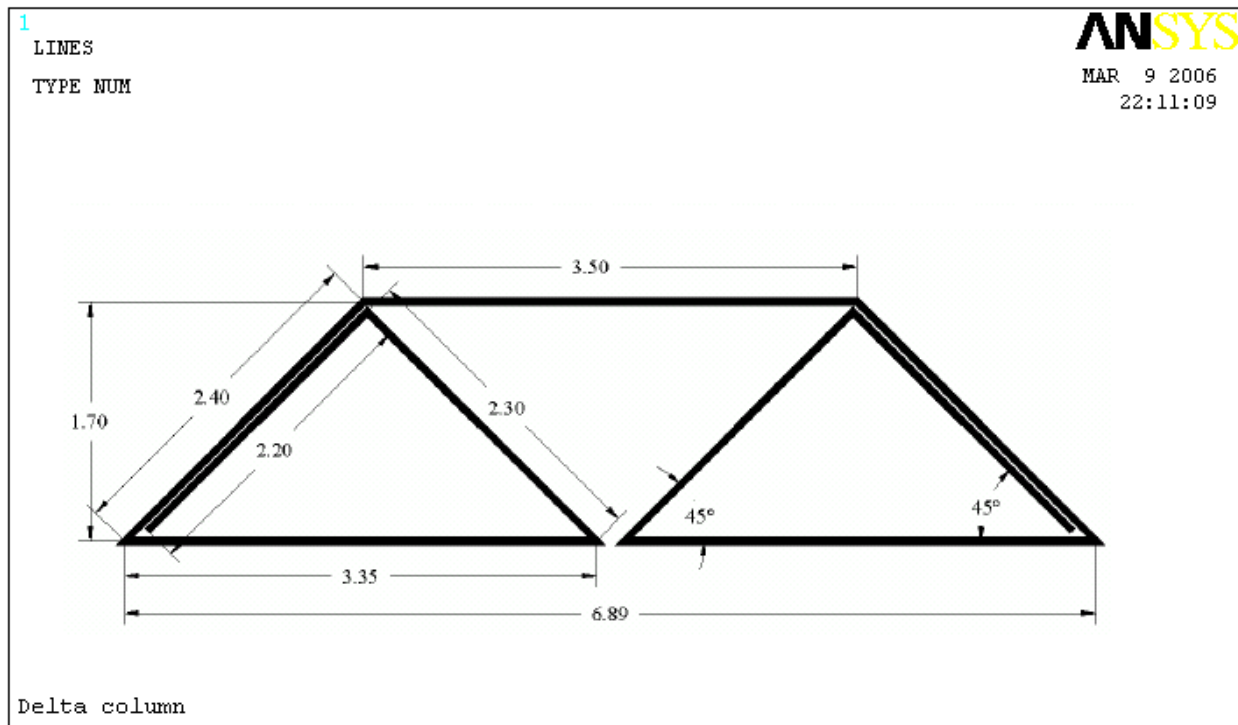
Figure 5.1 Cross-section of the Delta-shape column (unit: inches)

5.1.2 Finite element model of the Delta-shape column

Shell elements (Shell181) were used to model the Delta-shape column. Figure 5.2 shows the elevation of the Delta-shape column model. The column was divided into 54 – 2 inches elements in height. Figure 5.3 shows the three-dimensional view of the Delta-shape column model. The model was restrained with pin supports at the top of the column and fix supports at the bottom except the rotation about X direction, as shown in Figure. 5.4.
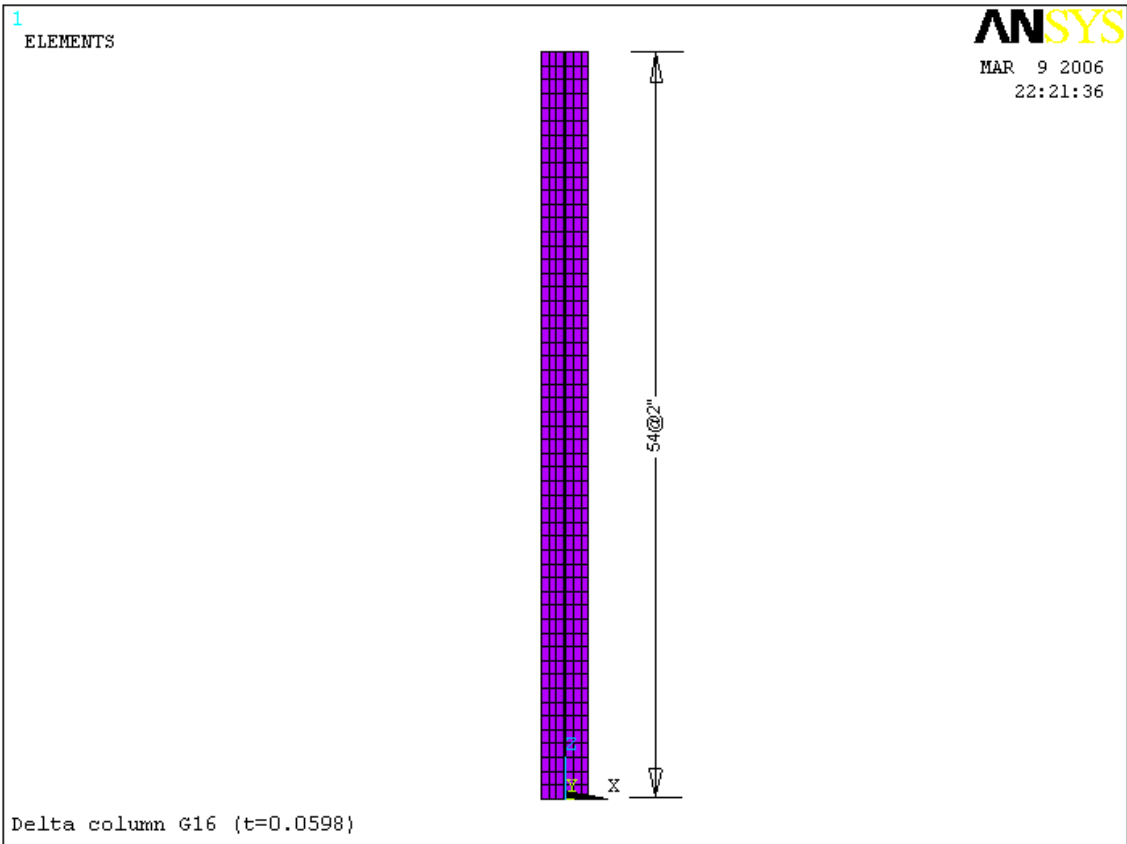
Figure 5.2 Elevation of the Delta-shape column
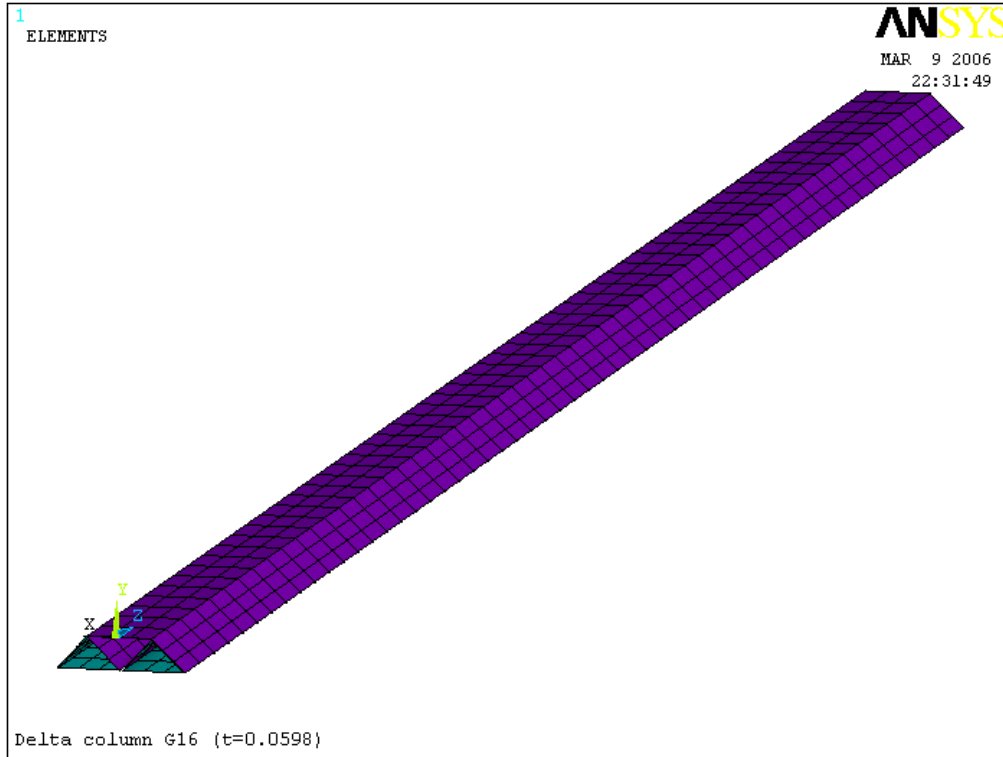
Figure 5.3 3-D Delta-shape column model
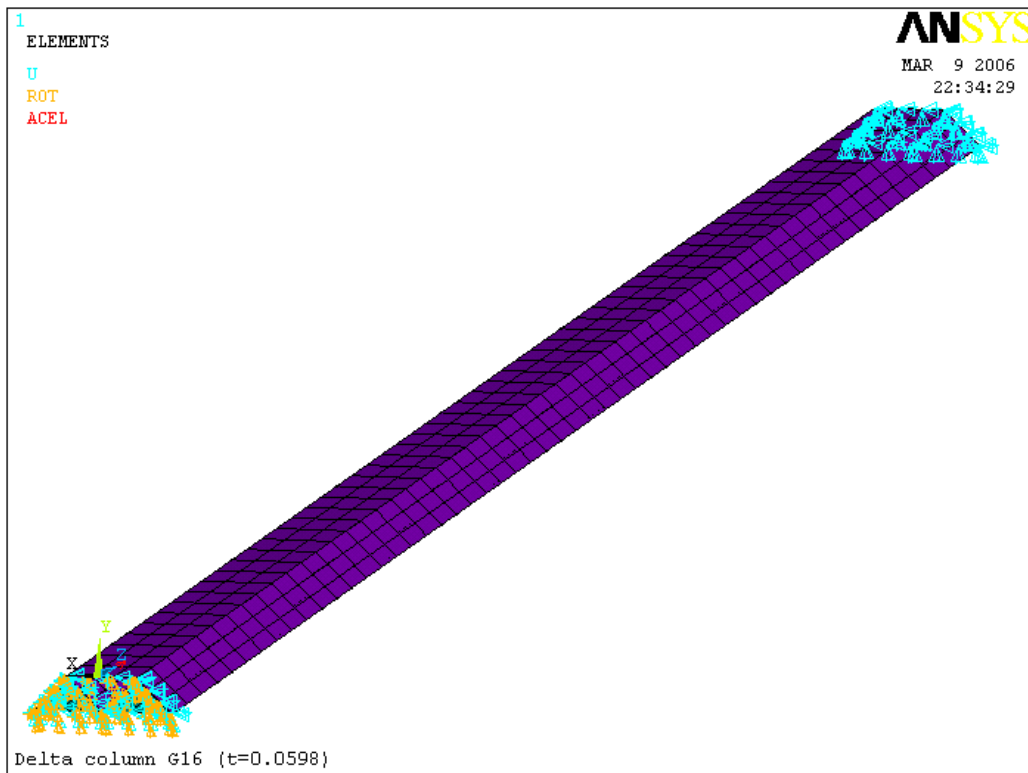
Figure 5.4 Delta-shape column model with end restraints

5.1.3 Loads

Table 5.1 Applied load of the Delta-shape columns

Gage #	Dead load (lbs)	Live load (lb/in)	Wind load (psi)	
			Case 1	Case 2
Gage 16	43.962	79.503	0.1360	1.3989
Gage 18	35.14	79.503	0.1360	1.3989
Gage 20	26.392	79.503	0.1360	1.3989

Note:

     1. Case 1 denotes columns carry the wind load based on column area only;

     2. Case 2 denotes columns carry the wind load based on 36 in wide tributary area.

Figure 5.5 was an example of the Delta-shape column with loads. It was assumed that the column will resist wind load on its front side.
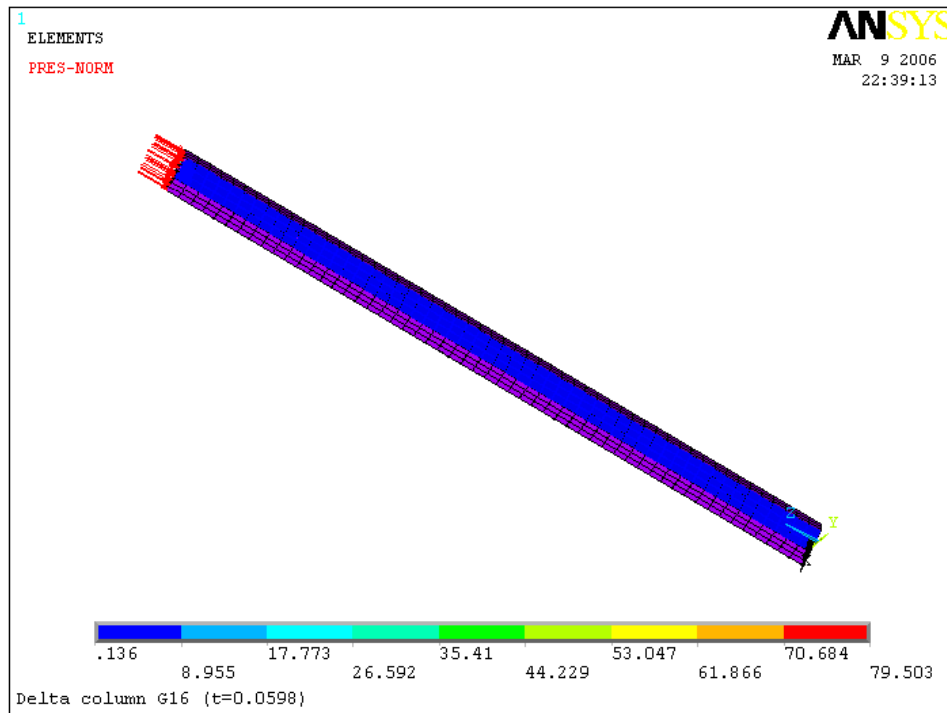
Figure 5.5 Loads on the column with Delta-shape

(Positive values denote the pressure act into the areas)

5.2 Analytical Results of the Delta-shape Column

5.2.1 Deformation

Figures 5.6 through 5.8 show the deformation of Delta-shape columns with Gage 16, 18 and Gage 20 under the load Case 1. Figures 5.9 through 5.11 show the deformation of Delta-shape column with Gage 16, 18 and Gage 20 under the load Case 2.

5.2.1.1 Deformation of Delta-shape column under the load Case 1
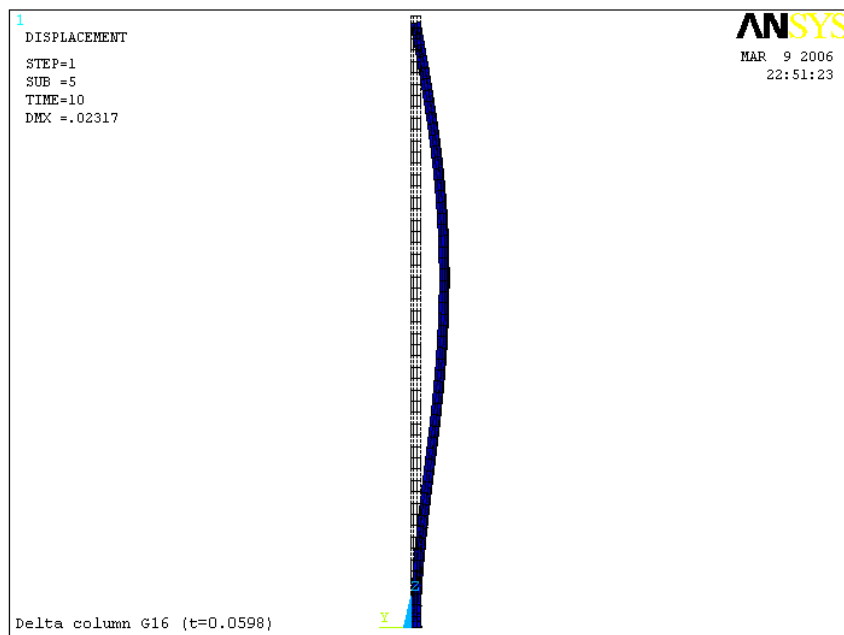
Figure 5.6 Deformation of the Delta-shape column with 16 Gage (unit: inches)
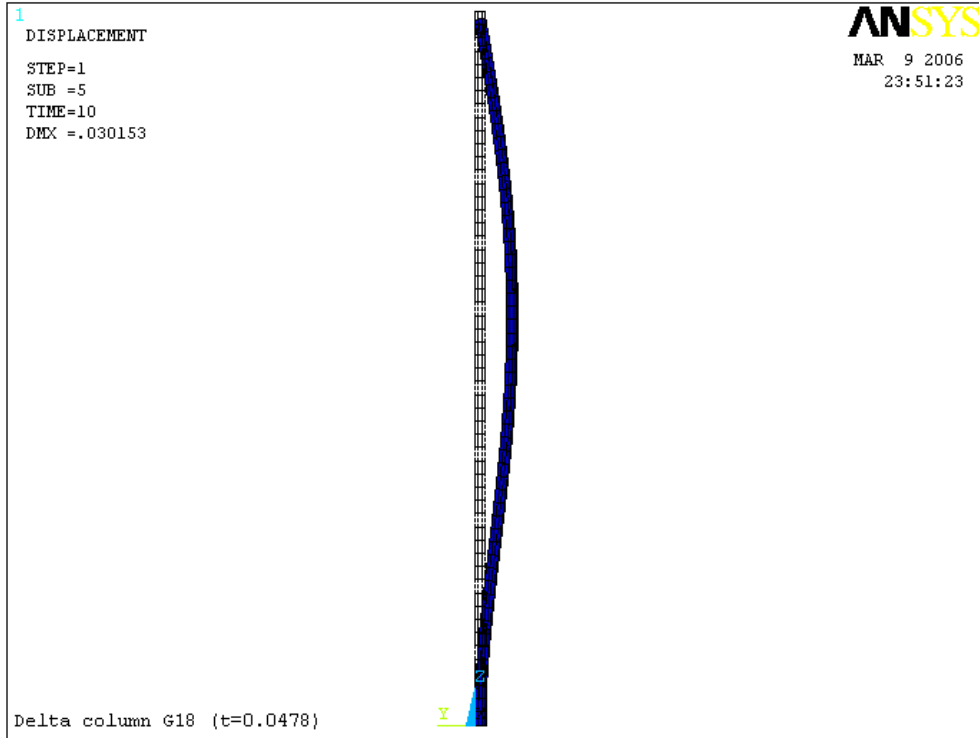
Figure 5.7 Deformation of the Delta-shape column with 18 Gage (unit: inches)
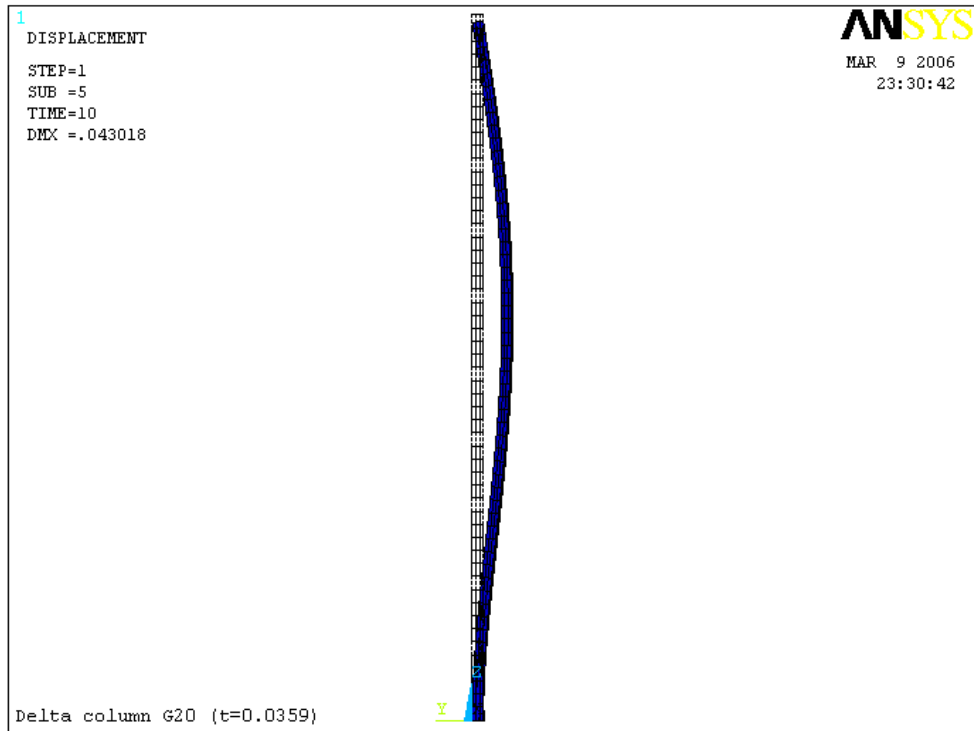
Figure 5.8 Deformation of the Delta-shape column with 20 Gage (unit: inches)

5.2.1.2 Deformation of Delta-shape column under the load Case 2
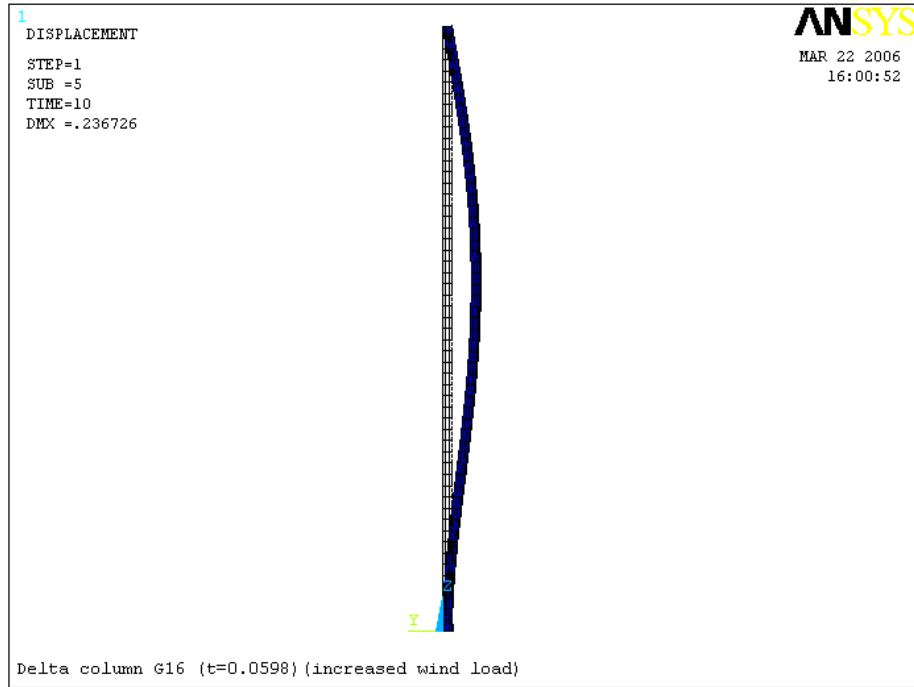
Figure 5.9 Deformation of the Delta-shape column with 16 Gage (unit: inches)
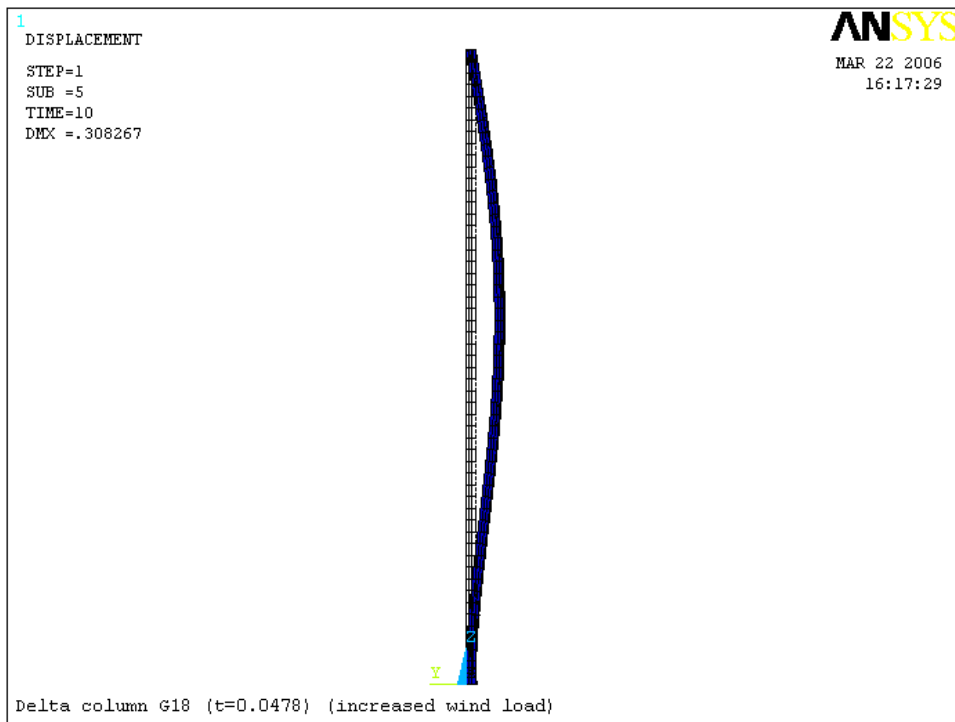
Figure 5.10 Deformation of the Delta-shape column with 18 Gage (unit: inches)
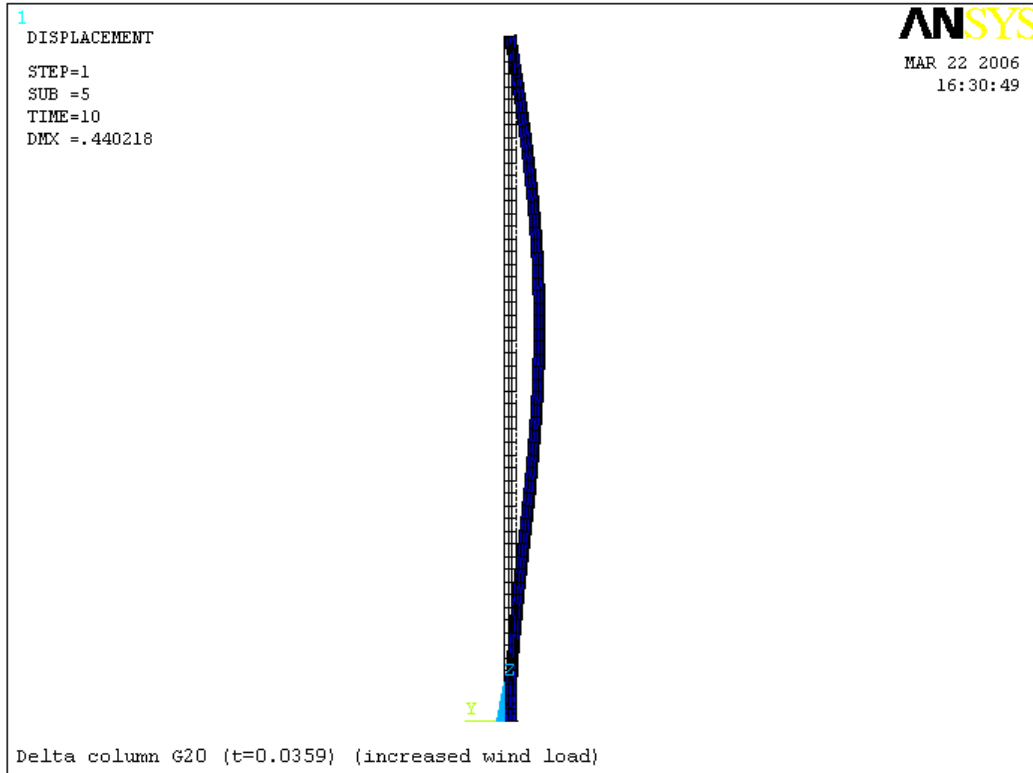
Figure 5.11 Deformation of the Delta-shape column with 20 Gage (unit: inches)

The Delta-shape column clearly had a strong axis and weak axis in the cross-section. The deformation occurred predominantly in the lateral direction, or about the weak axis. Little twisting was observed for all of the column dimensions and load cases studied. The maximum deformation of the Delta columns increased as thickness of steel decreased. For example, the maximum deformation of the Delta columns increased from 0.02317 in. to 0.0430 in. as the steel thickness changed from 16 gage to 20 gage. Under load Case 2, due to a larger lateral deformation of column, the deformation limit L/360 was the controlling criteria.

5.2.2 Stresses of the Delta-shape columns

Figures 5.12 through 5.17 show the stresses of Delta-shape columns made of 16, 18 and 20 gage steel under the load Case 1. Figures 5.18 through 5.23 show the stresses of Delta-shape column made of 16, 18 and 20 gage steel under the load Case 2.

5.2.2.1 Stresses in longitudinal direction of Delta-shape column under load Case 1
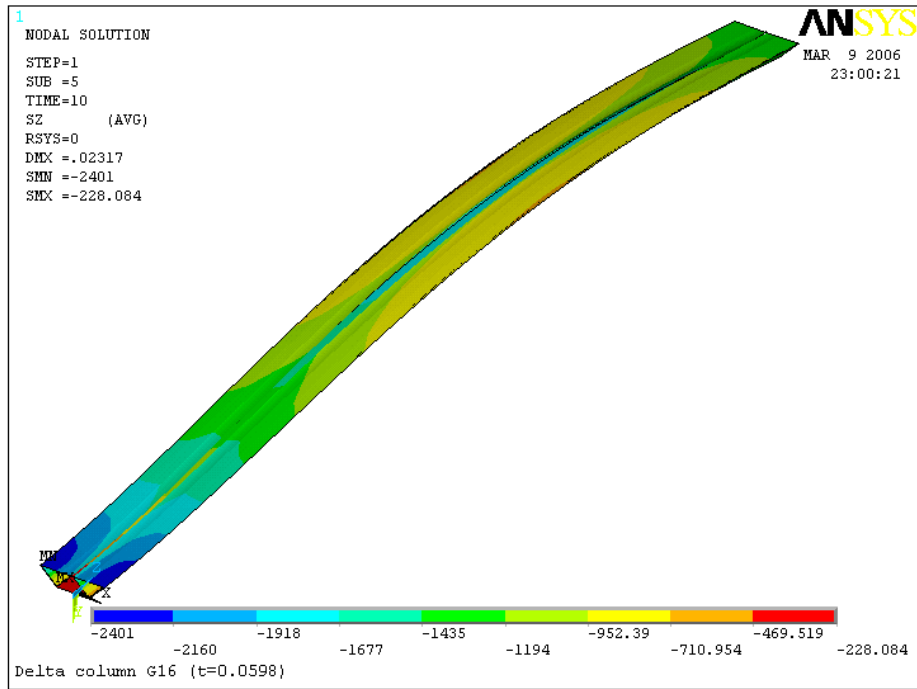
Figure 5.12 Stresses in the back side of the delta-shape column with 16 Gage (unit: psi)
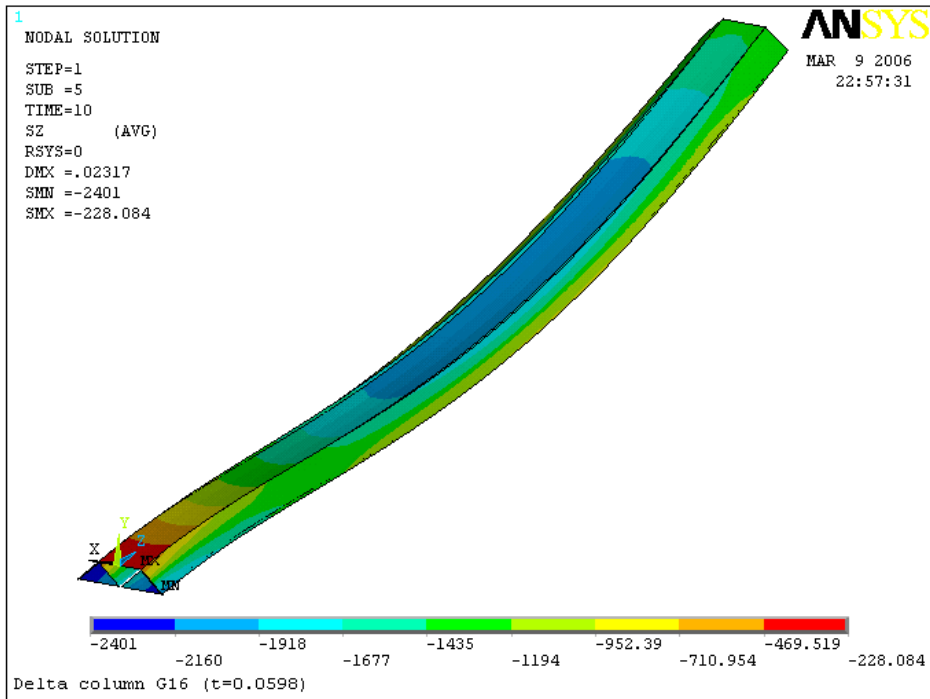
Figure 5.13 Stresses in the front side of the delta-shape column with 16 Gage (unit: psi)
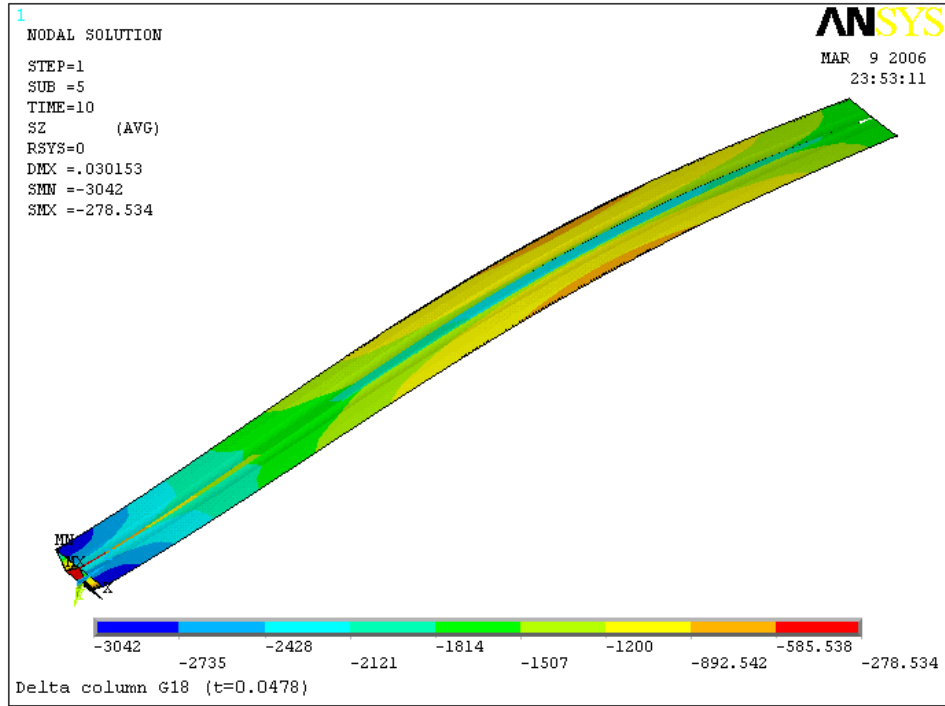
Figure 5.14 Stresses in the back side of the delta-shape column with 18 Gage (unit: psi)
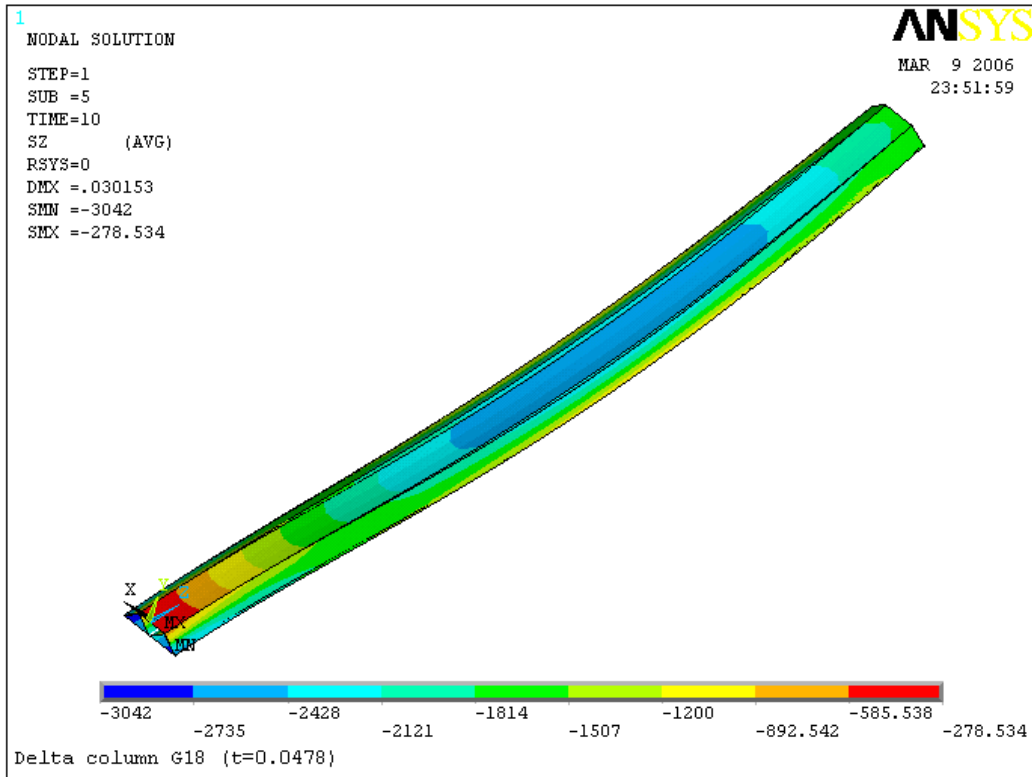
Figure 5.15 Stresses in the front side of the delta-shape column with 18 Gage (unit: psi)
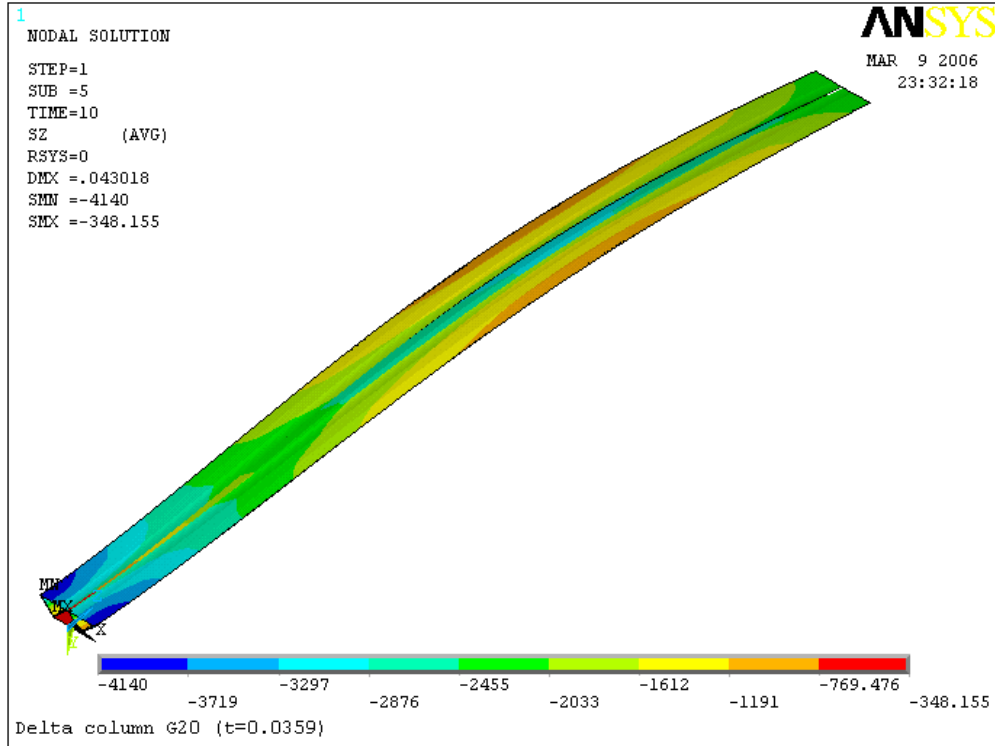
Figure 5.16 Stresses in the back side of the delta-shape column with 20 Gage (unit: psi)
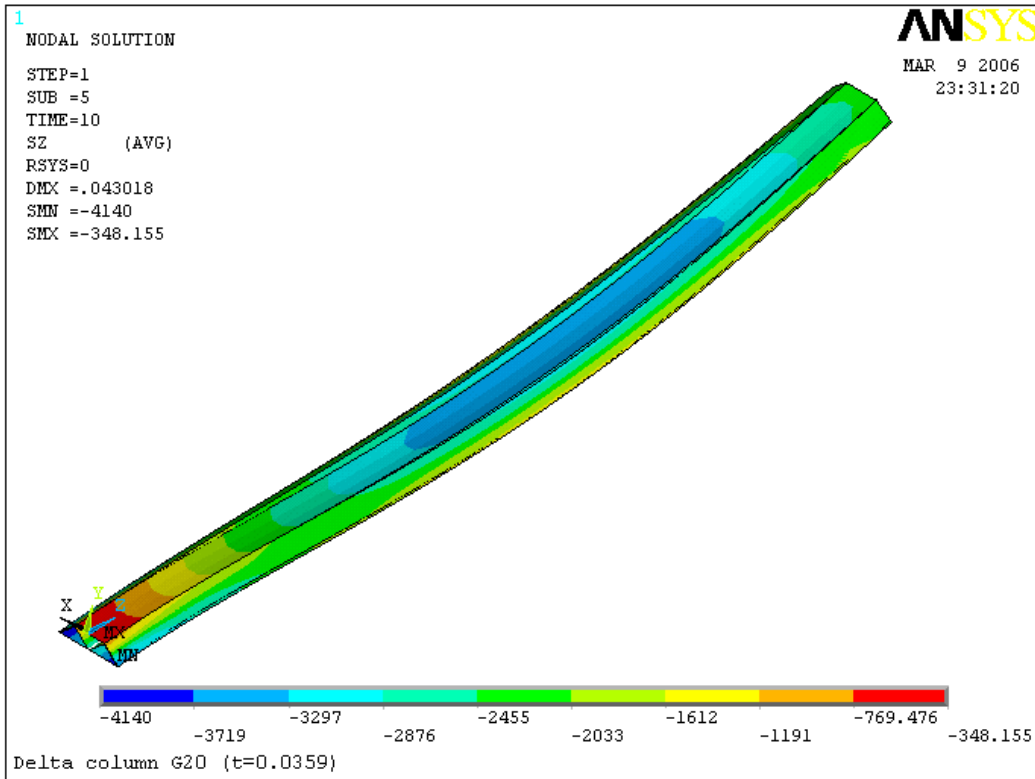
Figure 5.17 Stresses in the front side of the delta-shape column with 20 Gage (unit: psi)

5.2.2.2 Stresses in longitudinal direction of Delta-shape column under load Case 2
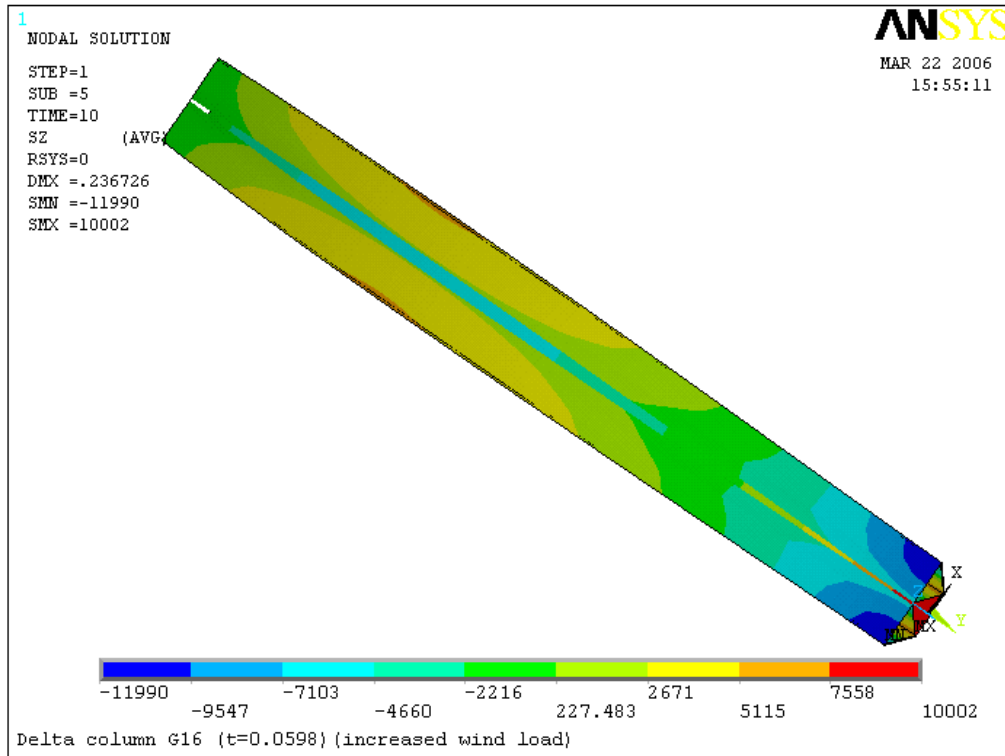
Figure 5.18 Stresses in the back side of the delta-shape column with 16 Gage (unit: psi)
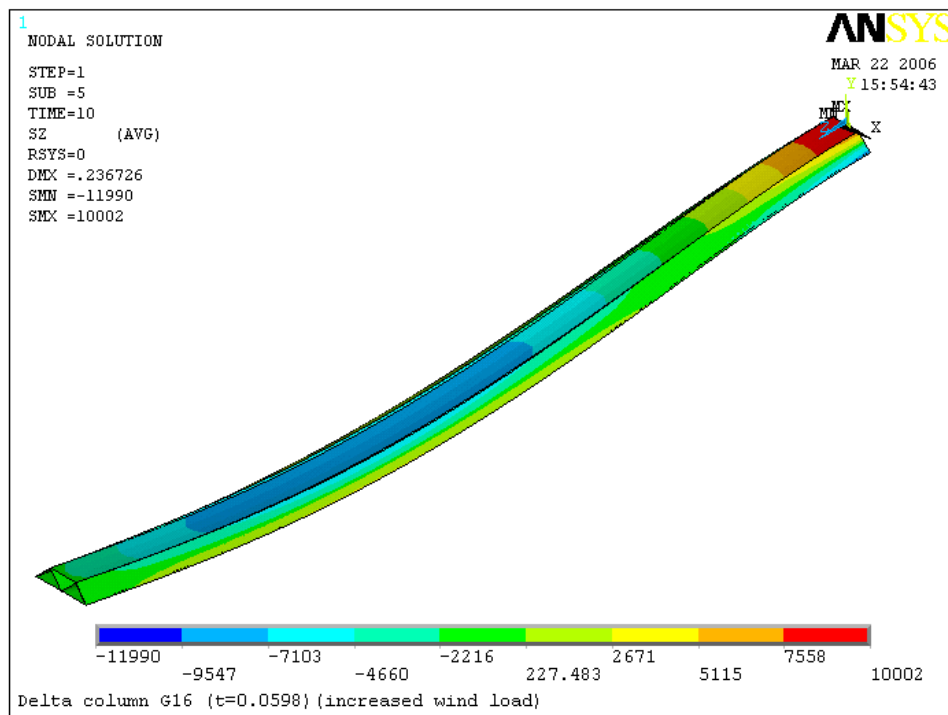
Figure 5.19 Stresses in the front side of the delta-shape column with 16 Gage (unit: psi)

68
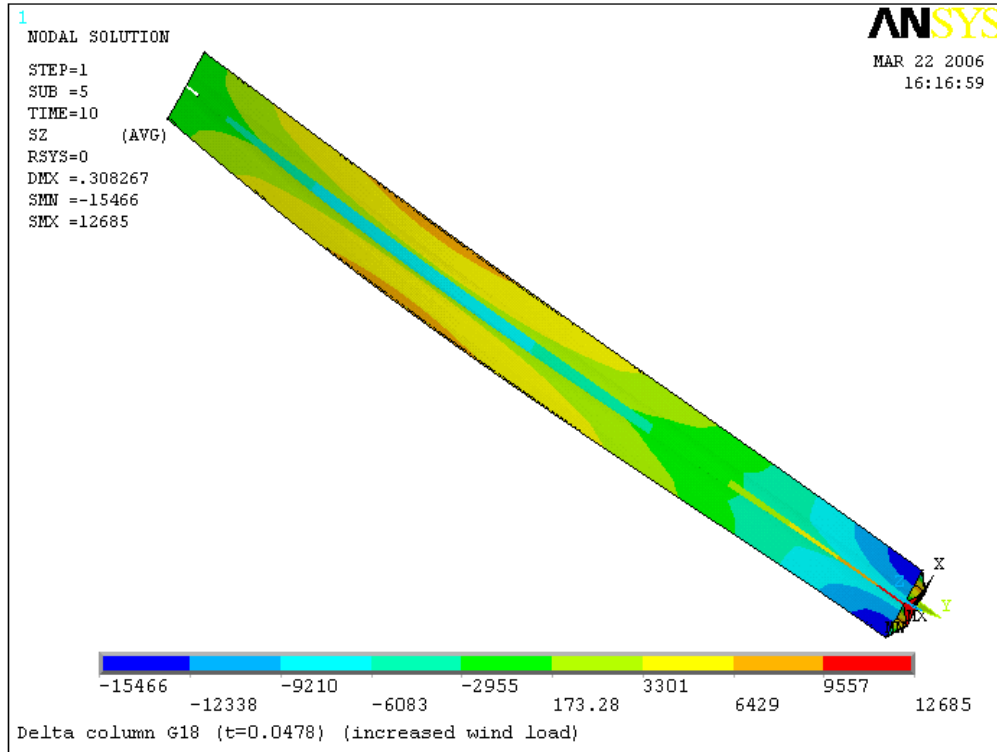
Figure 5.20 Stresses in the back side of the delta-shape column with 18 Gage (unit: psi)
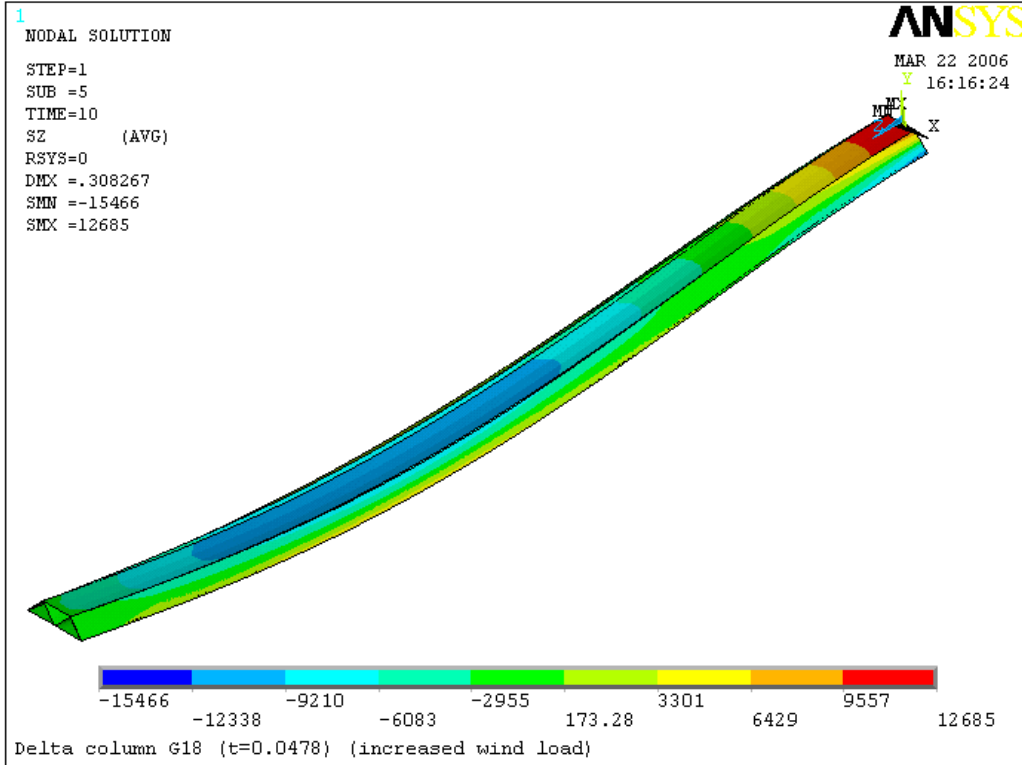
Figure 5.21 Stresses in the front side of the delta-shape column with 18 Gage (unit: psi)
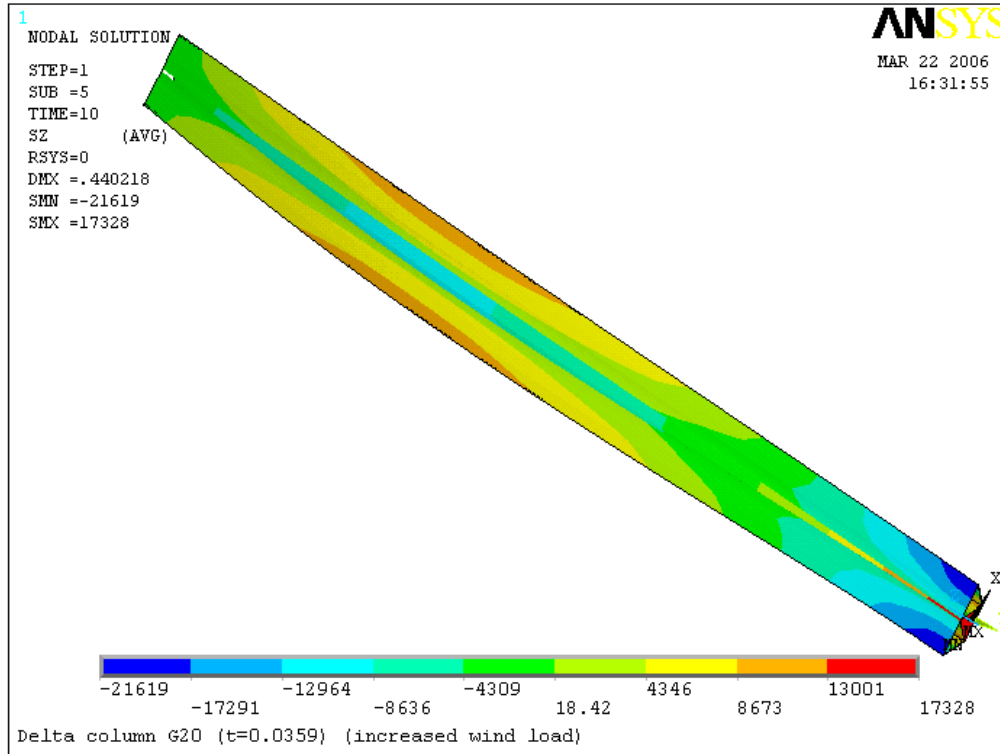
Figure 5.22 Stresses in the back side of the delta-shape column with 20 Gage (unit: psi)
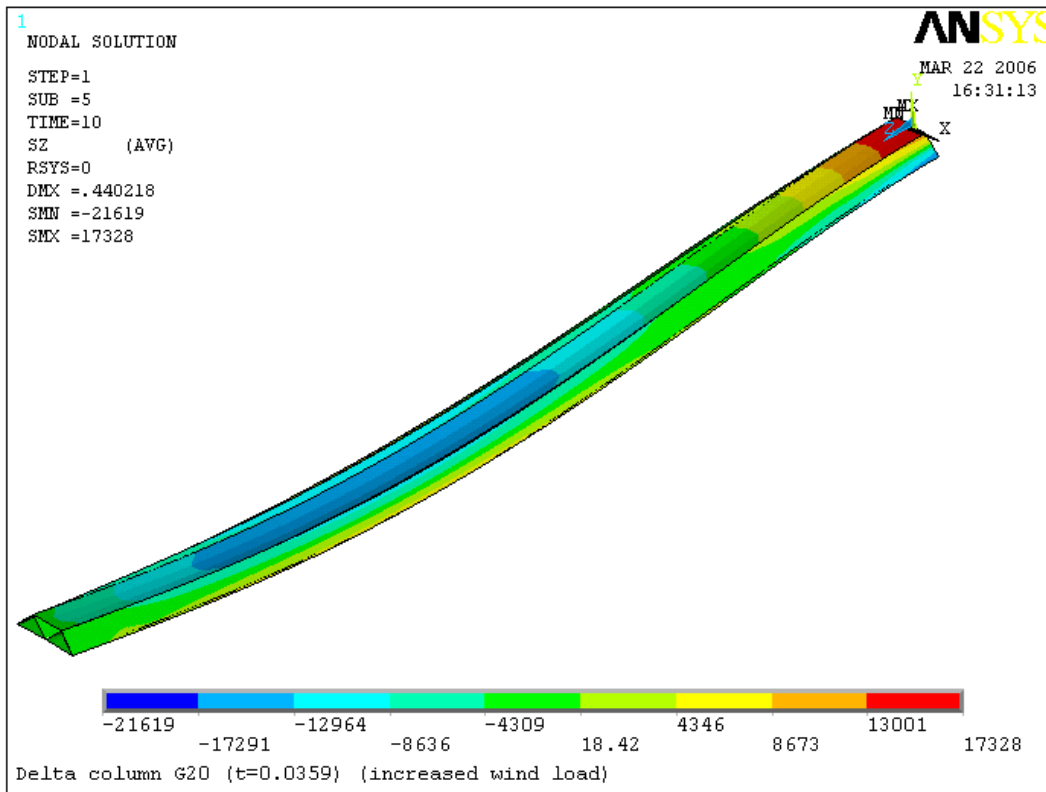
Figure 5.23 Stresses in the front side of the delta-shape column with 20 Gage (unit: psi)

The maximum longitudinal stress of the Delta-shape columns occurred at the bottom of the column. The stress at the mid-height of the column, the larger deformation location, was also relative high. Tensile was not observed in all the studied Delta-shape columns under load Case 1, which was the same as the C-shape columns. As the thickness of the steel decreased, the stresses in the columns increased. For example, the maximum stresses of the Delta-shape columns increased from 2,401 psi to 4,140 psi as the steel thickness changed from 16 to 20 gages under load Case 1. The stresses in the columns under load Case 2 exhibited the same trends.

5.3 Load Capability of the Delta-shape Column

The load capabilities of the Delta-shape columns were determined based on the factored load combinations. Wind load (W) equals 0.136 psi in the load Case 1, and increases to 1.399 psi in load Case 2, which was described in Section 2.3.2.

5.3.1 Load Capability of the Delta-shape Column under the load Case 1

5.3.1.1 Vertical load capability of the Delta-shape column

Vertical load capability of the Delta-shape column can be determined from combination (2):

1.2D+1.6R+0.8W

Table 5.2 Vertical load capability (Rain load) of the Delta-shape column

Steel thickness	R (psi)	Stress in steel (ksi)	
		Maximum positive stress (Tension)	Maximum negative stress (Compression)
16 Gage	218.2	-----	**28.033**
18 Gage	173.0	-----	**28.045**
20 Gage	127.9	-----	**28.040**

Note: 1. $\phi F_{steel} = 0.85 \times 33 = 28.05 ksi$

2. Dead load and wind load are constants.

5.3.1.2 Wind load capability of the Delta-shape column

Wind load capability of the Delta-shape column can be determined from combination (3):

1.2D+1.6W+0.5L+0.5S

Table 5.3 Horizontal load capability (Wind load) of the Delta-shape column

Steel thickness	W(psi)	Maximum deformation (inches)	Stress in steel (ksi)	
			Maximum positive stress (Tension)	Maximum negative stress (Compression)
16 Gage	2.21	0.597	**28.039**	27.506
18 Gage	1.72	0.606	27.497	**27.948**
20 Gage	1.21	0.610	26.008	**27.956**

Note: 1. $\phi F_{steel} = 0.85 \times 33 = 28.05 ksi$

2. Dead load, live load and snow load are constants.

5.3.1.3 Deflection capability of the Delta-shape column

Deflection capability of the Delta-shape column can be determined from combination:

D+W+L+S (or Lr)

Table 5.4 Deformation vs. wind load (W) of the Delta-shape column

Steel thickness	W(psi)	Maximum deformation (inches)	Stress in steel(ksi)	
			Maximum positive stress (Tension)	Maximum negative stress (Compression)
16 Gage	1.77	**0.30**	13.015	14.808
18 Gage	1.36	**0.299**	12.284	15.084
20 Gage	0.96	**0.300**	11.098	15.475

Note: 1. $\phi F_{steel} = 0.85 \times 33 = 28.05 ksi$

2. Dead load, live load and snow load are constants.

3. The limitation of Delta-shape deformation was L/360=0.3 inch.

5.3.2 Vertical Load Capability of the Delta-shape Column under the load Case 2

Vertical load capability of the Delta-shape column can be determined from combination (2):
1.2D+1.6R+0.8W

Table 5.5 Vertical load capability (Rain load) of the Delta-shape column

Steel thickness	R(psi)	Stress in steel (ksi)	
		Maximum positive stress (Tension)	Maximum negative stress (Compression)
16 Gage	157.4	-----	**28.044**
18 Gage	109.7	----	**28.050**

Note: 1. $\phi F_{steel} = 0.85 \times 33 = 28.05 ksi$, 2. Dead load and wind load are constants.

CHAPTER 6

MODELING AND ANALYSIS OF THE ORIGINAL-SHAPE COLUMN

6.1 Description of Input and Modeling of the Original Column without foam

6.1.1 Dimensions and modeling of the original column without foam
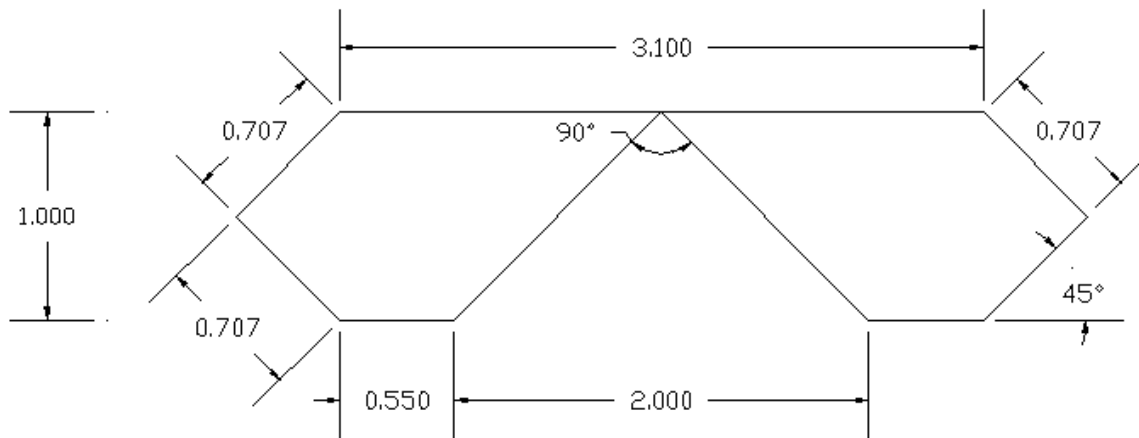
Figure 6.1 Cross-section of the original-shape column (unit: inches)
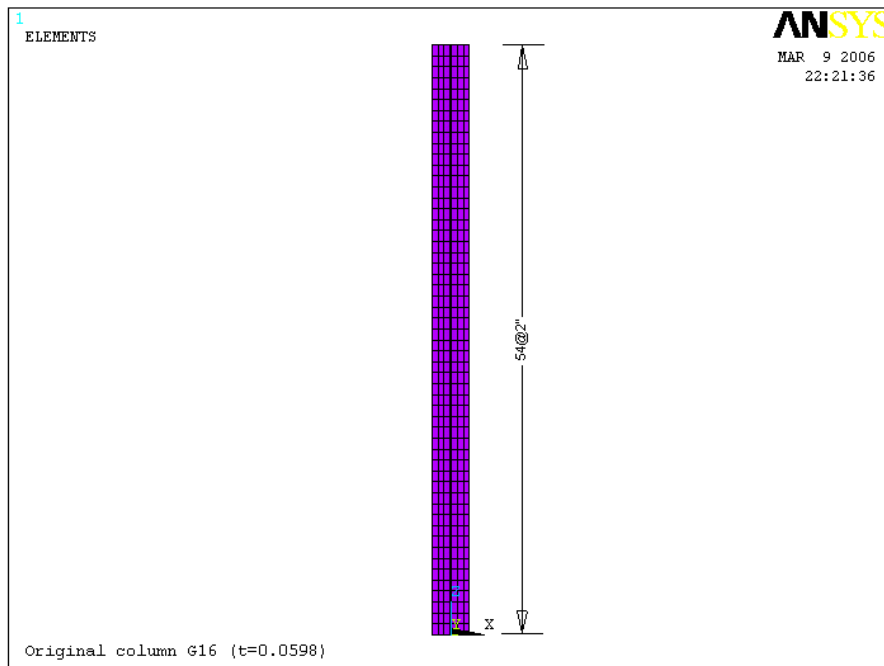
Figure 6.2 Elevation of the original column

6.1.2 Finite element model of the original column

Shell elements (Shell181) were used to model the Original. Figure 6.3 shows the three-dimensional view of the Original column model. The model was restrained with pin supports at the top of the column and fix supports at the bottom except the rotation about X direction, as shown in Figure. 6.4.
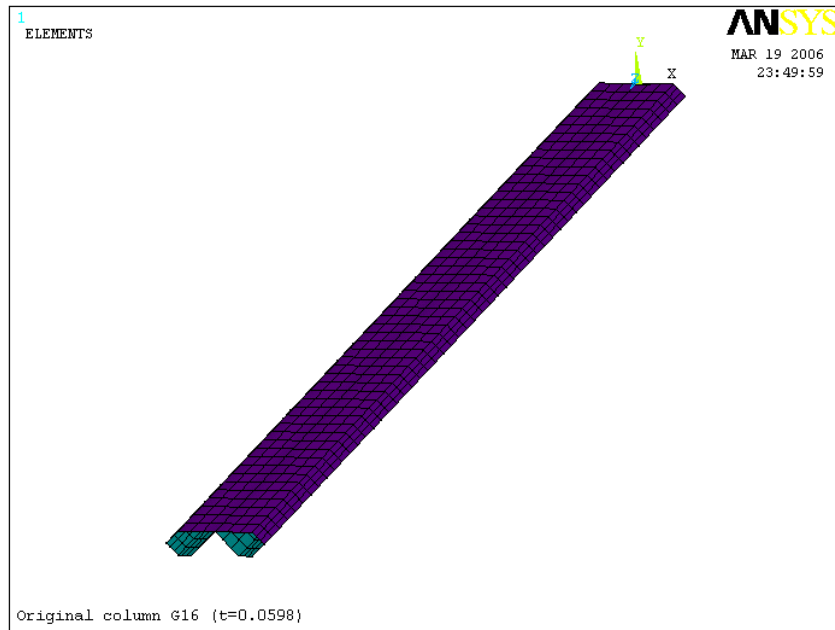
Figure 6.3 3-D original column model
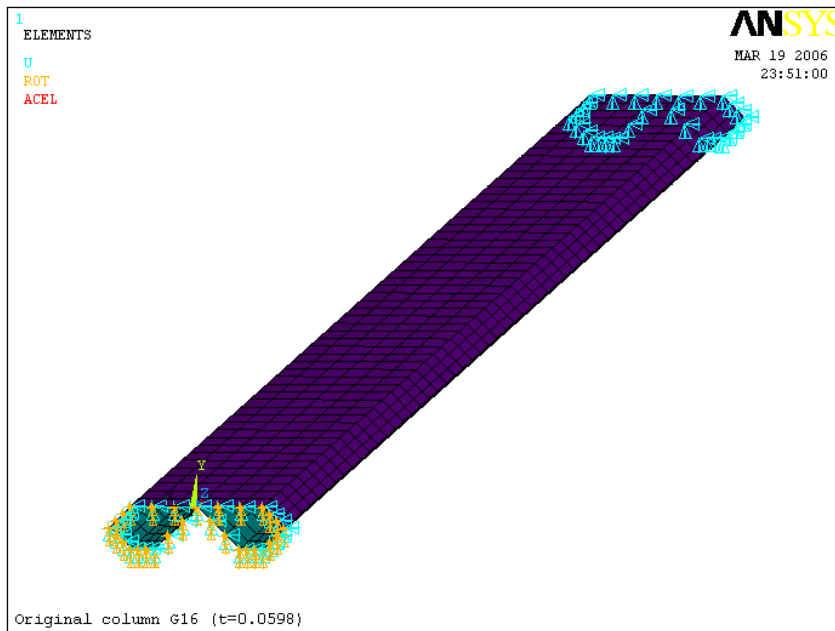
Figure 6.4 Original column model with end restraints

6.1.3 Loads

Table 6.1 Applied load of the original columns

Steel thickness	Dead load (lbs)	Live load (lb/in)	Wind load (psi)	
			Case 1	Case 2
16 Gage	23.730	147.285	0.136	1.579
18 Gage	18.968	147.285	0.136	----
20 Gage	14.246	147.285	0.136	----

Note:

    1. Case 1 denotes columns carry the wind load based on column area only;

    2. Case 2 denotes columns carry the wind load based on 36 in wide tributary area.

Figure 6.5 is an example of the Delta-shape column with loads. It was assumed that the column would resist wind load on its front side.
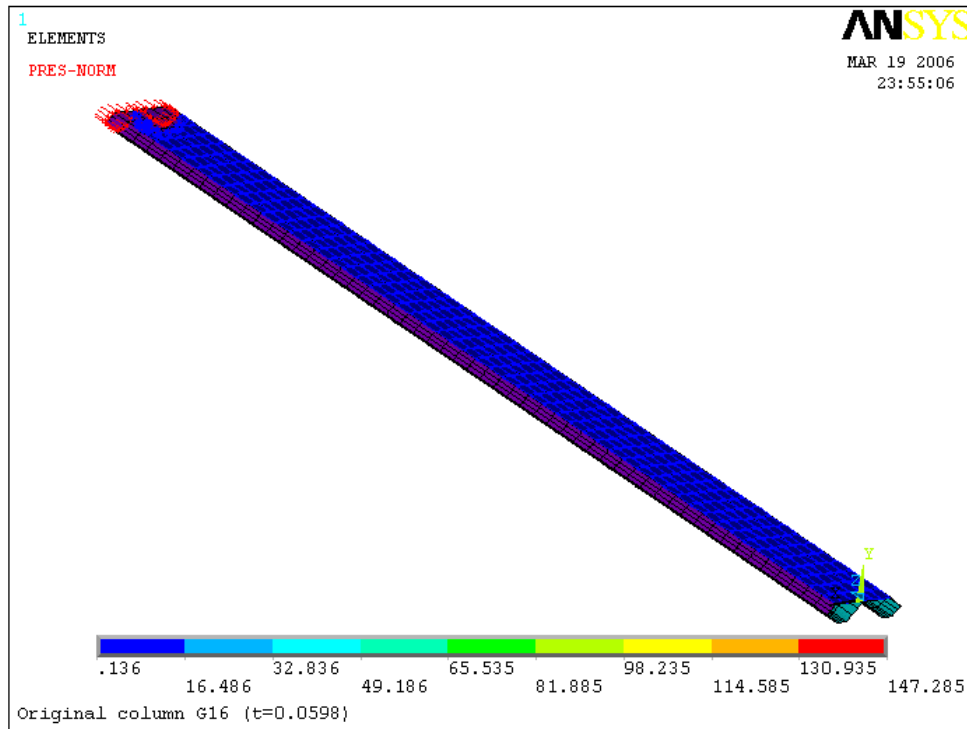
Figure 6.5 Loads on the original column

(Positive values denote the pressure act into the areas)

6.2 Analytical Results of the Original Column without Foam

6.2.1 Deformation

Figures 6.6 through 6.8 show the deformation of the original columns with Gage 16, 18 and Gage 20 under the load Case 1. Figures 6.9 show the deformation of the original column with Gage 16 under the load Case 2.

6.2.1.1 Deformation of original column under the load Case 1
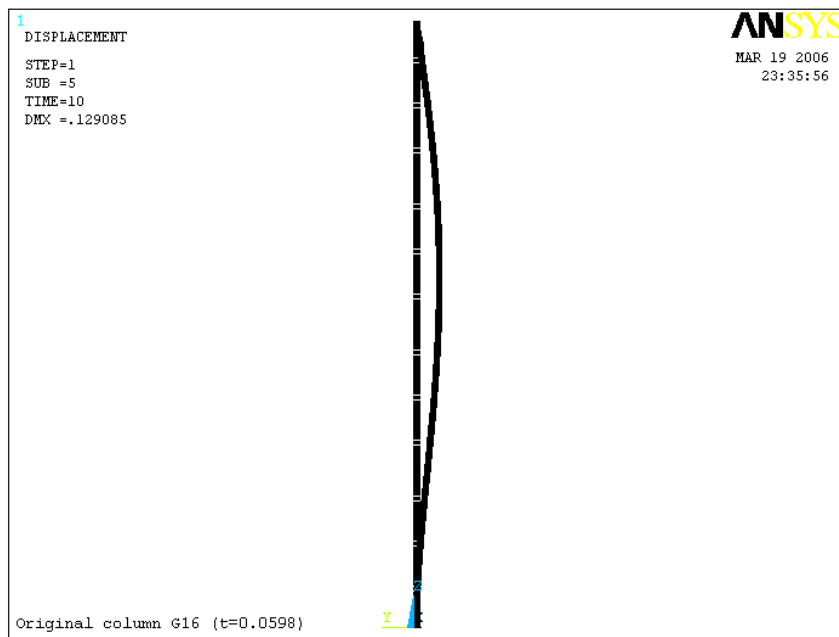
Figure 6.6 Deformation of the original column with 16 Gage (unit: inches)
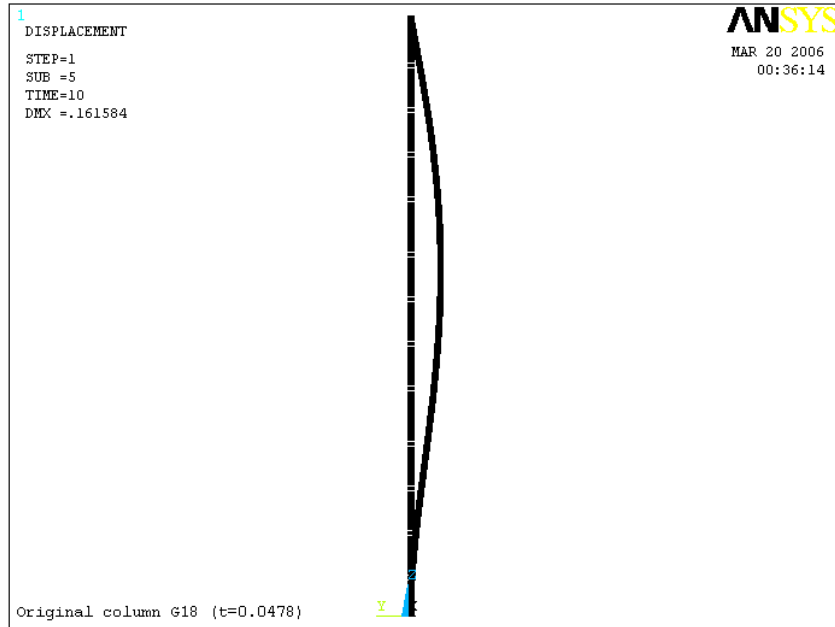
Figure 6.7 Deformation of the original column with 18 Gage (unit: inches)
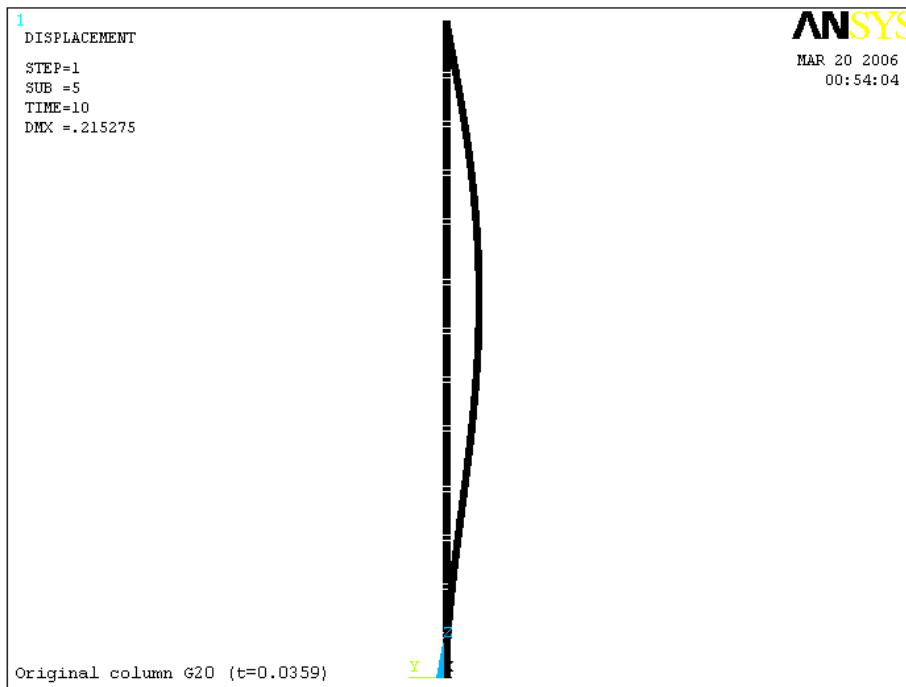
Figure 6.8 Deformation of the original column with 20 Gage (unit: inches)

6.2.1.2 Deformation of original column under the load Case 2


```
1
DISPLACEMENT                                                        ANSYS
STEP=1                                                           MAR 23 2006
SUB =5                                                              09:46:28
TIME=10
DMX =1.497




                                              Z
                                   Y

Original column G16 (t=0.0598)
```
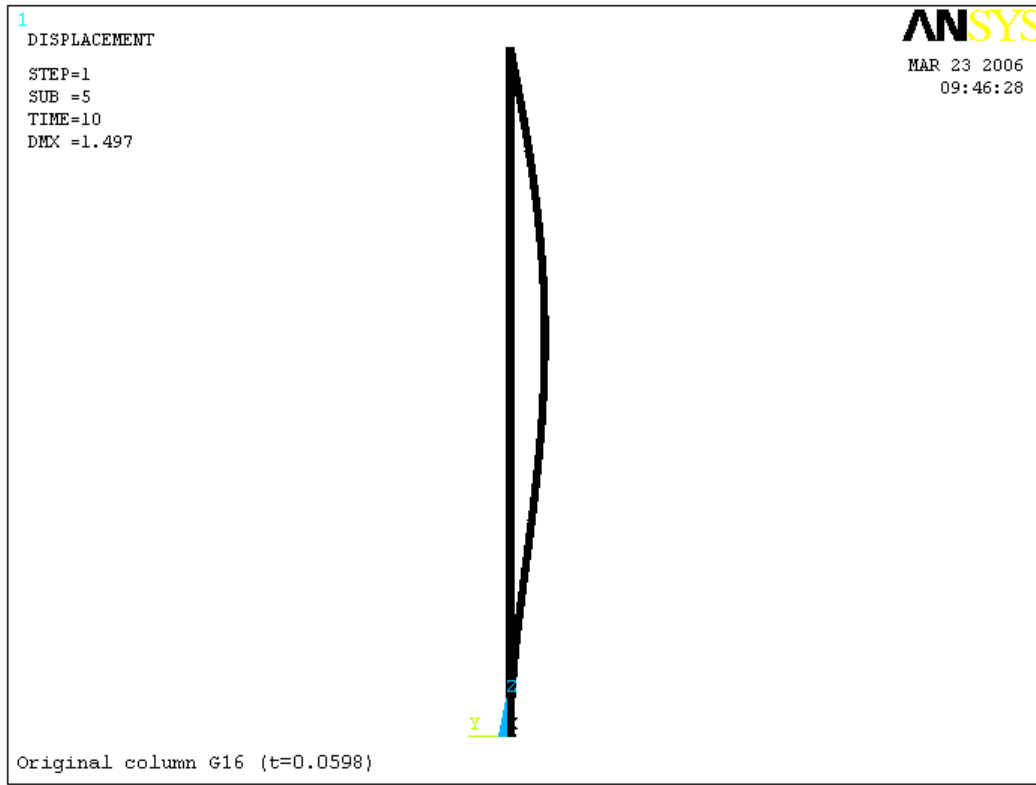
Figure 6.9 Deformation of the original column with 16 Gage (unit: inches)

No twisting was observing in the deformation of all original columns, which was the same as the Delta-columns. The maximum deformations of all original columns occurred at about 46" from the top surface. The maximum deformation of the original columns increased as the thickness of the steel facing decreased. For example, the maximum deformation of the original columns increased from 0.129 in. to 0.215 in. as the steel thickness changed from 16 gage to 20 gage. As far as the maximum deformations under load Case 1, all original columns can be acceptable, but the slenderness ratios of all original columns were around 284, which was greater than the limit of the code (AISC LRFD Specifications).

The lateral deformation of original columns made of 16 gage steel were very larger than the limit of L/360 when columns were subjected to wind load based on 36 in wide tributary area. (The limitation of Delta deformation is L/360=0.3 inch).

Compared to the C-shape column and Delta-shape column with the same steel thickness under the same load, the maximum deformation of the original column was the largest. For example, the maximum deformation of the Delta column made of 16 gage steel was 0.0232 inch, while the maximum deformation of the original 16 gage column was 0.1291 inch under load Case 1.

6.2.2 Stresses of the original columns

Figures 6.10 through 6.15 show the stresses of original columns made of 16, 18 and 20 gage steel under the load Case 1. Figures 6.16 through 6.17 show the stresses of the original column with Gage16 under the load Case 2.

6.2.2.1 Stresses in longitudinal direction of original column under load Case 1
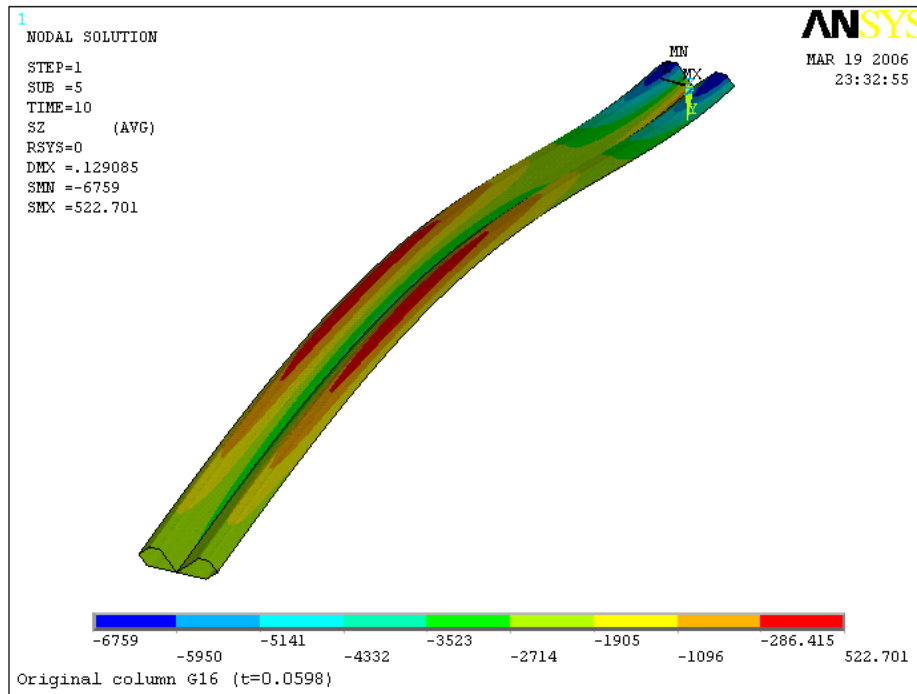
Figure 6.10 Stresses in the back side of the Original column with 16 Gage (unit: inches)
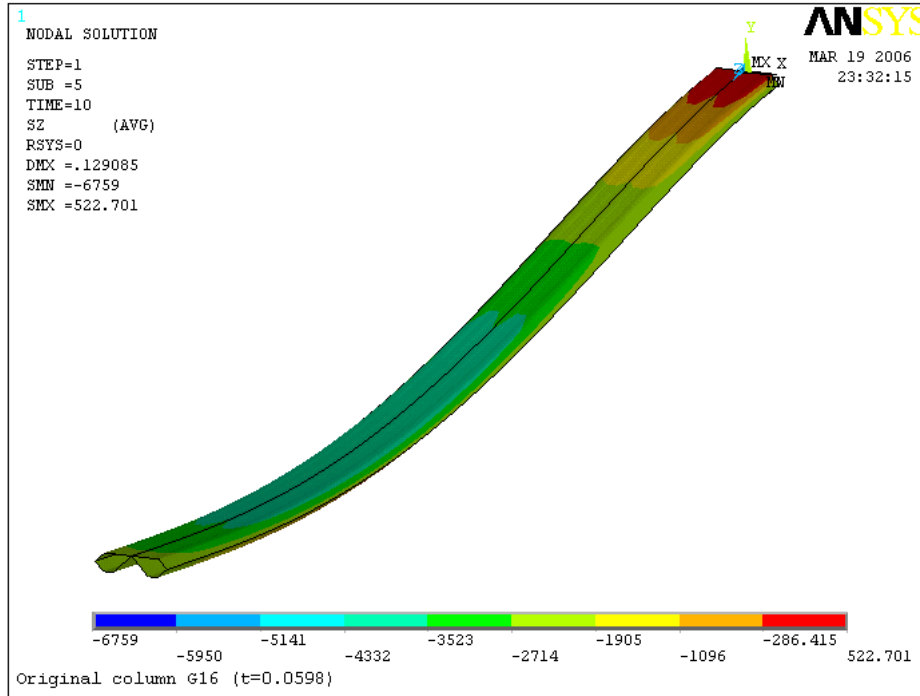
Figure 6.11 Stresses in the front side of the Original column with 16 Gage (unit: inches)
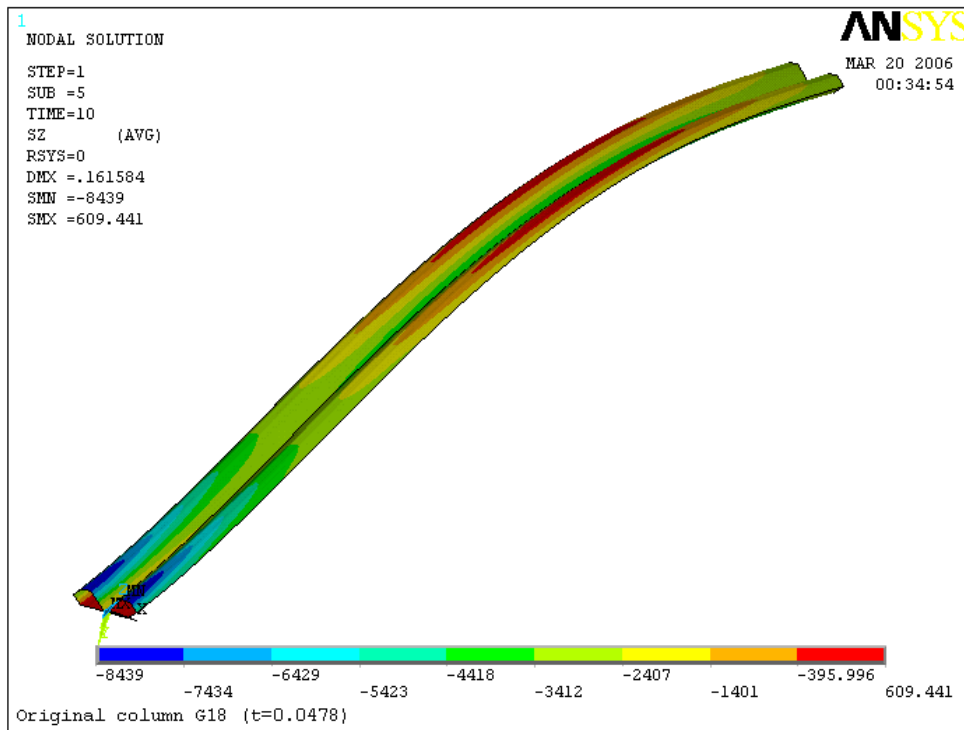
Figure 6.12 Stresses in the back side of the Original column with 18 Gage (unit: inches)
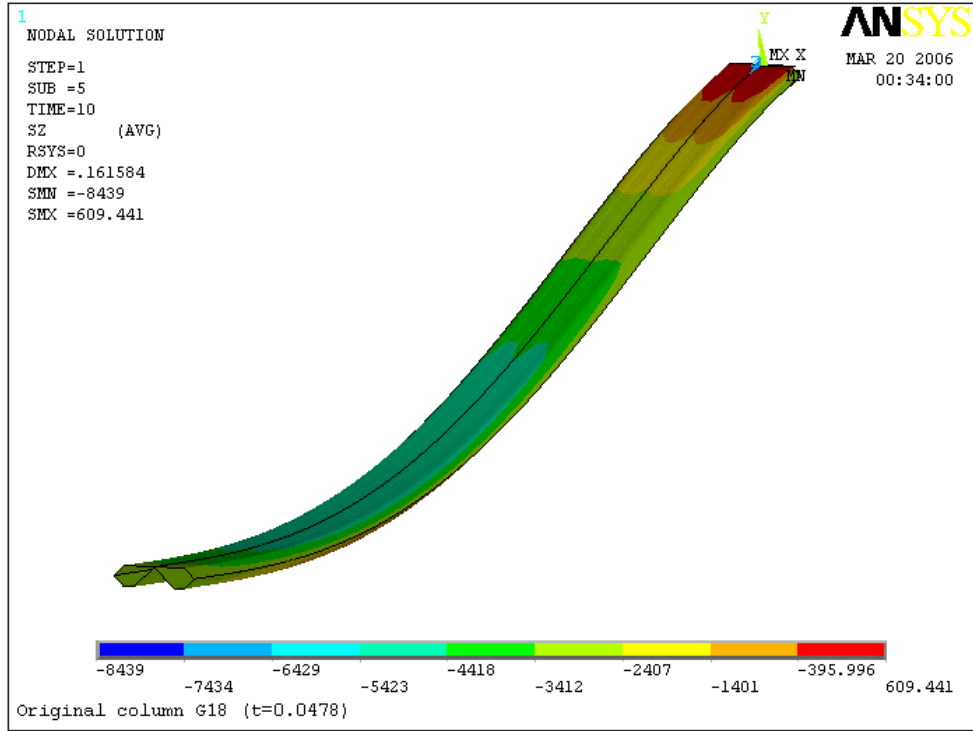
Figure 6.13 Stresses in the front side of the Original column with 18 Gage (unit: inches)
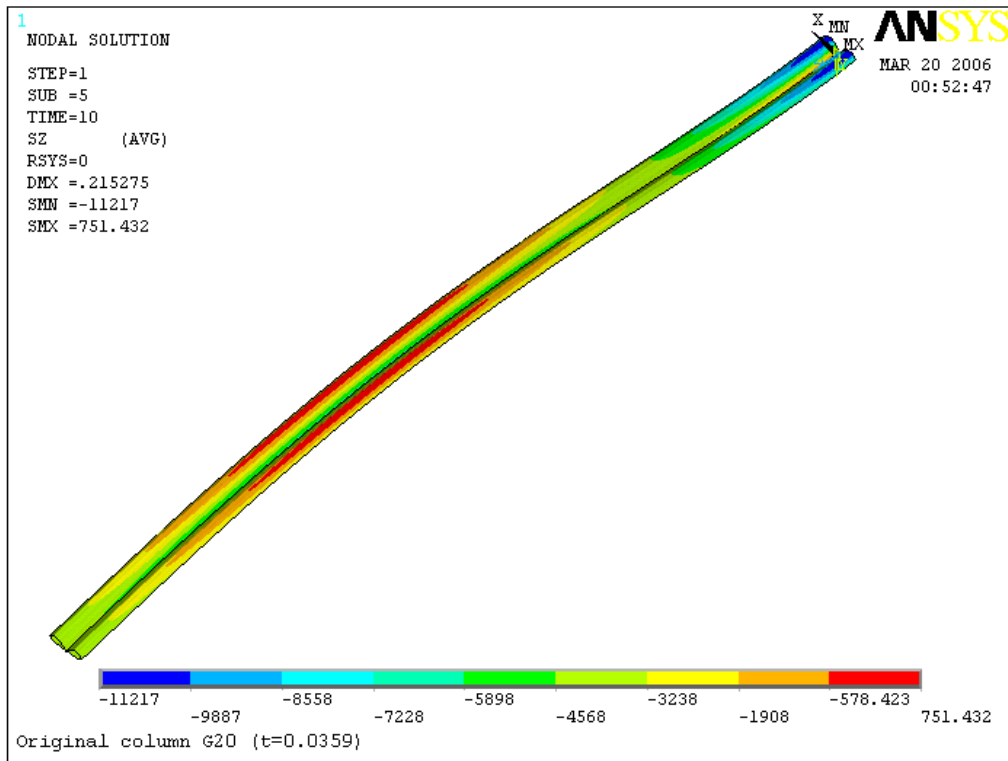
Figure 6.14 Stresses in the back side of the Original column with 20 Gage (unit: inches)
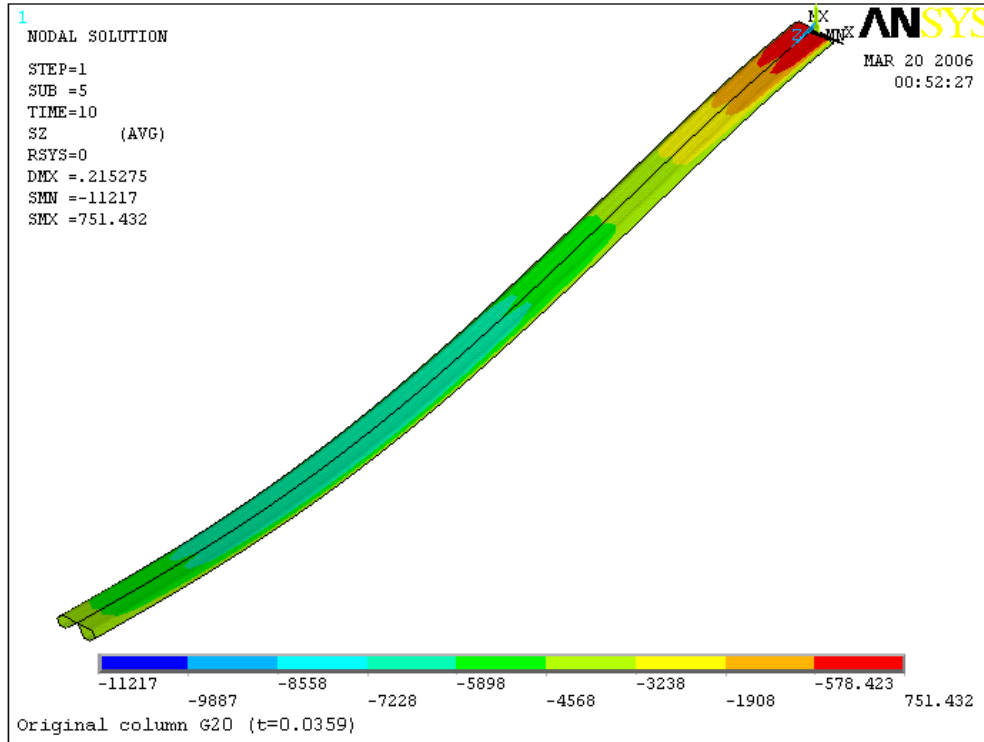
Figure 6.15 Stresses in the front side of the Original column with 20 Gage (unit: inches)

In the longitudinal direction, the maximum compressive stresses and tensile stresses of all

the original columns occurred at the bottom of the columns under load Case 1. In addition, the

stresses of the columns at the upper positions were relative high. The stresses of the original

columns increased as the thickness of the steel decreased. For example, the maximum stresses of

the original columns increased from 6759 psi to 11217 psi as the steel thickness changed from 16

gage to 20 gage under load Case 1.

The maximum stress of the original column was larger than the stresses of the C-shape and

Delta-shape columns with the same steel thickness and under the same loads. For example, the

maximum stress of the Delta column made of 16 gage steel was 2401psi, while the maximum

stress of the original column made of 16 gage steel was 6759 psi under load Case 1.

6.2.2.2 Stresses in longitudinal direction of original column under load Case 2
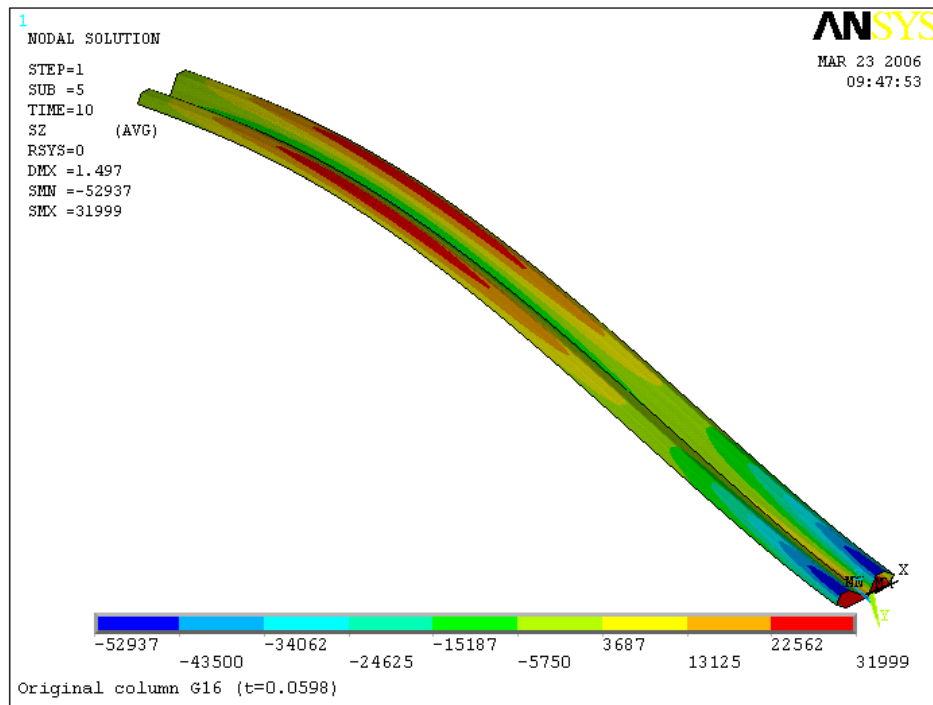
Figure 6.16 Stresses in the back side of the Original column with 16 Gage (unit: inches)
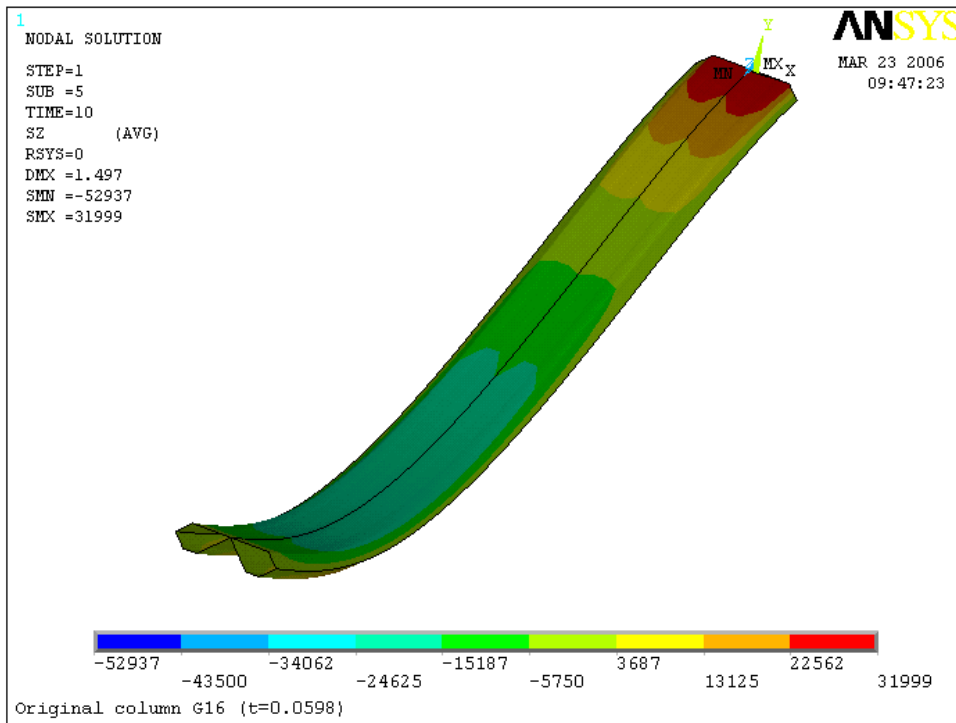
Figure 6.17 Stresses in the front side of the Original column with 16 Gage (unit: inches)

The stresses in the columns under load Case 2 exhibited the same trends as the ones under load Case 1. The stresses of the original column made of 16 gage steel were too large to satisfy the deformation limitation when the column subjected to wind load based on 36 in wide tributary area. Compared to the maximum stresses of the maximum stress of the original column was larger than the stresses of the C-shape and Delta-shape columns with same steel thickness under the same loads. For example, the maximum stress of the Delta column made of 16 gage steel was 2401 psi, while the maximum stress of the original column made of 16 gage steel was 6759 psi under load Case 1.

6.3 Description of Input and Modeling of the Original Column with foam

6.3.1 Dimensions and modeling of the original column with foam

The original column with foam made of 16 gage steel under Case 1 was studied.
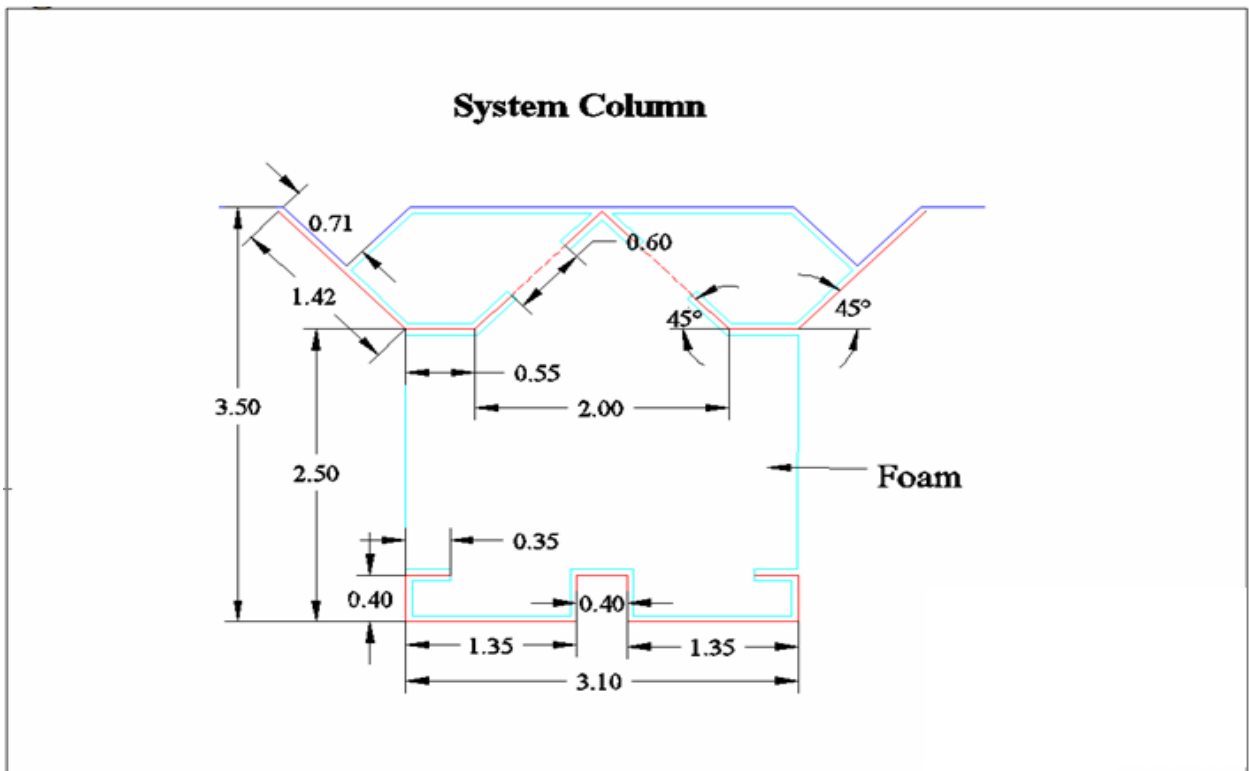
Figure 6.18 Cross-section of the original column with foam (unit: inches)
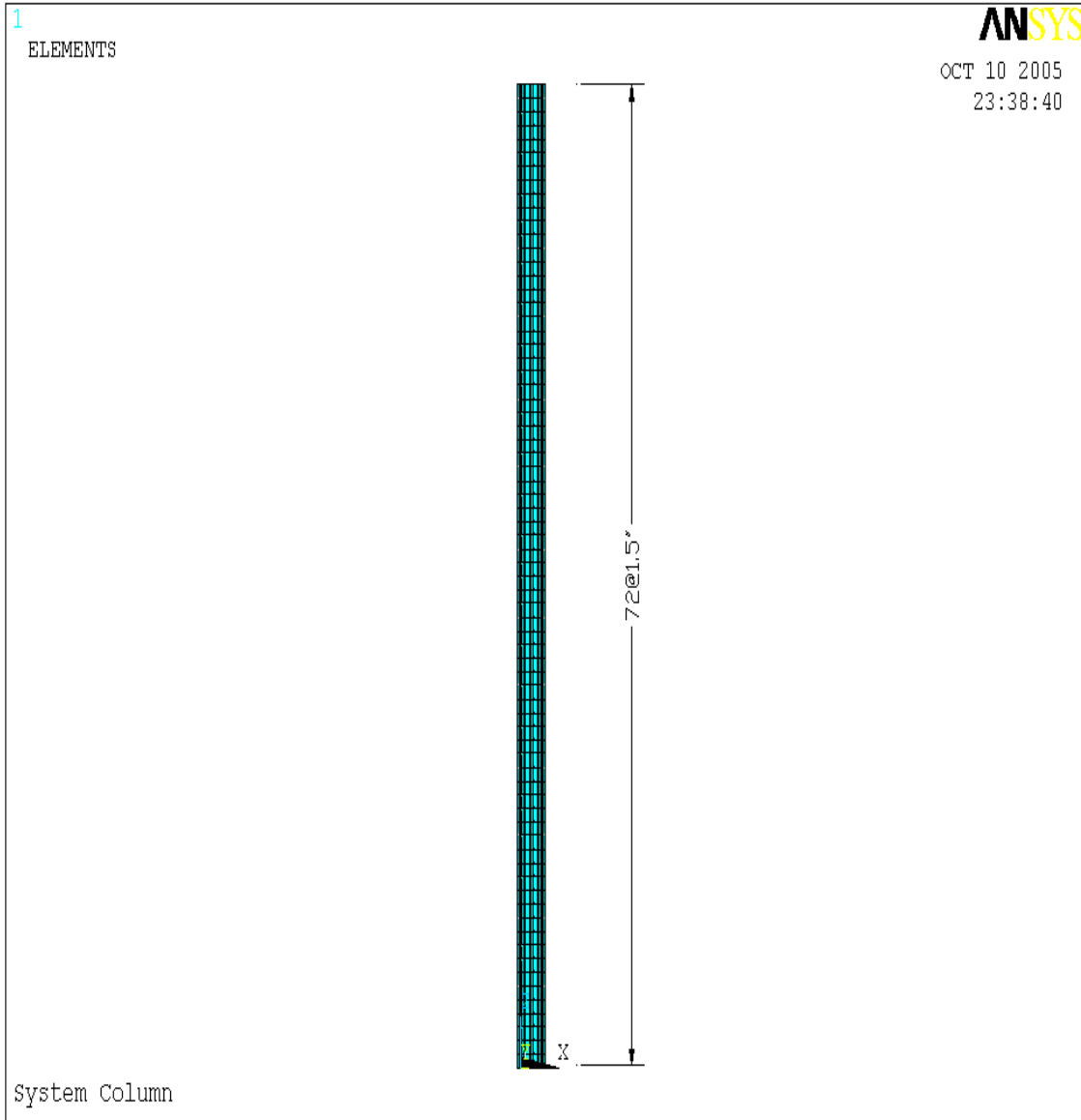
Figure 6.19 Elevation of the original column with foam

6.3.2 Finite element model of the original column with foam

Shell elements (Shell181) are used to model the metal facings and solid elements (Solid45) are used to model the foam between the facings. As shown in Figure 6.21, the model is restrained with pin supports at the top of the column and fix supports at the bottom except the rotation about x direction.
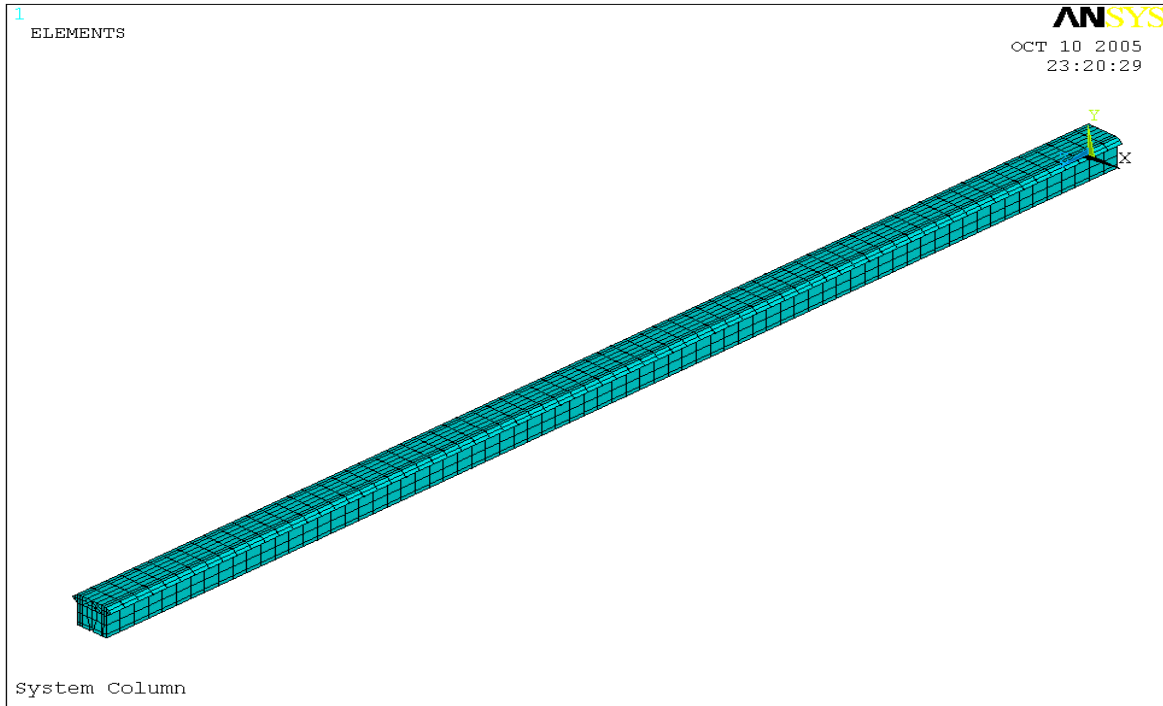
Figure 6.20 Original column model with foam
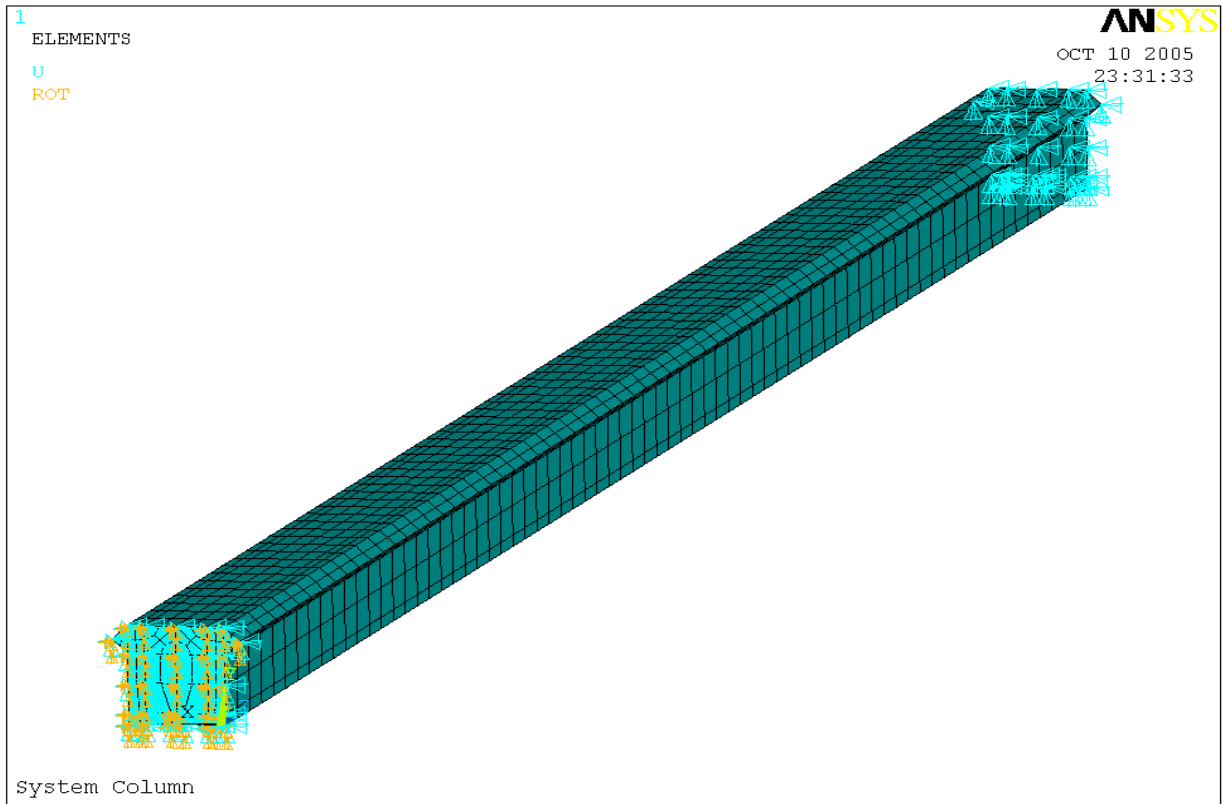
Figure 6.21 End restrains of the original column with foam

6.3.3 Loads

Dead load - Self-weight of the original column made of 16 gage steel with foam:

Foam: 2.0545 lbs

Steel sheets: 16.75 lbs

Live load: $7604^{psf} = 52.807^{psi}$, applied on the top of the original column.

Wind load: $19.60^{psf} = 0.136^{psi}$, applied on the facing of the original column.
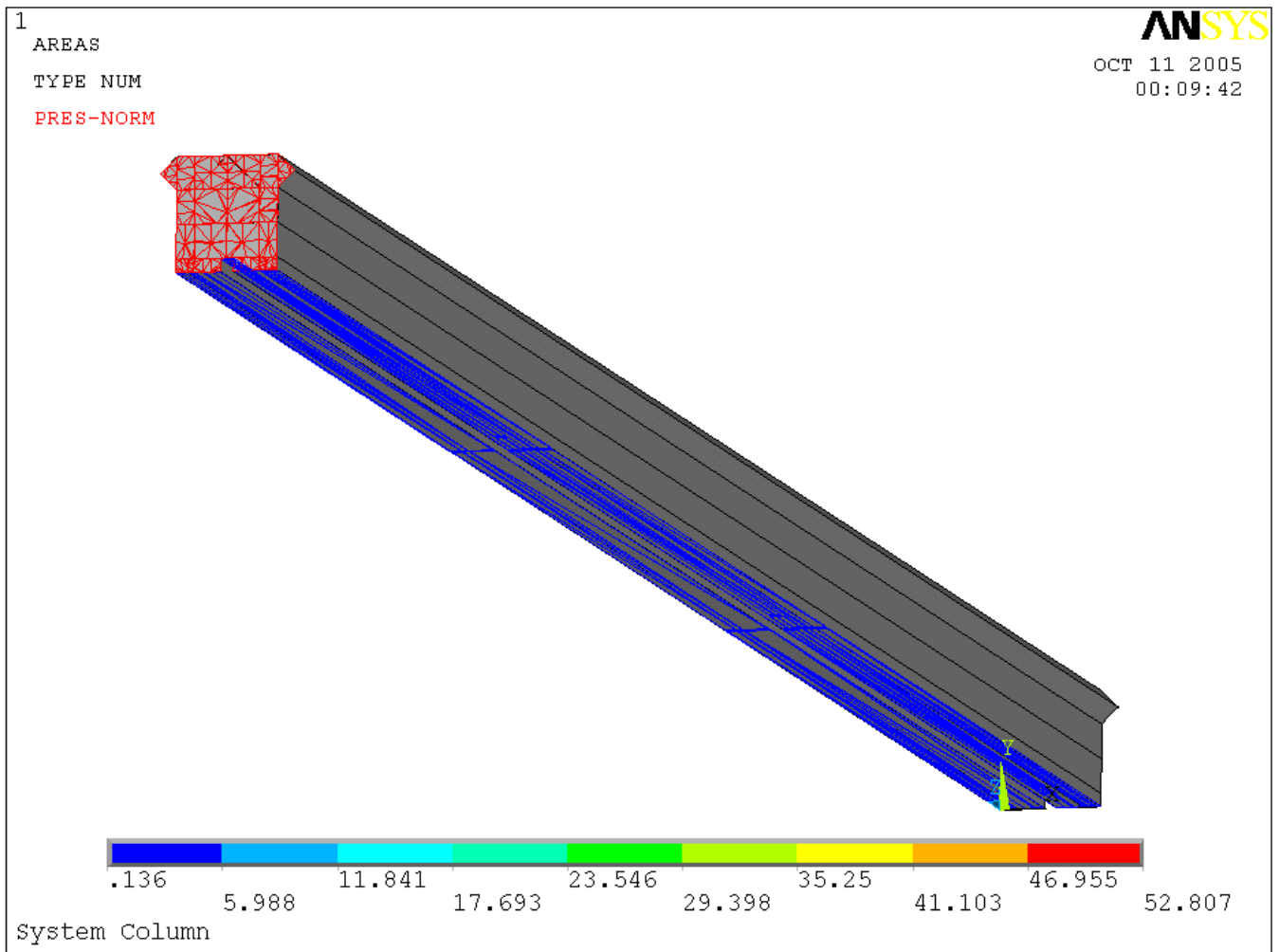
Figure 6.22 Loads on the original column with foam

(Positive values denote the pressure act into the areas)

6.4 Analytical Results of the Original Column with Foam

6.4.1 Deformation of the original column with foam
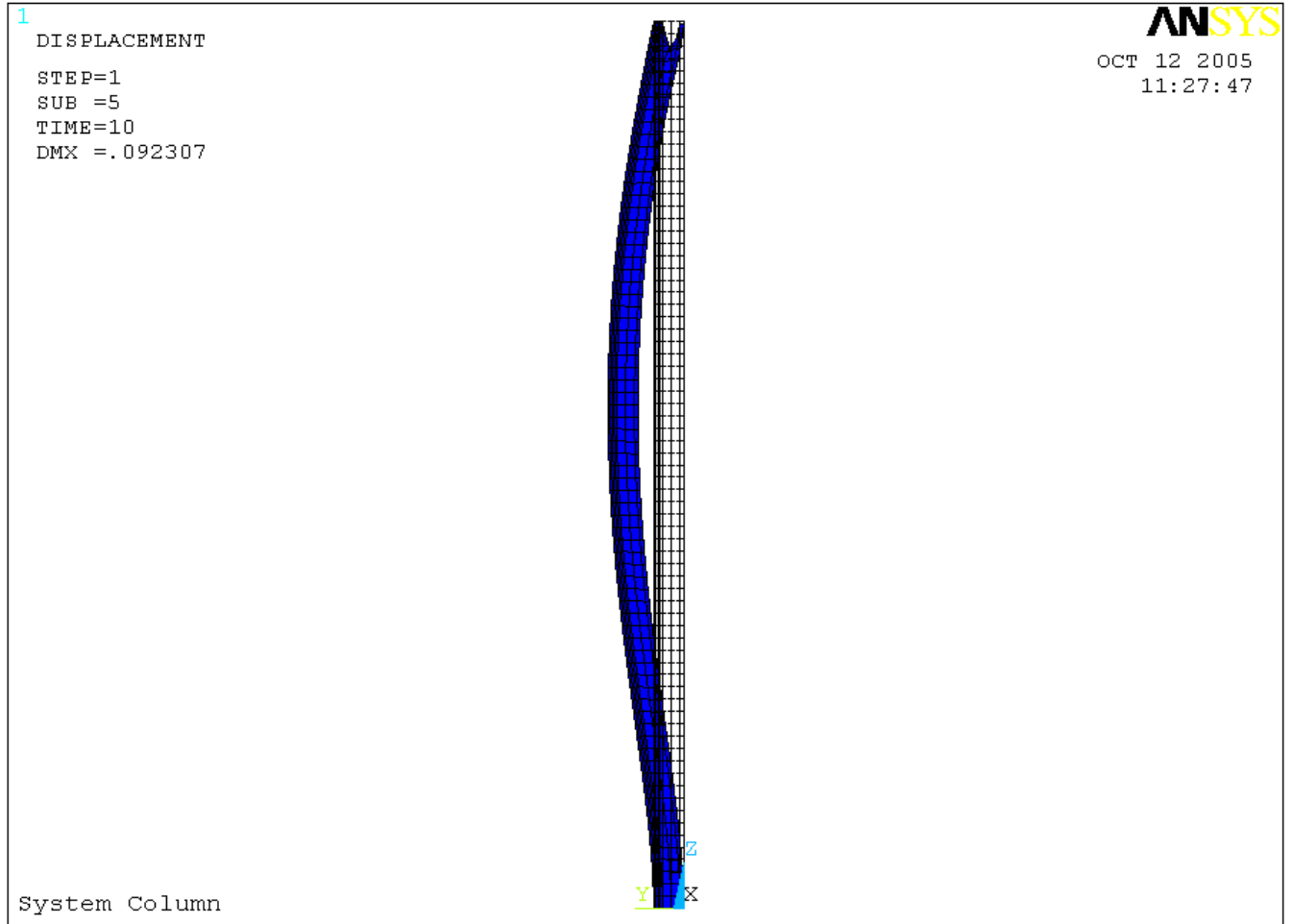
Figure 6.23 Deformation of the original column with foam (unit: inches)

6.4.2 Stresses of the original column with foam
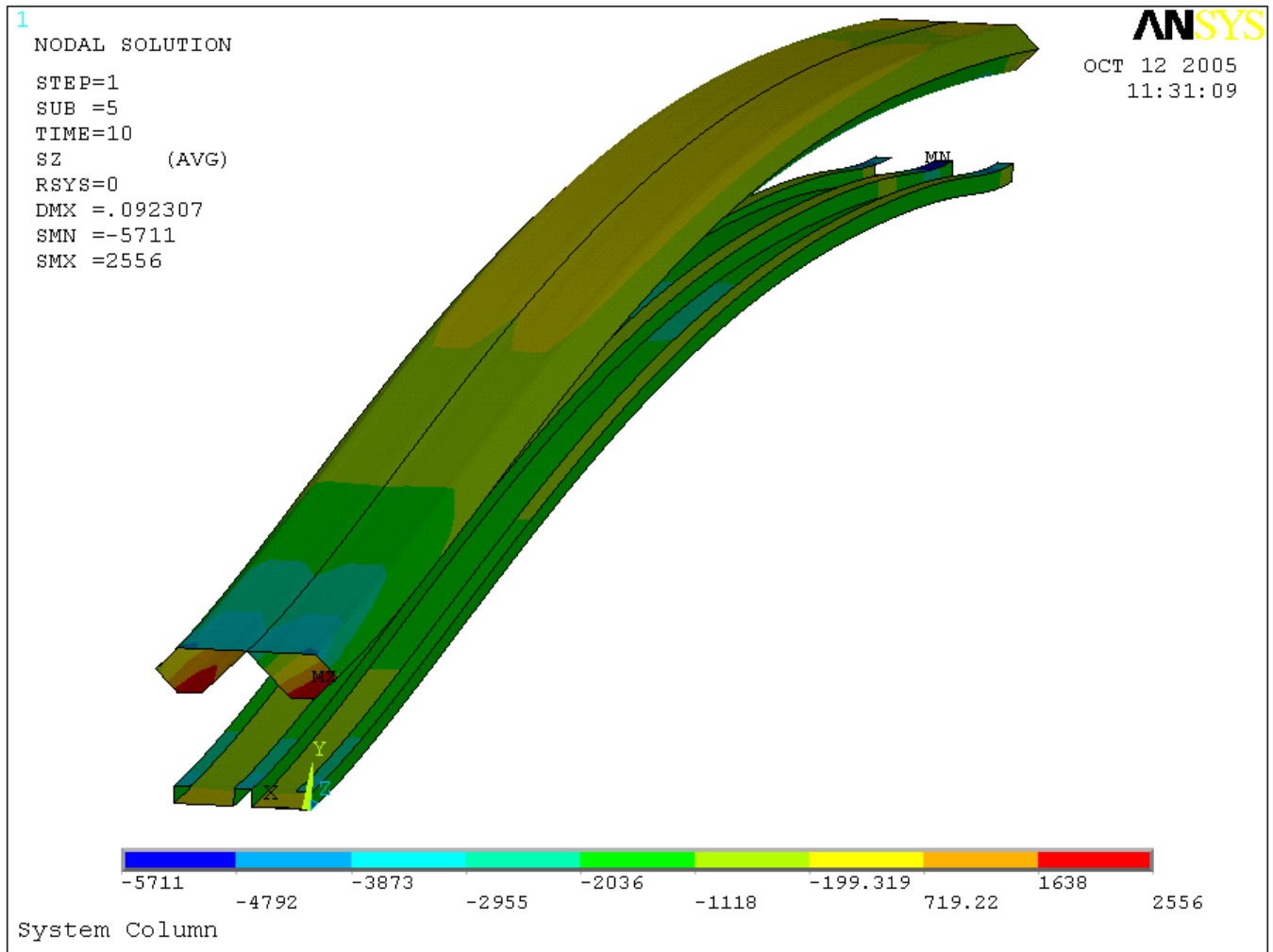
Figure 6.24 Stresses in the longitudinal direction at the steel facings (unit: psi)
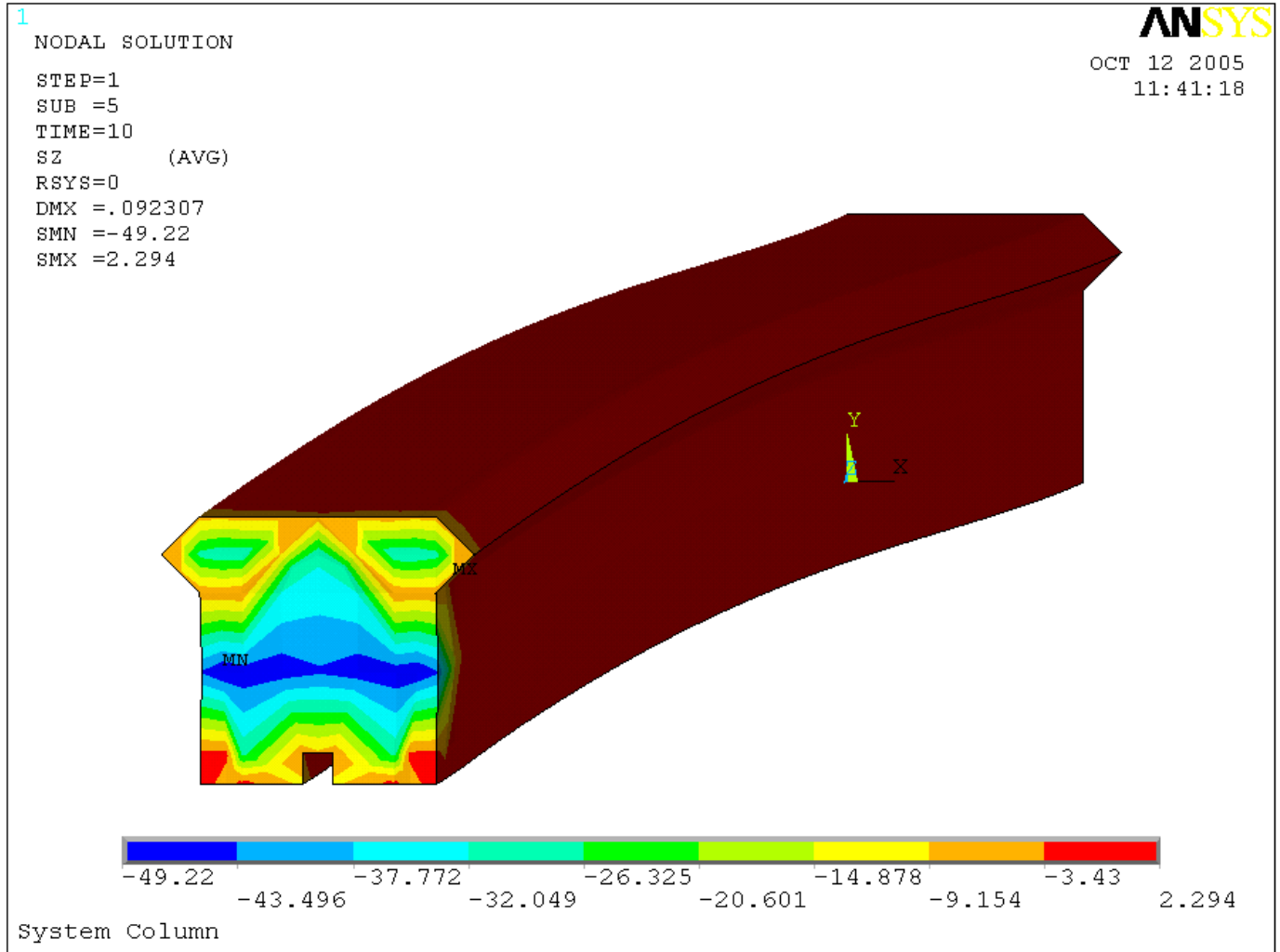
Figure 6.25 Stresses in the longitudinal direction in foam (unit: psi)

6.4.3 Results comments of the original columns with foam

(a) The maximum deformation in the system column occurs at about 46.5" from the top surface.

(b) For the stresses in longitudinal direction, the maximum compressive stress occurs at 3" from the top of the front steel facing and the maximum tensile stress occurs at about 1.5" from the bottom surface of the middle steel facing. The maximum tensile and compressive stresses in the PU foam are 2.294 psi and 49.22 psi, respectively.

Table 6.2 Summary of the maximum stresses in the original column with foam

Element	Maximum tensile stress (psi)	Maximum compressive stress (psi)
Steel sheet (front)	1426	5711
Steel sheet (middle)	2556	3187
Steel sheet (back)	1242	4207
PU foam	2.294	49.22

(a) The stress in the PU foam was almost equal to zero compared to the stress in steel sheets; indicating steel facings carried most of the loads.

(b) The magnitude of deformation is dependent on the modulus of elasticity of foam, E_{foam}, as shown in Figure 6.26
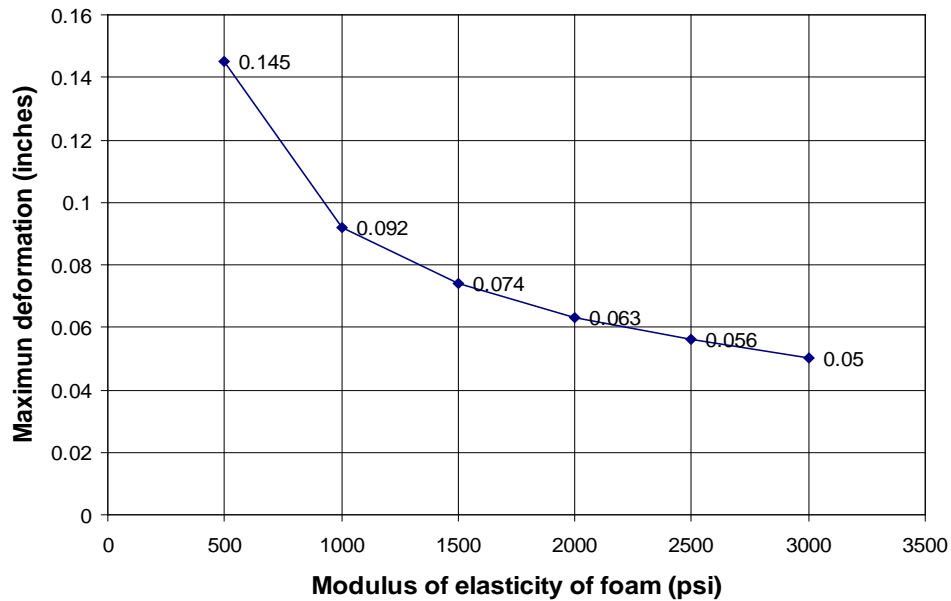
Figure 6.26 Maximum deformation of original column vs. modulus of elasticity of foam

CHAPTER 7

MODELING AND ANALYSIS OF THE WINDOW HEADER

7.1 Description of Input and Modeling of the window header

7.1.1 Dimensions and modeling of the window header

The material properties of the window header are same as the panel and column. The window header made of 16 gage steel was studied.
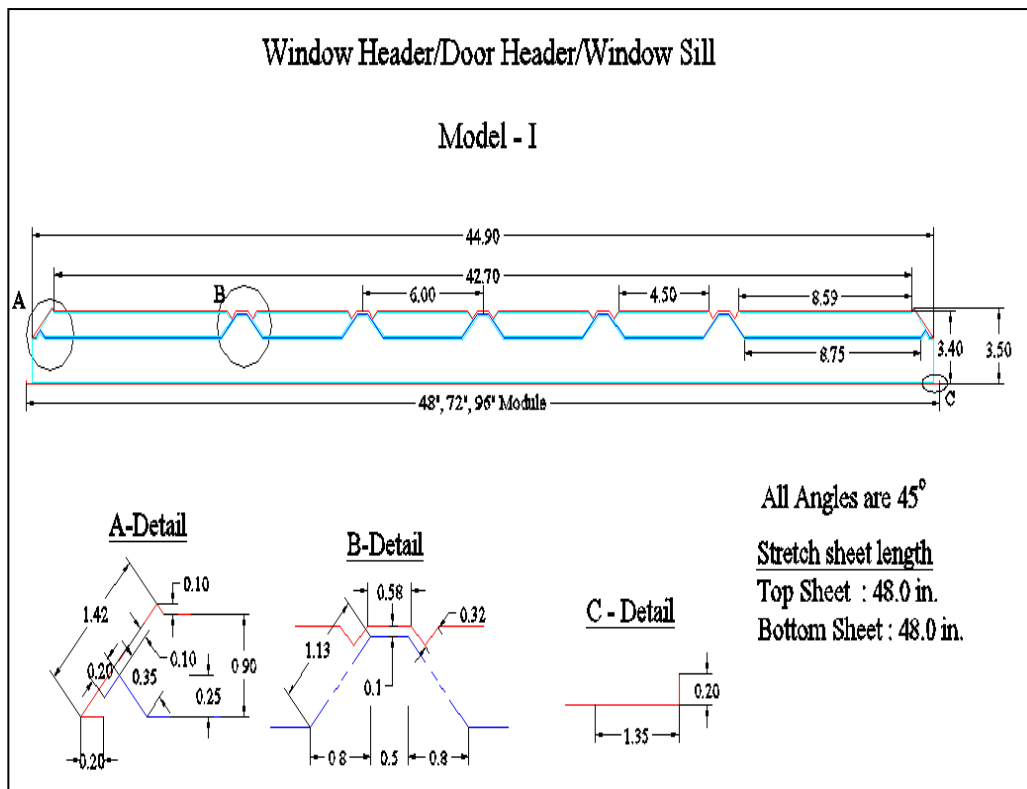
Figure 7.1 Cross-section of the window header model (unit: inches)
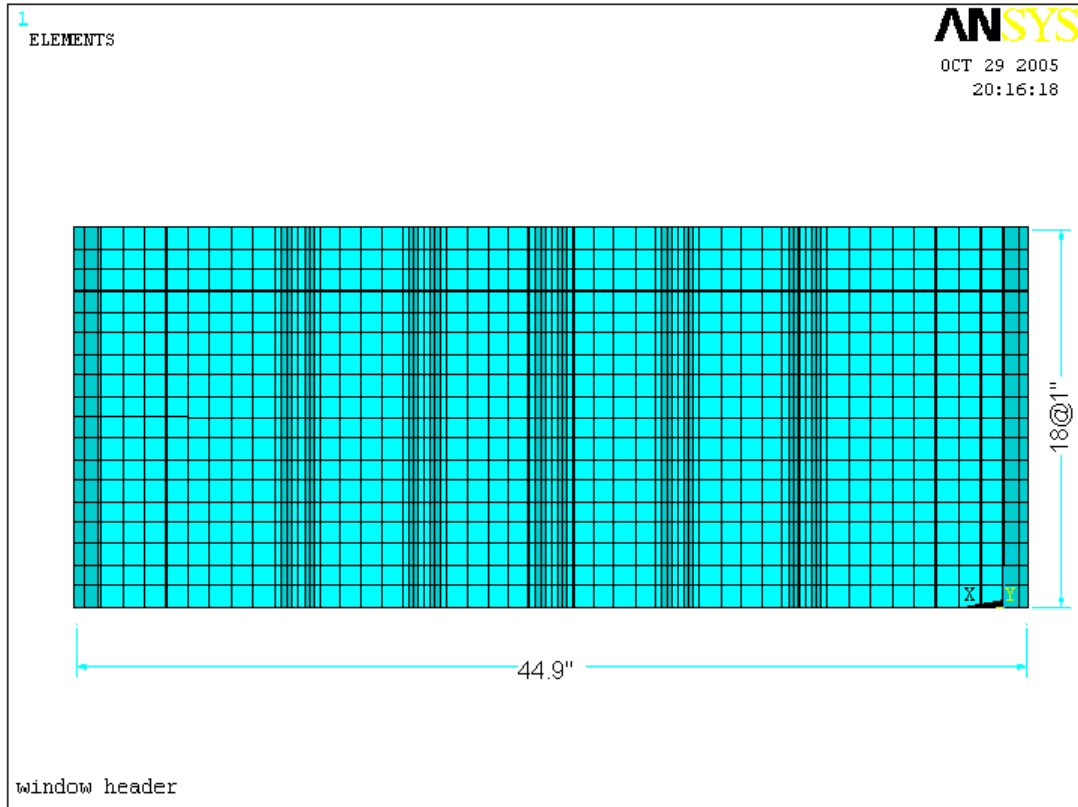
Figure 7.2 Elevation of the window header model

7.1.2 Finite element model of the window header model

Shell elements (Shell181) were used to model the header's metal facings and solid elements (Solid45) were used to model the foam between the facings. As shown in Figure 7.4, pin supports were applied on the ends of the bottom of the window header, and translation restraints in X and Y directions were applied on the top of the header at the positions of columns.
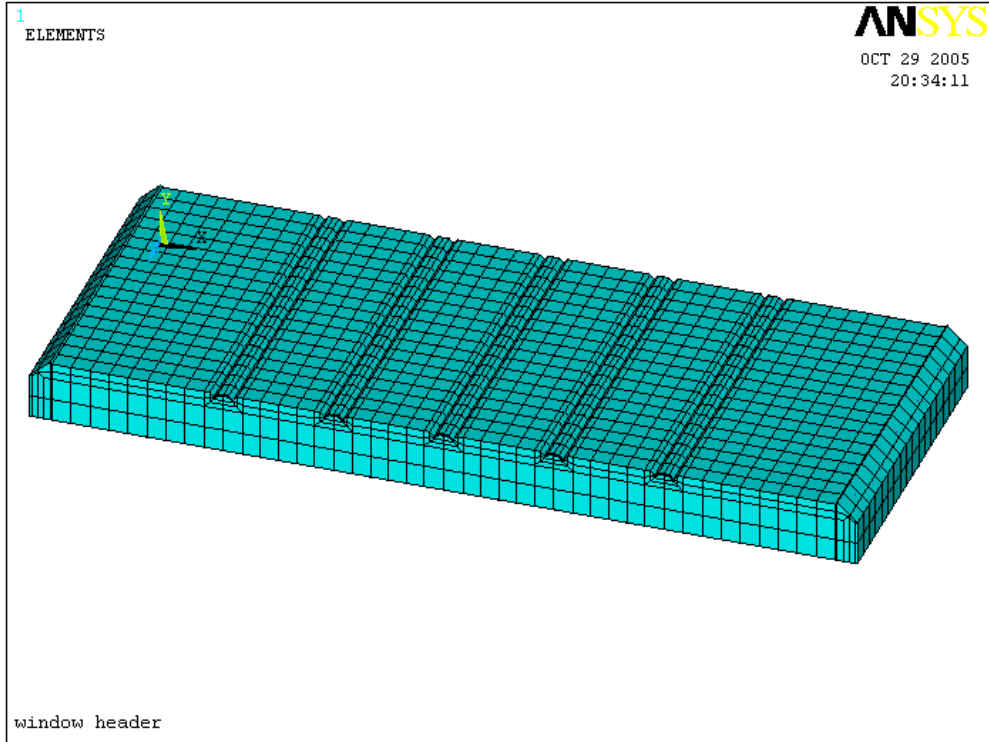
Figure 7.3 Window header finite element model
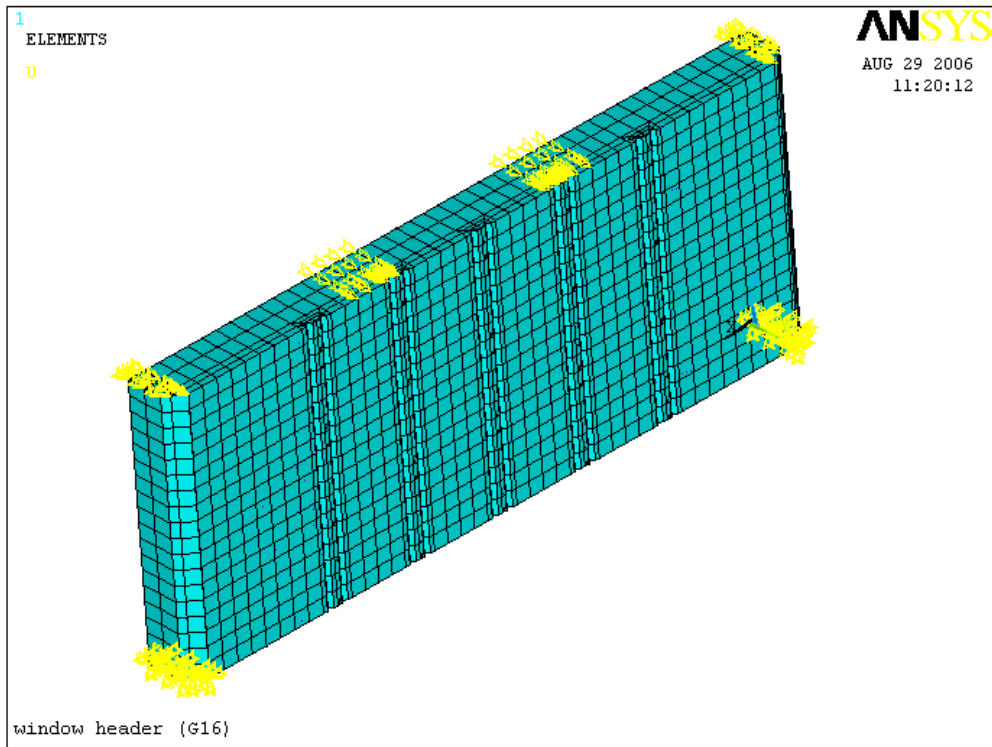
Figure 7.4 Window header model with end restrains

7.1.3 Loads

Dead load - Self-weight of the window header:

Foam: 4.65 lbs

Steel sheets: 26.72 lbs

Live load: 1.164^{psi}, applied on the top C-shape track of the window header.

Wind load: $19.60^{psf} = 0.136^{psi}$, applied on the curved facing of the window header.
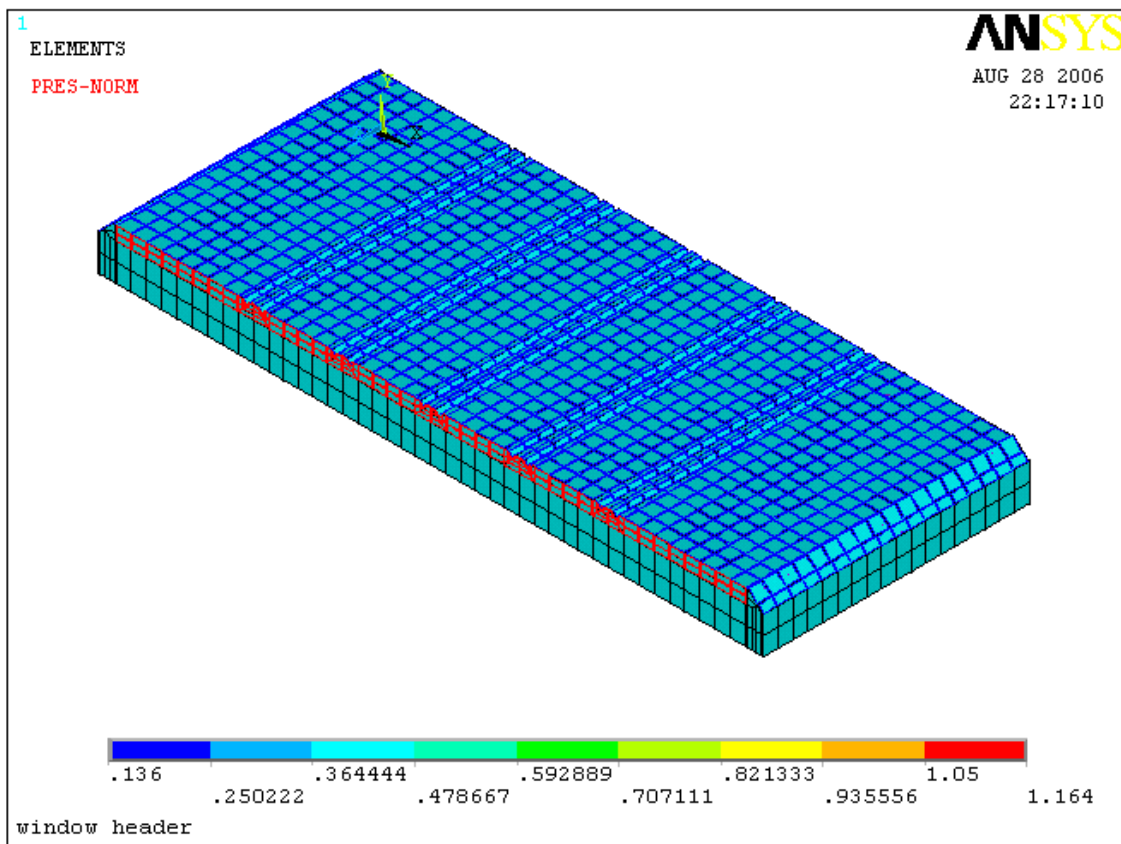
Figure 7.5 Loads on the window header model

(Positive values denote the pressure act into the areas)

7.2 Analytical results of the window header

Figure 7.6 shows the deformation of the window header with Gage 16. Figures 7.7 through 6.10 show the stresses of window header under the load Case 1.
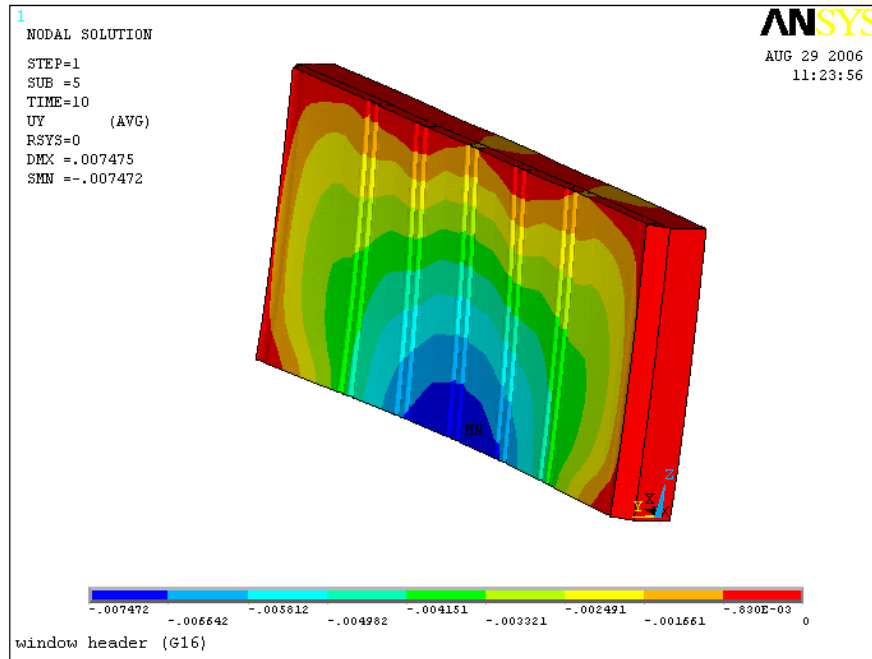
Figure 7.6 Deformation of the window header model (unit: inches)
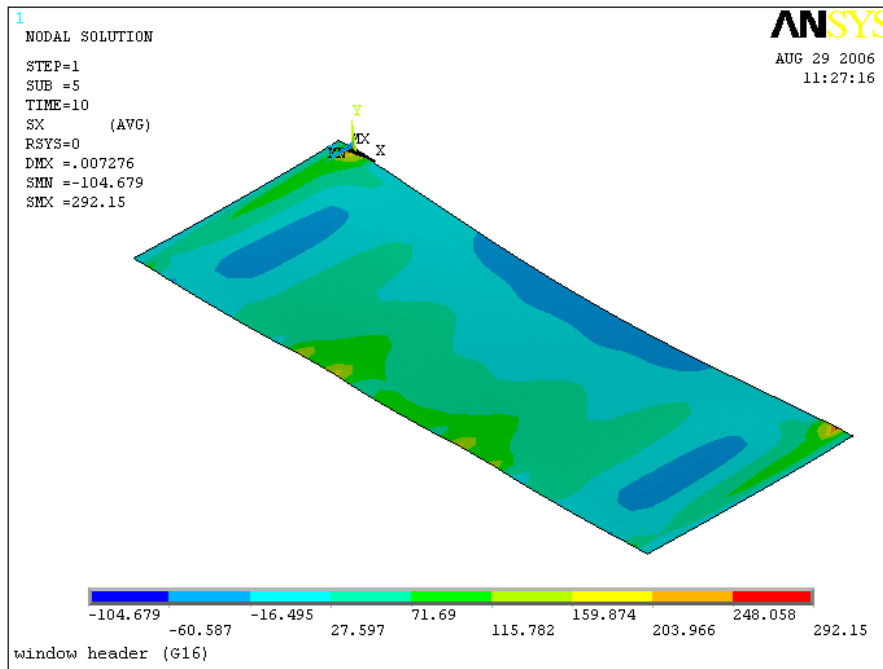
Figure 7.7 Stresses in x direction in the back steel facing y=0 (unit: psi)

99
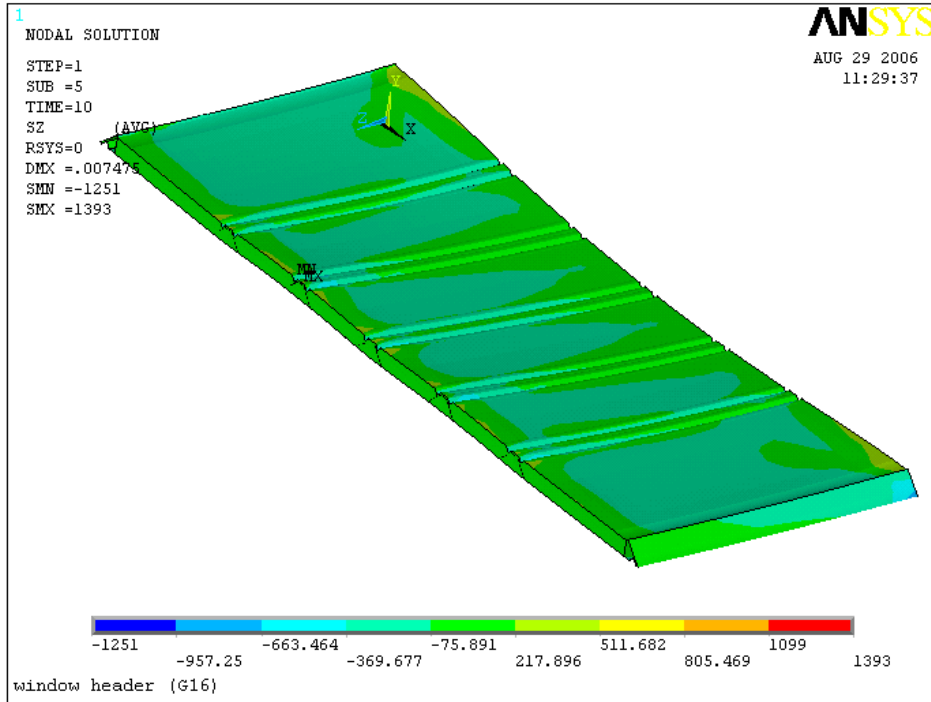
Figure 7.8 Stresses in longitudinal direction in the front steel facing (unit: psi)
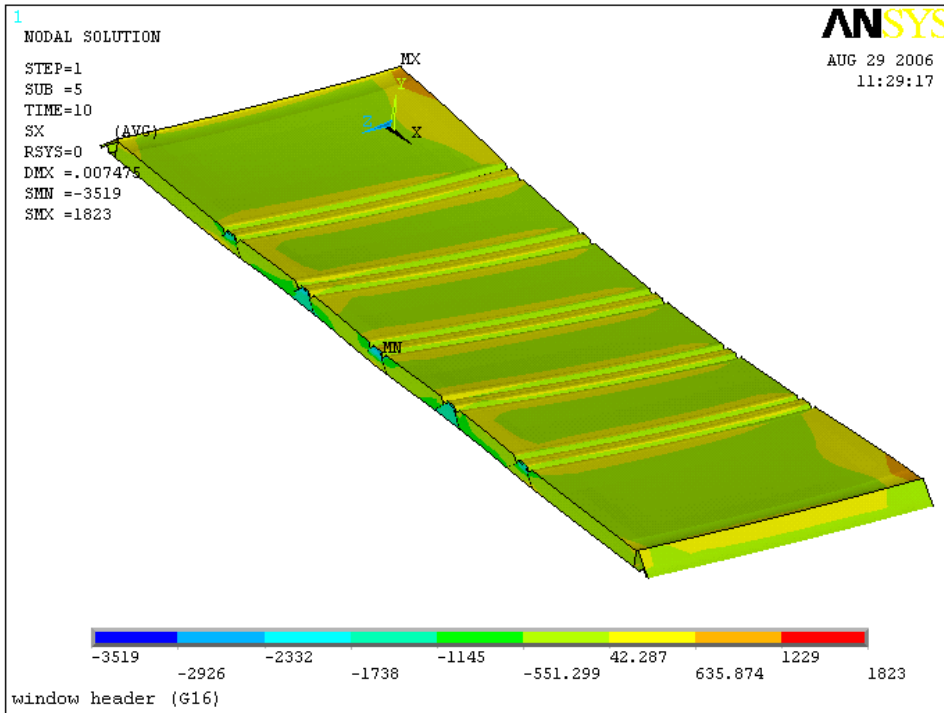
Figure 7.9 Stresses in x direction in the front steel facing (unit: psi)
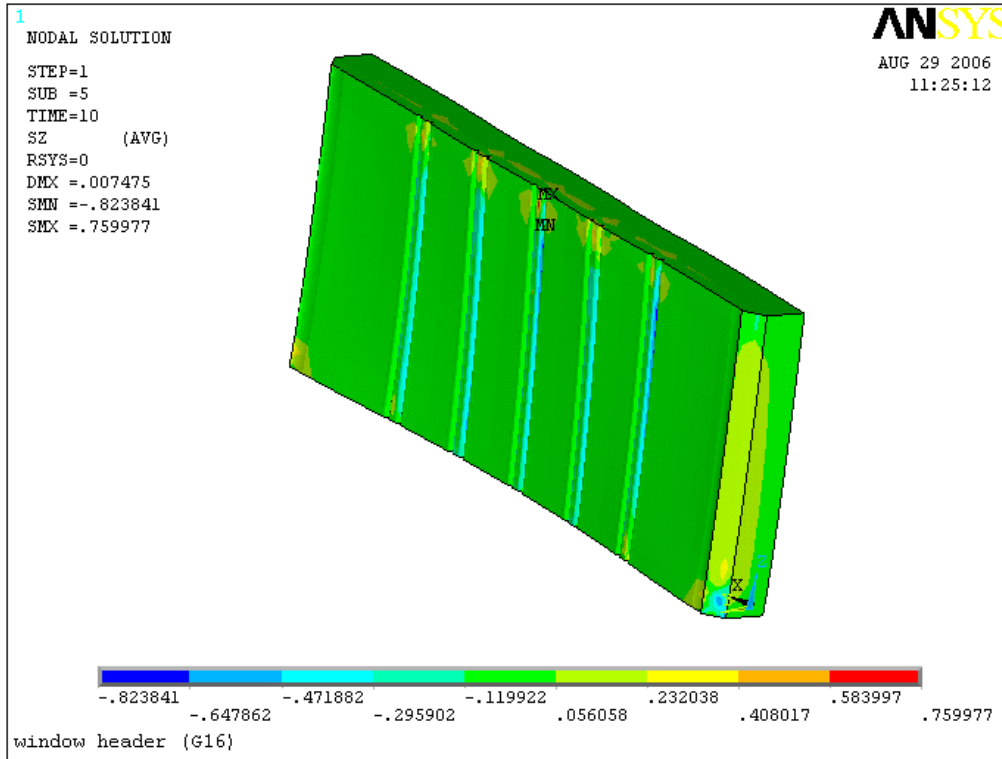
Figure 7.10 Stresses in longitudinal direction in foam (unit: psi)

It was observed that the maximum deformation in the window header occurred at the bottom of the front steel facing (y = 2.5 ft). For the stresses in longitudinal direction, the maximum compressive stress and the maximum tensile stress occurred at the top of the front steel facing. The stress in the PU foam was almost equal to zero; indicating steel facings carried most of the loads.

Table 7.1 Summary of the maximum stresses in the window header

Element	Maximum positive stress (Tension) (psi)	Maximum negative stress (Compression) (psi)
Steel sheets (front)	1823	3519
Steel sheet (back)	104.68	292.15
PU foam	0.82	0.76

7.3 Capability of the Window Header

When the wind load was kept unchanged (Wind load: 0.136 *psi*, applied on the shaped facing of the window header), the maximum vertical live load on the window header could be obtained based on allowable stress in steel facings. Figure 7.11 through 7.15 shows the deformations and stresses under the maximum live load on the window header.
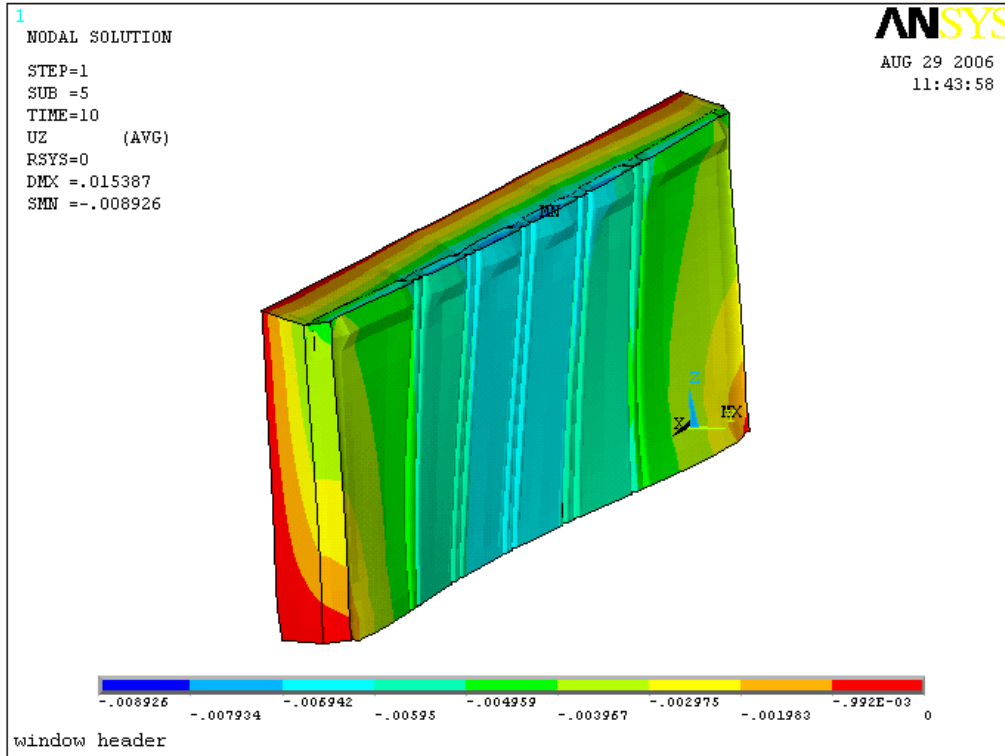
Figure 7.11 Deformation of the window header model (unit: inches)
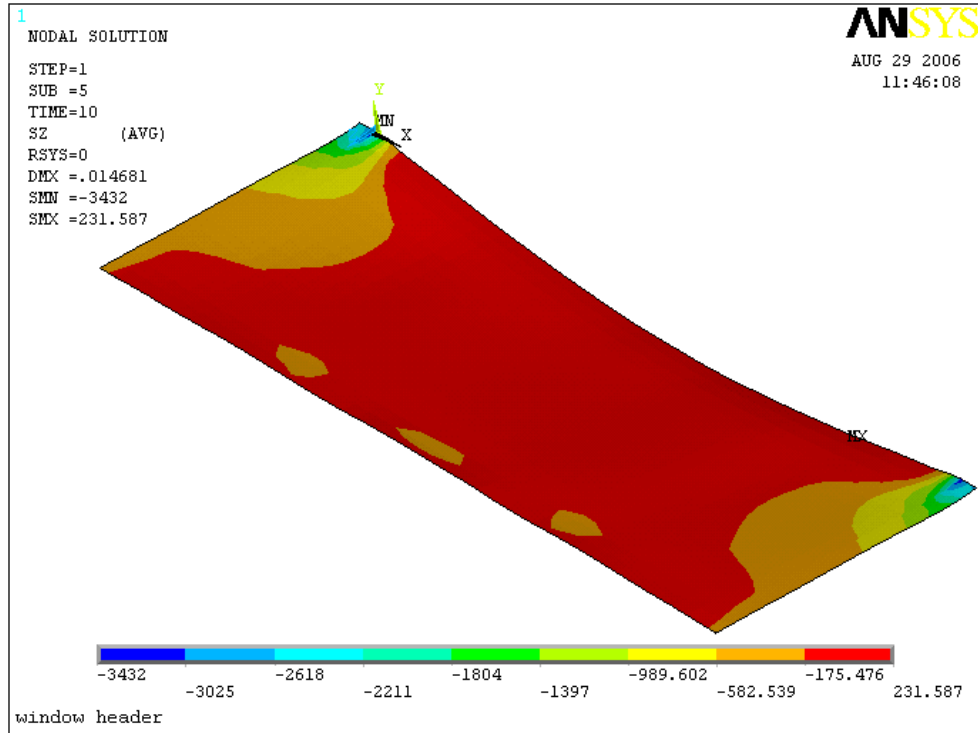
Figure 7.12 Stresses in longitudinal direction in the back steel facing y=0 (unit: psi)
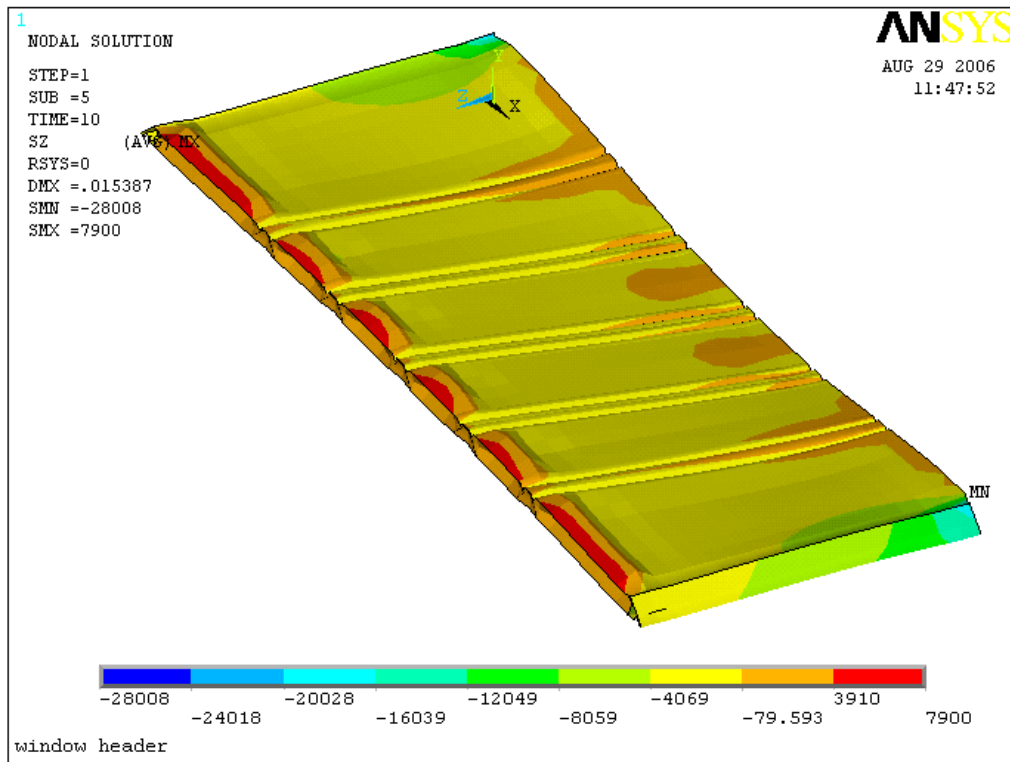
Figure 7.13 Stresses in longitudinal direction in the front steel facing (unit: psi)

103
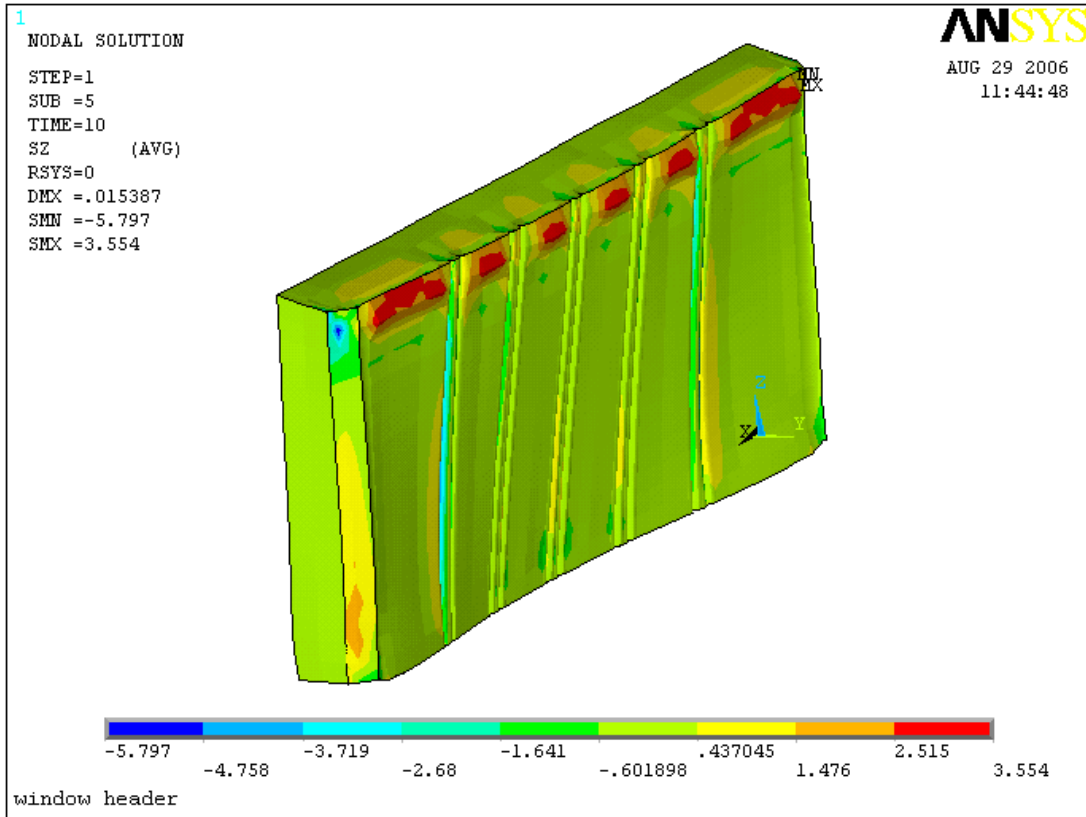
Figure 7.14 Stresses in longitudinal direction in foam (unit: psi)

Under the maximum vertical load, the window header exhibited the same performance as the normal load case – load Case 1. The maximum deformation of the window header was 0.0154 inch which occurred at the midsapn, bottom of the header. Under the larger vertical live load, the maximum stress in steel facing was 28,000 psi while the maximum stress in foam was only 5.797 psi, which showed the steel facings carry majority of the applied loads. The maximum negative stress of the window header occurred at the bottom of the front steel facings and close to the supports. The maximum positive stress occurred in the steel facing at the top of the header.

CHAPTER 8

CONCLUSION AND RECOMMENDATION

8.1 Conclusion and recommendation about the basic panel

1. For all the panels of metal facings made of 24, 25 and 26 gage steel studied, the maximum deformation occurred at about middle height of the panels. The magnitude of deformation decreased with the modulus of elasticity of foam increased. Under self-weight, wind load and live load, the maximum deformation was less than the limit of the code when the modulus of elasticity was 1000 psi.

2. The maximum tensile stress in longitudinal direction occurred at the bottom of the front steel facing and the maximum compressive stress occurred at about 45" from the top surface of the front steel facing. Under the normal loads (load Case 1), the stress of foam was much smaller than the stress of the steel facing, and the stress of the foam could be neglected. For example, in the panel made of 24 gage steel, the maximum stress of the foam was 13.565 psi while the maximum stress of the steel facing was 11428 psi.

3. In determination of the vertical load capacity, the stress in the foam was a key factor for the maximum value of the vertical load and the stress of the steel facing did not change much. In pursuing the horizontal wind load capacity, the stress of the steel facing was a key factor while the stress of the foam could be neglected because the steel facings carried almost all the loads.

8.2 Conclusions and recommendations about the system column

8.2.1 Comparison of Slenderness Ratio

The slenderness ratio was an important term for columns behavior. According to the AISC LRFD Specifications, Article B7, the slenderness ratio of a compression member, KL/r, should not exceed 200. The calculations of the slenderness ratio of all columns are shown in the following.

Table 8.1 Comparison of Slenderness Ratio for the Studied columns

	C-shape column				Delta-shape column			Original column		
	16G-C2×4	16G-C2×6	20G-C2×4	20G-C2×6	16G	18G	20G	16G	18G	20G
A (in^2)	0.3919	0.5086	0.2353	0.3071	1.4352	1.1472	0.8616	0.5894	0.4711	0.3538
I (in^4)	0.7598	2.1565	0.4561	1.3143	0.603	0.4819	0.3619	0.085	0.0679	0.051
r (in.)	1.3924	2.059	1.3923	2.069	0.6482	0.6481	0.6480	0.3798	0.3796	0.38
L (in.)	108.0	108.0	108.0	108.0	108.0	108.0	108.0	108.0	108.0	108.0
KL/r	77.56	52.5	77.6	52.2	166.61	166.64	166.67	284.4	284.5	284.2

Note:
1. I is the least moment of inertia of the column section;

2. $r = \sqrt{\dfrac{I_{33}}{A}}$.

According to Table 8.1, the slenderness ratios of the C-shape and Delta-shape columns were less than the limitation of slenderness ratio 200, while the slenderness ratios of the original columns were greater than the limit.

8.2.2 Comparison of deformations and stresses for columns under load Case 1

Table 8.2 Deformations and Stresses of the Studied Columns under Load Case 1

Steel thickness	Column	Maximum Deflection (in.)	Maximum Rotation (rad.)	Maximum positive stress (Tension) (psi)	Maximum negative stress (Compression) (psi)	Slenderness ratio (KL/r)	Check Code
16 Gage	2 × 4 C-shape	0.0678	0.0232	---	6132	77.56	**OK**
	2 × 6 C-shape	0.0335	0.0097	---	4492	52.5	**OK**
20 Gage	2 × 4 C-shape	0.1424	0.0503	---	11,130	77.6	**OK**
	2 × 6 C-shape	0.0644	0.0202	---	8108	52.2	**OK**
16 Gage	Delta-shape	0.0232	0	---	2401	166.61	**OK**
18 Gage	Delta-shape	0.0302	0	---	3042	166.64	**OK**
20 Gage	Delta-shape	0.0430	0	---	4140	166.67	**OK**
16 Gage	Original column	0.1291	0	522.701	6759	<u>284.4</u>	**NG**
18 Gage	Original column	0.1616	0	609.441	8439	<u>284.5</u>	**NG**
20 Gage	Original column	0.2153	0	751.432	11,217	<u>284.2</u>	**NG**

Note:

1. Limitations:

      a. The limitation of steel stress $\phi F_{steel} = 0.85 \times 33 = 28.05 ksi$.

      b. The limitation of panel deformation is L/360=0.30 inch.

      c. The limitation of slenderness ratio is 200.

2. The underlined values are unacceptable compared with the above limitations.

8.2.3 Comparison of deformations and stresses for columns under load Case 2

Table 8.3 Deformations and Stresses of the Studied Columns under Load Case 2

Steel thickness	Column	Maximum Deflection (in.)	Maximum Rotation (rad.)	Maximum positive stress (Tension) (psi)	Maximum negative stress (Compression) (psi)	Slenderness ratio (KL/r)	Check Code
16 Gage	2×4 C-shape	<u>1.079</u>	0.370	<u>31.102</u>	<u>45.051</u>	77.56	**NG**
	2×6 C-shape	<u>0.529</u>	0.156	19.16	<u>32.216</u>	52.5	**NG**
16 Gage	Delta-shape	0.2367	0	10,002	11,990	166.61	**OK**
18 Gage	Delta-shape	<u>0.3083</u>	0	12,685	15,466	166.64	**OK**
20 Gage	Delta-shape	<u>0.4402</u>	0	17,328	21,619	166.67	**NG**
16 Gage	Original column	<u>1.497</u>	0	<u>31,999</u>	<u>52,937</u>	<u>284.4</u>	**NG**

Note:
1. Limitations:
     a. The limitation of steel stress $\phi F_{steel} = 0.85 \times 33 = 28.05 ksi$.
     b. The limitation of panel deformation is L/360=0.30 inch.
     c. The limitation of slenderness ratio is 200.
2. The underlined values are unacceptable compared with the above limitations.

8.2.4 Conclusion from analysis of system columns

Based on the analytical results, following conclusions were drawn:

1. Twist or torsional deformation could be clearly observed in the C-shape columns under

loading due to the asymmetry about the weak axis in the cross-section. The delta-shape and

original columns exhibited flexural buckling deformation only. The maximum deformations of

delta-shape and original columns occurred at about 45" - 46" from the top surfaces of the columns.

2. The maximum compression of all the columns occurred at the bottom of the columns under load Case 1 and Case 2. Under load Case 1, the maximum tensile of the original column occurred at the bottom of the columns, and no tensile occurred at the C-shape and Delta-shape columns. The maximum tensile stresses of all the columns occurred at the bottom of the columns under load Case 2.

3. The stresses, deformations and slenderness ratios in C-channel columns and Delta columns were acceptable when columns were subjected to wind load based on column area only (load Case 1). The slenderness ratio of original columns was unacceptable.

4. Only Delta columns made of 16 and 18 gage steel met all of the design criteria when the columns subjected to wind load based on 36 in wide tributary area (24 in. for C-shape column). For columns with the same Gage and under the same loads, Delta column had the smallest stress and original column had the largest stress.

Considering the deformation, slenderness ratio and stresses of the columns, Delta-columns made of 16 and 18 gage steel were the best choice among the columns studied in this project.

8.3 Conclusions on the window header

For the stresses in the longitudinal direction of the window header, the maximum tensile and compressive stresses occurred at the bottom of the front steel facing. The maximum compressive stress in the PU foam were almost zero, indicating the steel facings carried almost all of the loads on the window header. Even under the larger vertical live load, the maximum stress in steel facing was 28,000 psi while the maximum stress in foam was only 5.797 psi.

CHAPTER 9

PLANS FOR FUTURE COLLABORATION

The main purpose of this project was development and analysis of a new building envelope technology that maximizes internal integration by utilizing a highly-efficient building envelope with high-R thermal insulation, active thermal mass and superior air-tightness. The project team approach was to combine four common building technologies in a novel way. Structural Insulated Panel (SIP) technology was utilized as a structural vehicle and for high-R thermal insulation. Novel approach to panel-to-panel connections provided excellent air and moisture tightness, but it also works in a similar way as conventional wall framing.

It is expected that follow-up energy performance analysis for heating and cooling dominated climates and enhanced with full scale field testing in several U.S. locations can be considered as future collaboration targets.

INTERNAL DISTRIBUTION

1. A. Desjarlais
2. B. DeVault
3. J. Green
4. P. Hughes
5. J. Kosny
6. Laboratory Records–RC
7. Laboratory records for submission to OSTI

EXTERNAL DISBRIBUTION

1. Sally Gaskin, sally@sgiventures.net
2. X. Sharon Huo, xhuo@tntech.edu
3. Marilyn Brown, Marilyn.brown@pubpolicy.gatech.edu